HYDRAULIC MODEL STUDIES OF STEWART MOUNTAIN DAM SPILLWAY

Hydraulics Branch
Division of General Research
Engineering and Research Center
Bureau of Reclamation

July 1975
GR-6-75

MS-230 (8-70)
Bureau of Reclamation

TECHNICAL REPORT STANDARD TITLE PAGE

1. REPORT NO.	2. GOVERNMENT ACCESSION NO.	3. RECIPIENT'S CATALOG NO.
GR-6-75		

4. TITLE AND SUBTITLE	5. REPORT DATE
Hydraulic Model Studies of Stewart Mountain Dam Spillway	July 1975
	6. PERFORMING ORGANIZATION CODE
7. AUTHOR(S)	8. PERFORMING ORGANIZATION REPORT NO.
P. L. Johnson	GR-6-75
9. PERFORMING ORGANIZATION NAME AND ADDRESS	10. WORK UNIT NO.
Engineering and Research Center Bureau of Reclamation Denver, Colorado 80225	11. CONTRACT OR GRANT NO.
	13. TYPE OF REPORT AND PERIOD COVERED
12. SPONSORING AGENCY NAME AND ADDRESS	
Salt River Project Phoenix, Arizona	14. SPONSORING AGENCY CODE

15. SUPPLEMENTARY NOTES

16. ABSTRACT

Hydraulic model studies were performed to develop a means to eliminate the possibility of erosion undercutting the spillway chute at Stewart Mountain Dam, Arizona. The chute, which was completed in 1936, was designed so that the water would flow through the chute down a granitic slope to the river. The granite, which was initially thought to be sound, contains a major fault. Erosion along this fault is compromising the chute structure. Operational modifications, the addition of a divider wall or flip structures, and modifications and protection of the granitic surface were considered. Flow velocities across the surface and impact pressures on the rock surface were evaluated. The divider wall as well as several of the topographic modifications, when combined with protective surfacing of various extents of the rock, offered potential solutions.

17. KEY WORDS AND DOCUMENT ANALYSIS

a. DESCRIPTORS--/ hydraulic models/ *chute spillways/ spillway piers/ *model studies/ *model tests/ *rock competency/ impact tests/ slope protection/ erosion control

b. IDENTIFIERS--/ *Stewart Mountain Dam, AZ

c. COSATI Field/Group 13M

18. DISTRIBUTION STATEMENT	19. SECURITY CLASS. (THIS REPORT)	21. NO. OF PAGES
	UNCLASSIFIED	90
	20. SECURITY CLASS (THIS PAGE)	22. PRICE
	UNCLASSIFIED	

GR-6-75

HYDRAULIC MODEL STUDIES OF STEWART MOUNTAIN DAM SPILLWAY

by
P. L. Johnson
For the Salt River Project
Phoenix, Arizona

Hydraulics Branch
Division of General Research
Engineering and Research Center
Denver, Colorado
July 1975

UNITED STATES DEPARTMENT OF THE INTERIOR * BUREAU OF RECLAMATION

ACKNOWLEDGMENT

The studies were reviewed by T. J. Rhone, Applied Hydraulics Section Head, under the supervision of the Hydraulics Branch Chief, D. L. King. The final plans developed through the cooperation of the Salt River Project and the Hydraulics Branch, Division of General Research, Bureau of Reclamation. Input by James Legas, Division of Design, Bureau of Reclamation, was appreciated.

CONTENTS

	Page
Purpose	1
Results	1
Application	2
Introduction	3
Model	9
The Investigation	16
Conclusions	47

LIST OF FIGURES

Figure		Page
1	Stewart Mountain Dam and spillway	4
2	Location map, Stewart Mountain Dam	5
3	Plan of spillway, Stewart Mountain Dam	7
4	Topographic map of region below spillway	10
5	Stewart Mountain Dam and spillway with erosion shown	11
6	Hydraulic model	13
7	Impact geometry	14
8	Spillway calibration	18
9	Drawing of flip structures	24
10	Operating toothed flip	25
11	Operating solid flip	27
12	Divider wall	28
13	First topographic model modification	30
14	Second topographic model modification	33
15	Intermediate topographic model modification	35
16	Final topographic configuration with protective surfacing	37

LIST OF FIGURES - Continued

Figure		Page
17	Plan and elevation splitter piers	46
18	Splitter piers operating	48
19	Possible flow surface protection	51

APPENDIX A

Figure		Page
A-1	Initial model topography	55
A-2	Velocity contours for a discharge of 13,000 ft^3/s (initial model topography)	56
A-3	Impact pressures for a discharge of 13,000 ft^3/s (initial model topography)	57
A-4	Velocity contours for a discharge of 30,000 ft^3/s (initial model topography)	58
A-5	Impact pressures for a discharge of 30,000 ft^3/s (initial model topography)	59
A-6	Velocity contours for a discharge of 60,000 ft^3/s (initial model topography)	60
A-7	Impact pressures for a discharge of 60,000 ft^3/s (initial model topography)	61

APPENDIX A - Continued

Figure		Page
A-8	Velocity contours for a discharge of 140,000 ft^3/s (initial model topography)	62
A-9	Impact pressures for a discharge of 140,000 ft^3/s (initial model topography)	63
A-10	First topographic model modification	64
A-11	Velocity contours for a discharge of 13,000 ft^3/s (first topographic model modification)	65
A-12	Impact pressures for a discharge of 13,000 ft^3/s (first topographic model modification)	66
A-13	Velocity contours for a discharge of 30,000 ft^3/s (first topographic model modification)	67
A-14	Impact pressures for a discharge of 30,000 ft^3/s (first topographic model modification)	68

APPENDIX A - Continued

Figure		Page
A-15	Velocity contours for a discharge of 60,000 ft^3/s (first topographic model modification)	69
A-16	Impact pressures for a discharge of 60,000 ft^3/s (first topographic model modification)	70
A-17	Velocity contours for a discharge of 140,000 ft^3/s (first topographic model modification)	71
A-18	Impact pressures for a discharge of 140,000 ft^3/s (first topographic model modification)	72
A-19	Second topographic model modification	73
A-20	Velocity contours for a discharge of 13,000 ft^3/s (second topographic model modification)	74
A-21	Impact pressures for a discharge of 13,000 ft^3/s (second topographic model modification)	75

APPENDIX A - Continued

Figure		Page
A-22	Velocity contours for a discharge of 30,000 ft^3/s (second topographic model modification)	76
A-23	Impact pressures for a discharge of 30,000 ft^3/s (second topographic model modification)	77
A-24	Velocity contours for a discharge of 60,000 ft^3/s (second topographic model modification)	78
A-25	Impact pressures for a discharge of 60,000 ft^3/s (second topographic model modification)	79
A-26	Velocity contours for a discharge of 140,000 ft^3/s (second topographic model modification)	80
A-27	Impact pressures for a discharge of 140,000 ft^3/s (second topographic model modification)	81
A-28	Final topographic model configuration	82

APPENDIX A - Continued

Figure		Page
A-29	Velocity contours for a discharge of 13,000 ft^3/s (final topographic model configuration)	83
A-30	Impact pressures for a discharge of 13,000 ft^3/s (final topographic model configuration)	84
A-31	Velocity contours for a discharge of 30,000 ft^3/s (final topographic model configuration)	85
A-32	Impact pressures for a discharge of 30,000 ft^3/s (final topographic model configuration)	86
A-33	Velocity contours for a discharge of 60,000 ft^3/s (final topographic model configuration)	87
A-34	Impact pressures for a discharge of 60,000 ft^3/s (final topographic model configuration)	88

APPENDIX A - Continued

Figure		Page
A-35	Velocity contours for a discharge of 140,000 ft^3/s (final topographic model configuration)	89
A-36	Impact pressures for a discharge of 140,000 ft^3/s (final topographic model configuration)	90

PURPOSE

These studies were made to find a means for eliminating the possibility of erosion undercutting the spillway chute structure at Stewart Mountain Dam, Ariz.

RESULTS

1. The undercutting of the chute, which is of immediate concern, is caused by a back eddy that flows over and erodes the poor quality rock in the discharge channel immediately downstream from the spillway. The back eddy results from deflection of the flow by a ridge that exists in the topography.

2. Releasing the flow through selected gates was not effective in controlling the erosion.

3. A divider wall that restricts flows of under 60,000 ft^3/s (1,700 m^3/s) to the right four-ninths of the chute effectively isolates the erosion zone from the flow. Such a wall must be at least 12 feet (3.7 m) high and extend the entire length of the chute.

4. Numerous modifications to the topography downstream from the chute were studied. Several eliminated the back eddy at all discharges. All modifications tested produced high-velocity flows

across, and flow impacts upon, poor-quality rock zones. Such flow conditions would require protective surfacing of these zones.

5. Possible sediment deposits downstream from the modified topography only minimally affected the hydraulic performance.

6. Splitter piers, or some other venting structure, should be installed to allow aeration of the underside of the free jet falling from the chute. Various pier designs were studied and a satisfactory design determined.

APPLICATION

Application of the results of these studies is basically limited to this specific structure. Not only are the results controlled by the spillway geometry, but also by the existing rock surface configuration and the geological features immediately downstream from the spillway. It is, therefore, quite unlikely that other structures exist to which the results of these studies could be directly applied. However, these results may provide initial direction for studies of structures with similar problems.

INTRODUCTION

Stewart Mountain Dam (fig. 1), a facility of the Salt River Project in central Arizona, is located on the Salt River about 30 miles (48 km) east of Phoenix (fig. 2). Completed in 1930 by the Salt River Valley Water Users Association, it is downstream from Roosevelt, Horse Mesa, and Mormon Flat Dams. Stewart Mountain Dam consists of a central arch between massive concrete abutments with gravity sections on each side between the abutments and the sides of the canyon. The height from the streambed to the maximum reservoir water surface level is 119 feet (36.3 m). The purpose of the dam is to provide hydro-power, irrigation storage, and re-regulation of upstream releases.

The spillway (fig. 3), on the left gravity section of the dam, is a 265-foot (80.8-m) wide ogee crest followed by a 450-foot (137-m) long chute. The crest, located at elevation 1506 feet (459 m), is controlled by nine 27-foot (8.2-m) wide by 23-foot (7.0-m) high radial gates. The chute turns through an arc of approximately 32° and at the same time drops from an elevation of 1506 feet (459 m) at the crest to an average elevation of 1475 feet (450 m) at the downstream end. To maintain a uniform water depth across the chute and to minimize side wall height, the chute was superelevated. The maximum discharge capacity of the structure is 140,000 ft^3/s (3,960 m^3/s) with the reservoir water surface at its maximum elevation of 1535 feet (467.9 m). The largest discharge ever passed by the structure is approximately

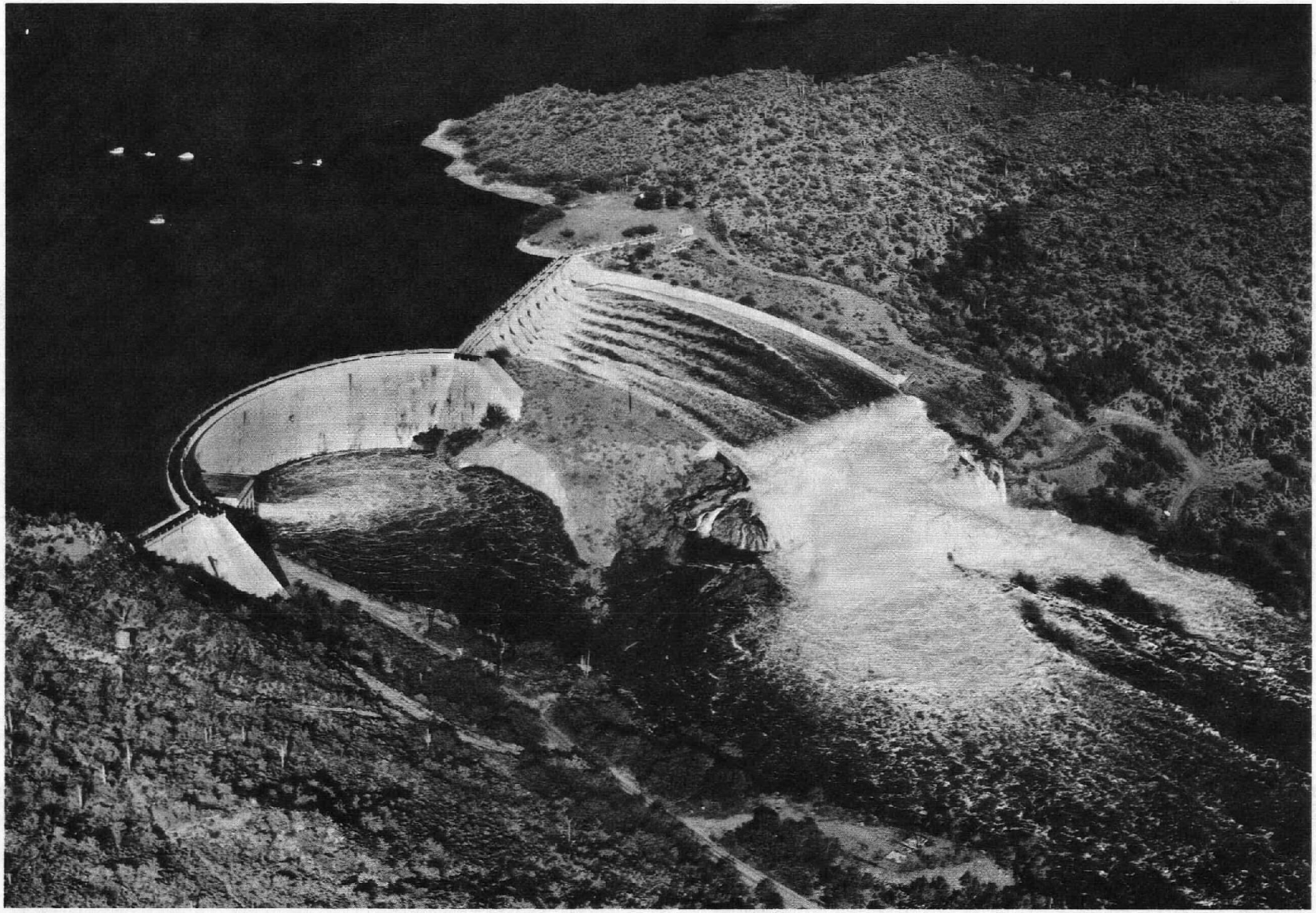

Figure 1. Stewart Mountain Dam and spillway.

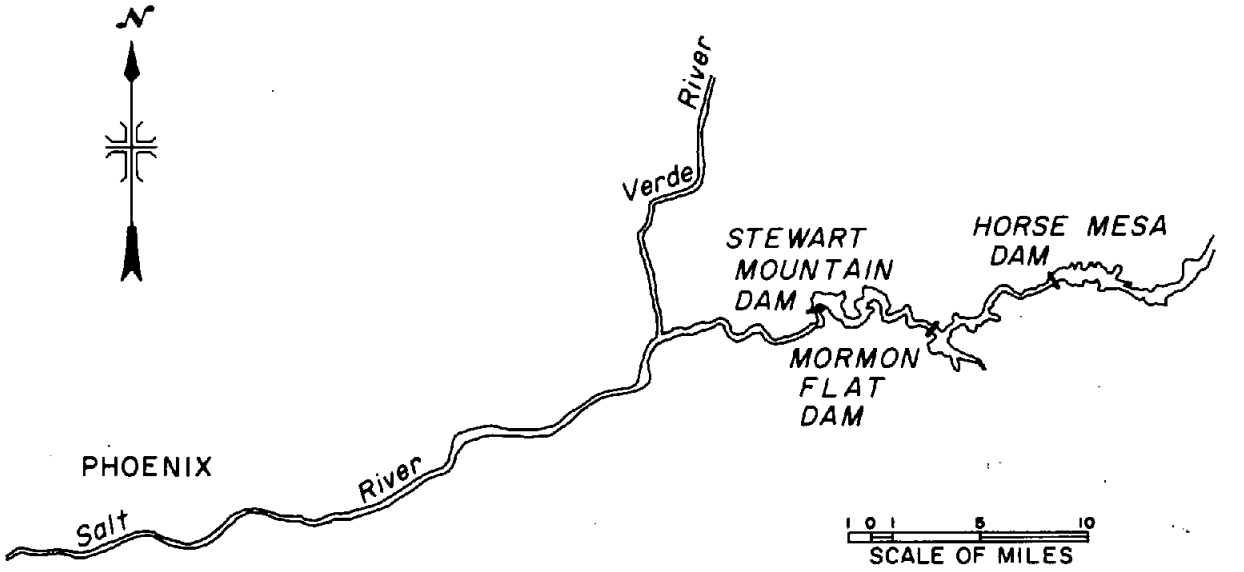

Figure 2. Location map, Stewart Mountain Dam.

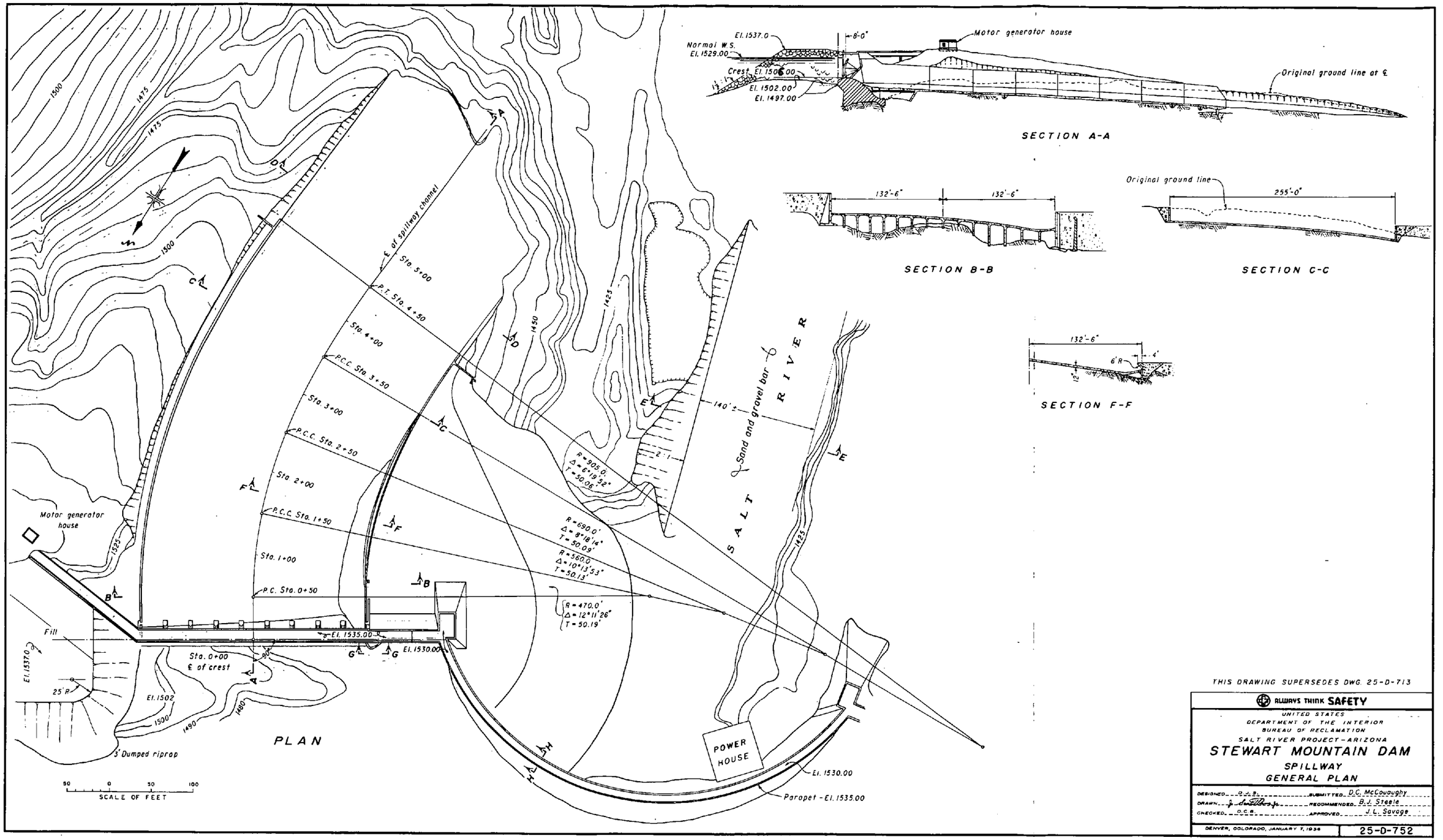

Figure 3. Plan of spillway, Stewart Mountain Dam.

35,000 ft^3/s (991 m^3/s). The structure is, however, usually dry. The 2-year release is approximately 1,000 ft^3/s (28.3 m^3/s). The spillway was originally built (1930) as an ogee crest with no downstream chute. However, because of concern about potential undercutting of the east abutment of the arch dam, the chute was added to the structure in 1936. At that time it was contemplated that erosion downstream from the chute would be negligible once the overburden was removed; also that the rock below the overburden was granite in fairly good condition. Both of these assumptions have since proven false. Not only is the rock in the region jointed, but a major fault (fig. 4) passes through the flow region and under the chute structure. The fault consists of a clay seam with highly fractured rock on both sides. This fault zone is highly susceptible to erosion. Erosion has consequently occurred and has now reached the point where the chute structure is being compromised (fig. 5).

MODEL

After an initial consideration of potential model scales, the scale ratio of 1:72 was selected as being most desirable. This scale was not only considered adequate to yield accurate test results, but also would yield a manageable model size that would fit into an existing model box. Using the existing model box significantly reduced the overall cost of the study. The 1:72 scale resulted in the 265-foot (80.8-m) wide crest

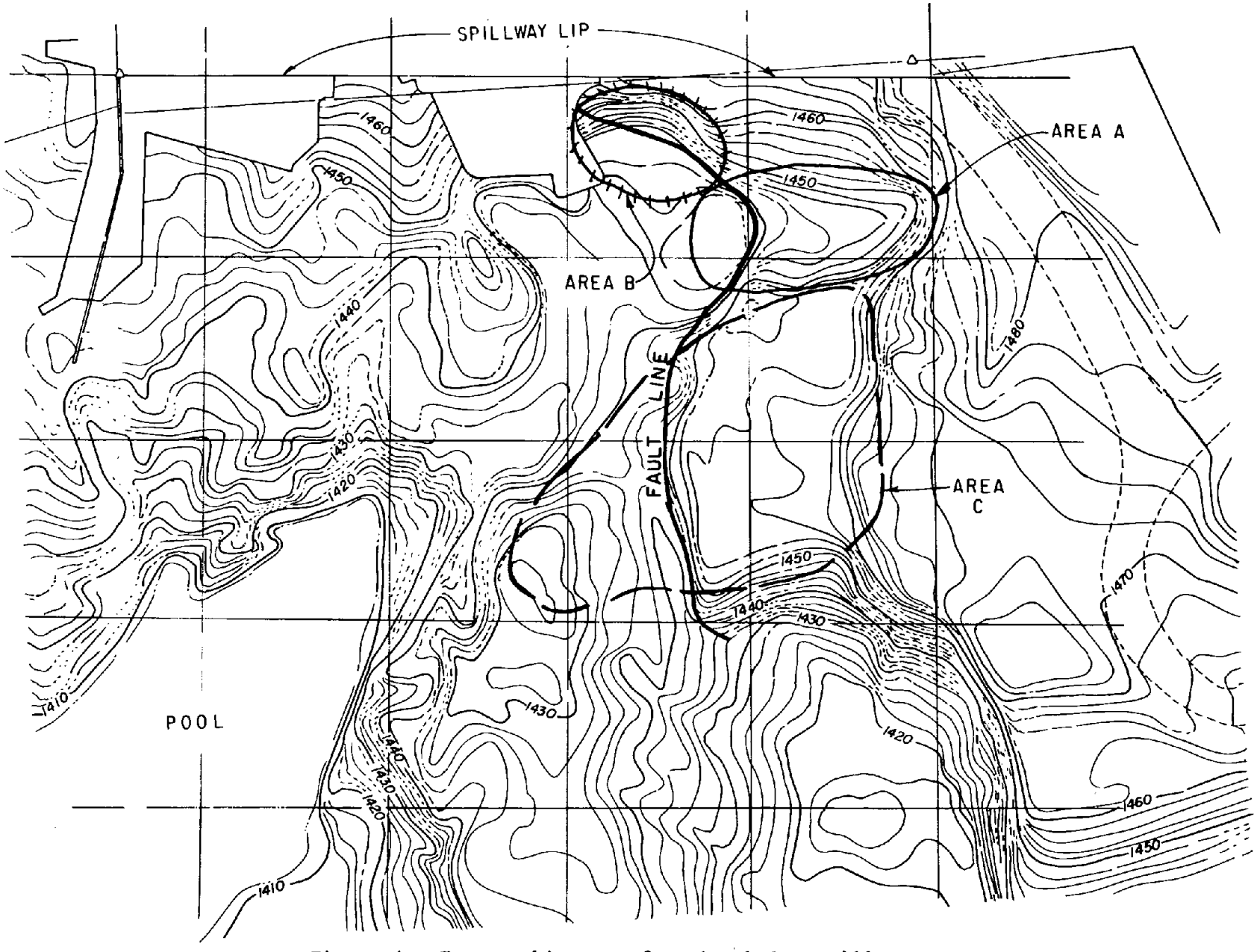

Figure 4. Topographic map of region below spillway.

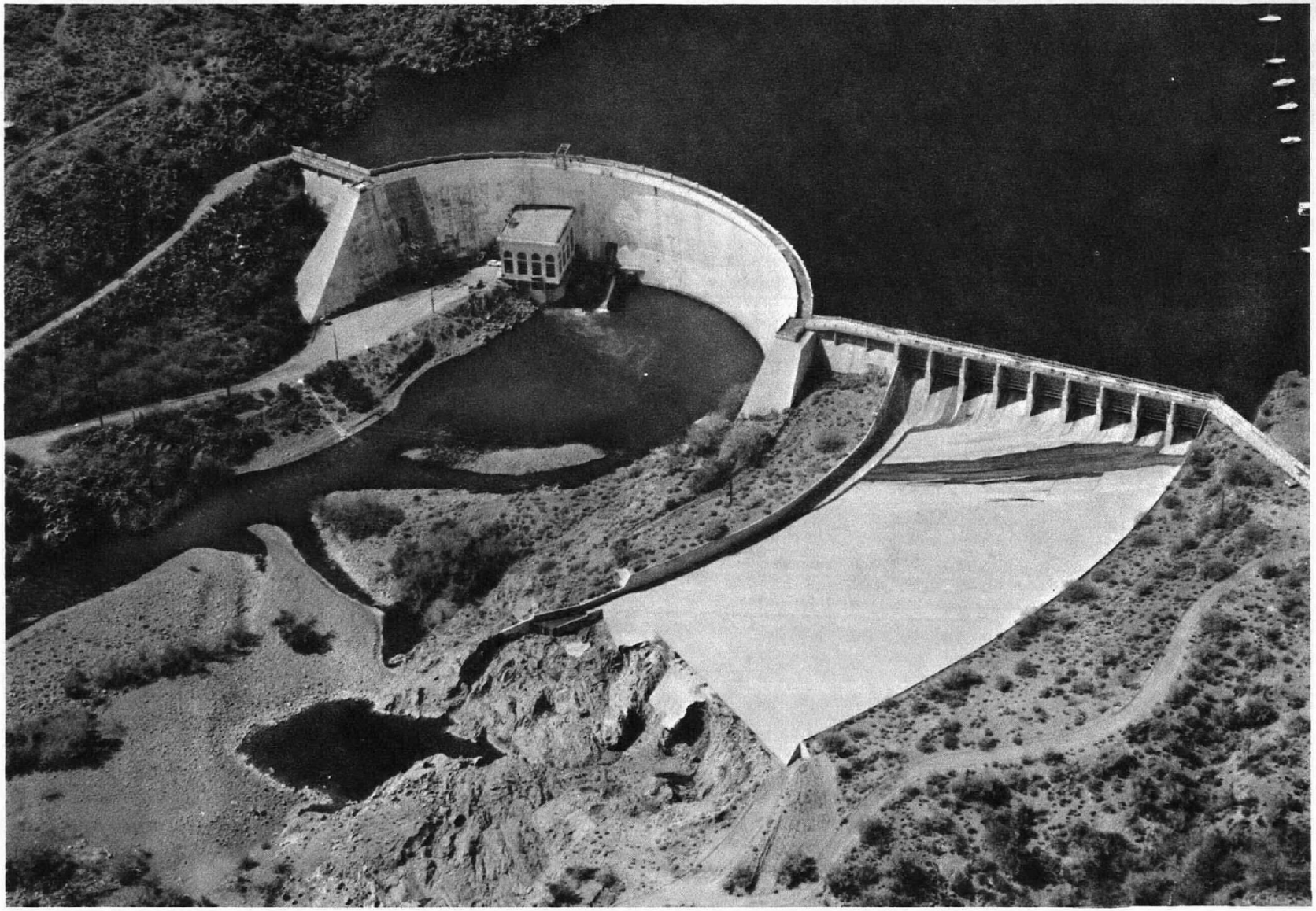

Figure 5. Stewart Mountain Dam and spillway with erosion shown.

having a model width of 3.68 feet (1.12 m). The 450-foot (137-m) long chute had a model length of 6.25 feet (1.91 m) and the 27- by 23-foot (8.2- by 7.0-m) radial gates were modeled by 4.5- by 3.83-inch (11.4- by 9.7-cm) slide gates. The 119-foot (36.3-m) height from the streambed to the maximum reservoir water surface was scaled to 1.62 feet (0.49 m). The maximum discharge of 140,000 ft^3/s (3,960 m^3/s) was modeled by a flow of 3.18 ft^3/s (0.090 m^3/s).

Photographs of the model are shown in figure 6. The slide gates were constructed from sheet metal, the piers were made of plastic, the spillway of a sand and epoxy concrete placed on a sheet metal frame, the box and dam of wood, and the topography of layered styrofoam. Use of the styrofoam in the topography construction had several advantages over previously used wood and concrete construction. It allowed considerably more detail to be placed in the topography. Detail was important in this particular study because of the concern with flow conditions over the poor rock zones and the need for detailed descriptions of the flow patterns. In addition, sections of the topography could be removed with a knife or saw and reattached with glue or wood screws. For this study, where many modifications were made to the topography, this ease of modification was essential. The styrofoam also allowed the placement of piezometers in the topography and, consequently, the direct measurement of impact pressures.

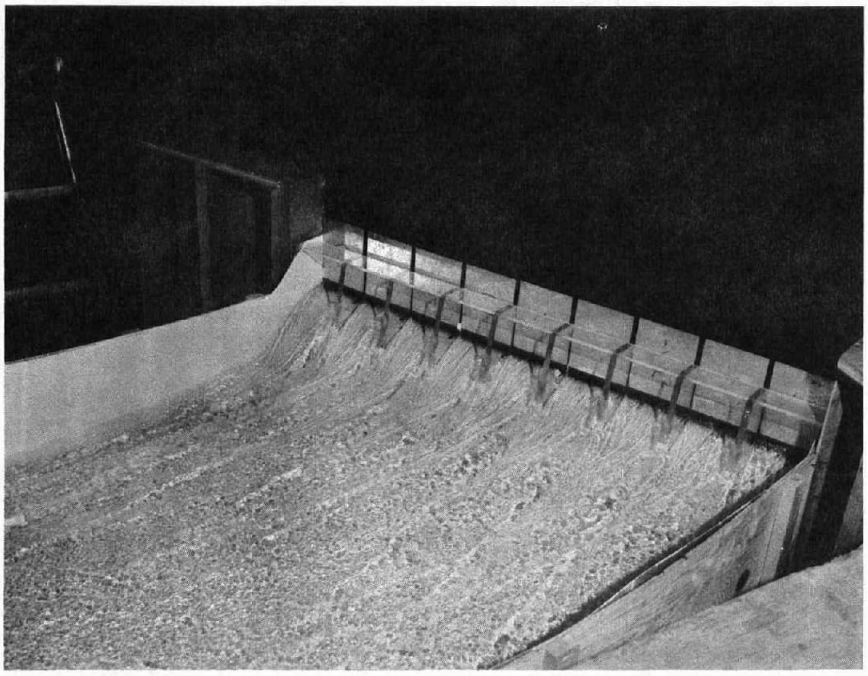

Figure 6. Hydraulic model. Photos P25-D-75889 and P25-D-75890.

Flows through the model were measured with Venturi meters. Water velocities through the model were measured with a Pitot tube. The number of piezometers placed in the topography proved insufficient to yield a complete picture of the impact pressure distribution. Even though 20 piezometers were scattered throughout the critical impact pressure regions, the impact areas were so large, because of both the overall size of the flow area and the changes in the impact areas resulting from changes in the spillway discharge, that they could not be adequately covered by piezometers. Therefore, the majority of the impact pressure data was determined by computing the velocity heads of the components of the flow that are normal to the impact surface. An example of this procedure follows:

Given a flow with a velocity, V, of 60 ft/s (18.3 m/s), passing across a horizontal surface, strikes a 1:4 (horizontal to vertical) slope at an impact angle of 40° (fig. 7).

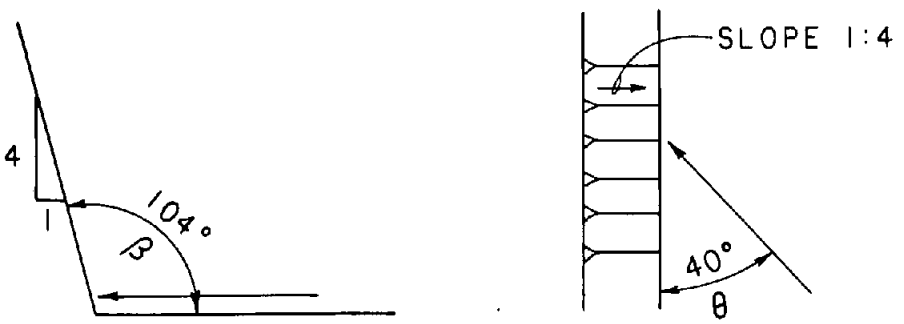

Figure 7. Impact geometry.

The component of the velocity, V_n normal to the impact surface (the 1:4 sloping surface) is:

$$V_n = V \sin \theta \sin \beta$$

$$V_n = (60 \text{ ft/s}) (\sin 40°) (\sin 104°) = 37.4 \text{ ft/s}$$

Where:

104° is the angular equivalent of the 1:4 slope. The impact head, h_v, (velocity head of the component of the flow which is normal to the impact surface) would be:

$$h_v = \frac{V_n^2}{2g}$$

$$h_v = \frac{(37.4)^2}{2g} = \frac{1,400}{64.4} = 21.7 \text{ feet of water}$$

The pressure data obtained from the piezometers were used to verify the computed impact pressures. In general, the piezometers yielded somewhat lower pressures than those computed. In some instances the piezometer pressures were in close agreement with or even higher than the computed pressures. These variations result from the fact that when a jet impinges on a smooth surface, the maximum impact pressure points are usually not clearly defined. There are transitions between the no-impact pressure zones and the full-impact pressure zones. If the piezometer is not in the full- or maximum-impact pressure zone, it would tend to show lower pressures. An impractical number of piezometers would be required to ensure that the maximum pressure is always read. Another complicating factor is that irregularities in the topography

may cause higher or lower impact heads than computed. When land features project into the flow, they expose surfaces that are more normal to the flow than the average impact surface. Therefore, it is possible to develop localized impact pressures considerably higher than computed. The maximum impact pressures that could be developed are equal to the total velocity head of the flow. For example (fig. 7), if the impact surface is normal to the 60-ft/s flow, the impact head, h_v, would be:

$$h_v = \frac{V^2}{2g}$$

$$h_v = \frac{(60)^2}{2g} = \frac{3,600}{64.4} = 55.9 \text{ feet of water}$$

Thus, potentially, pressures of up to 55.9 feet of water could develop even though the mean maximum impact pressure would be 21.7 feet of water. Likewise, when flow surfaces fall away from the flow, the angles of impact become more shallow and lower localized pressures would develop. It is possible that pressures well below atmospheric will occur. Such high- and low-impact pressure development is quite probable in the prototype where flow surfaces will be rough.

THE INVESTIGATION

Two assumptions about the operation of the spillway were applied throughout the testing. The first was that whenever a spill occurs,

the reservoir water surface would be at or near maximum elevation. Therefore, all data taken during this study were collected at the maximum reservoir water surface elevation. The second assumption was that if a spill occurs, all gates would be open an equal amount. This assumption was deviated from only when efforts were made to determine whether better flow conditions could be established by operating specific gates. However, all flow velocity and impact pressure data shown in this report were taken with all gates open an equal amount.

The first step in the model study was calibration of the spillway crest. Because the spillway is assumed to operate with the reservoir water surface at maximum elevation and with all gates open equally, the calibration became an exercise in determining the correct gate opening to pass each discharge. The curve obtained is shown in figure 8.

With the calibration complete, testing began. Flow conditions for the existing spillway and over downstream topography (fig. 4 and App. A, fig. A-1) were observed. The model was operated at discharges of 13,000, 30,000, 60,000, and 140,000 ft^3/s (368,850, 1,700, and 3,960 m^3/s). These discharges were selected for the following reasons:

1. 13,000 ft^3/s (368 m^3/s) is approximately the minimum discharge at which the flow covers the entire chute surface.

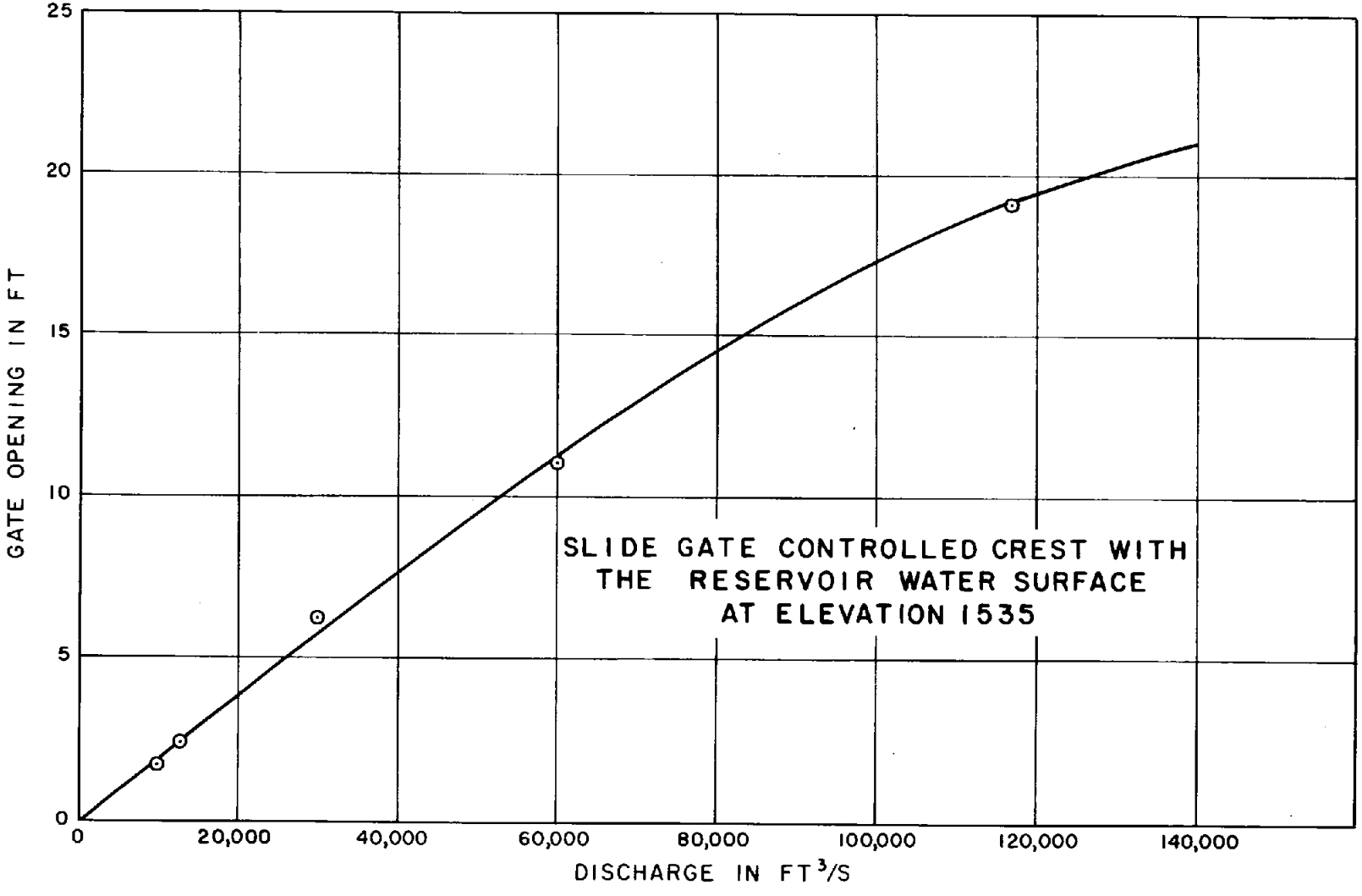

Figure 8. Spillway calibration.

2. 30,000 ft^3/s (850 m^3/s) is an intermediate discharge at which the prototype structure has operated on one occasion.

3. 60,000 ft^3/s (1,700 m^3/s) is a discharge greater than any at which the prototype structure has ever operated. It was the general consensus that this might be the appropriate discharge on which to base the modification design.

4. 140,000 ft^3/s (3,960 m^3/s) is the maximum discharge capacity of the spillway. The likelihood of its occurrence is considered quite small.

It was apparent that the main cause of undercutting of the spillway chute was the trough (area A, fig. 4). A portion of the flow entering the trough and striking either the bottom or the downstream slope of the trough was deflected back towards the chute. This backflow developed a strong eddy action over the fault zone near the downstream lip of the chute (area B, fig. 4). Indications were that the erosion caused by this eddy resulted in the undercutting of immediate concern. Other observed flow conditions for the initial downstream topographic configuration were as follows:

1. At 13,000 ft^3/s (368 m^3/s) discharge (figs. A-2 and A-3), no flow is able to pass over the ridge (area C, fig. 4). Therefore,

all the flow entering the trough (area A) passes down the gully and into the pool. The flow on the right (looking in the direction of the flow) generally passes directly down the slope and into the pool. The velocities observed for this discharge are shown in figure A-2. The eddy over the fault zone near the lip was quite shallow with a weak intensity and did not have sufficient depth for velocity measurement. Flow falling from the chute lip impinged directly on the fault (fig. A-3). As can be seen, there was also a secondary impact slightly downstream along the fault contact line.

2. At 30,000 ft^3/s (850 m^3/s) discharge (figs. A-4 and A-5), a portion of the flow passes over the ridge (area C, fig. 4) and down the channel on the left. A small portion of the flow passes completely over the center rock mass and down the back side; however, a majority of the flow entering the trough passes through the gully and into the pool on the right. Again, the flow from the right side of the chute generally passes directly down the slope and into the pool, and the eddy over the fault zone near the chute lip still occurred. The observed maximum velocity in the back eddy was approximately 14 ft/s (4.27 m/s). The flow entering the trough again impinged directly on the fault zone. Other impact regions that developed along the fault zone downstream from the initial impact point, are shown in figure A-4.

3. At 60,000 ft^3/s (1,700 m^3/s) discharge (figs. A-6 and A-7), the flow entering the trough (area A) impinges directly on the downstream, upsloping section of the trough (fig. A-7). Impact on the upslope results in a steeper angle of attack which in turn results in more water being deflected upstream toward the chute structure. The 60,000 ft^3/s (1,700 c^3/s) discharge caused the most severe back eddy yet observed. The maximum velocity in the back eddy was approximately 26 ft/s (7.9 m/s). It was also noted that even though a larger portion of the flow was deflected into the back eddy, a larger portion of the flow also passed over the ridge and into the left downstream channel. The larger flow over the ridge resulted because the initial impact was at a higher position on the ridge (in some areas nearly to the ridge crest). The flow from the chute still impacted directly on the fault zone. As before, a good portion of the flow passes down the gully and into the pool on the right, and the flow from the right side of the chute generally passes directly down the topography and into the pool.

4. At 140,000 ft^3/s (3,960 m^3/s) discharge (figs. A-8 and A-9), the flow patterns are similar to those for 60,000 ft^3/s (1,700 m^3/s) with two noticeable differences. First, the intensity of the back eddy near the chute had a maximum velocity of 18 ft/s which was less than at 60,000 ft^3/s (1,700 m^3/s), and second, the amount of flow passing over the ridge and into the left channel

was proportionately much larger than had been previously observed. These two conditions result because the flow on the left nearly passes over the trough before it impinges. Thus, a much smaller portion of the flow is deflected back toward the chute and into the back eddy, and a much larger portion of the flow passes over the ridge. Again, the flow from the chute impacted directly on the fault zone.

Based on these observations of the initial flow conditions, efforts were directed toward finding ways to minimize or eliminate the back eddy and the direct impact on the fault zone. Initially, manipulation of operating gates was considered a possible solution. Although there would be little flexibility to manipulate the gates at discharges near the maximum spillway capacity, it was noted that the largest discharge on record could have passed through three of the nine gates. It was thought that by selecting the correct gates, the flow could be generally concentrated on the right side of the chute. Thus, the flow leaving the chute would not enter the trough, form the back eddy, nor come in contact with the fault. Many combinations of operating gates were tried for discharges ranging from 10,000 to 60,000 ft^3/s (283 to 1,700 m^3/s). Very little improvement could be noticed. The length and the curvature of the chute were such that for almost any combination of operating gates the flow was evenly spread by the time it reached the end of the chute. Actually it was observed that at

lower discharges (below 10,000 ft^3/s or 283 m^3/s), uniform operation of the gates tended to concentrate the flow to the right side. This occurred because the thinly spread flow is quite susceptible to friction losses on the chute, which reduces the flow velocity and increases the effect of the superelevation on the flow. The superelevation pulls the flow to the right.

A second modification was the placement of a flip structure at or near the end of the chute. Two basic flip structure configurations were considered. Performance of the flips were evaluated visually and no physical measurements of the flow conditions were made. One configuration (fig. 9) consisted of a series of wedge-shaped blocks that were oriented so that the flow was deflected farther downstream and to the right. Generally, for the blocks to significantly deflect the flow to the right, their height and size must be quite large (5 feet (1.52 m) high and 10 to 15 feet (3.0 to 4.6 m) long or longer). Even with this size blocks, moderate and large discharges climbed the blocks and passed downstream with only a small deflection (fig. 10). Discharges above 20,000 ft^3/s (566 m^3/s) had too much mass, velocity, and total momentum to be easily turned. The smaller discharges were turned through greater angles, but because their trajectory lengths were short, displacement of the flow to the right was still relatively small. The second configuration considered was a solid triangular sill that ran the complete length of the

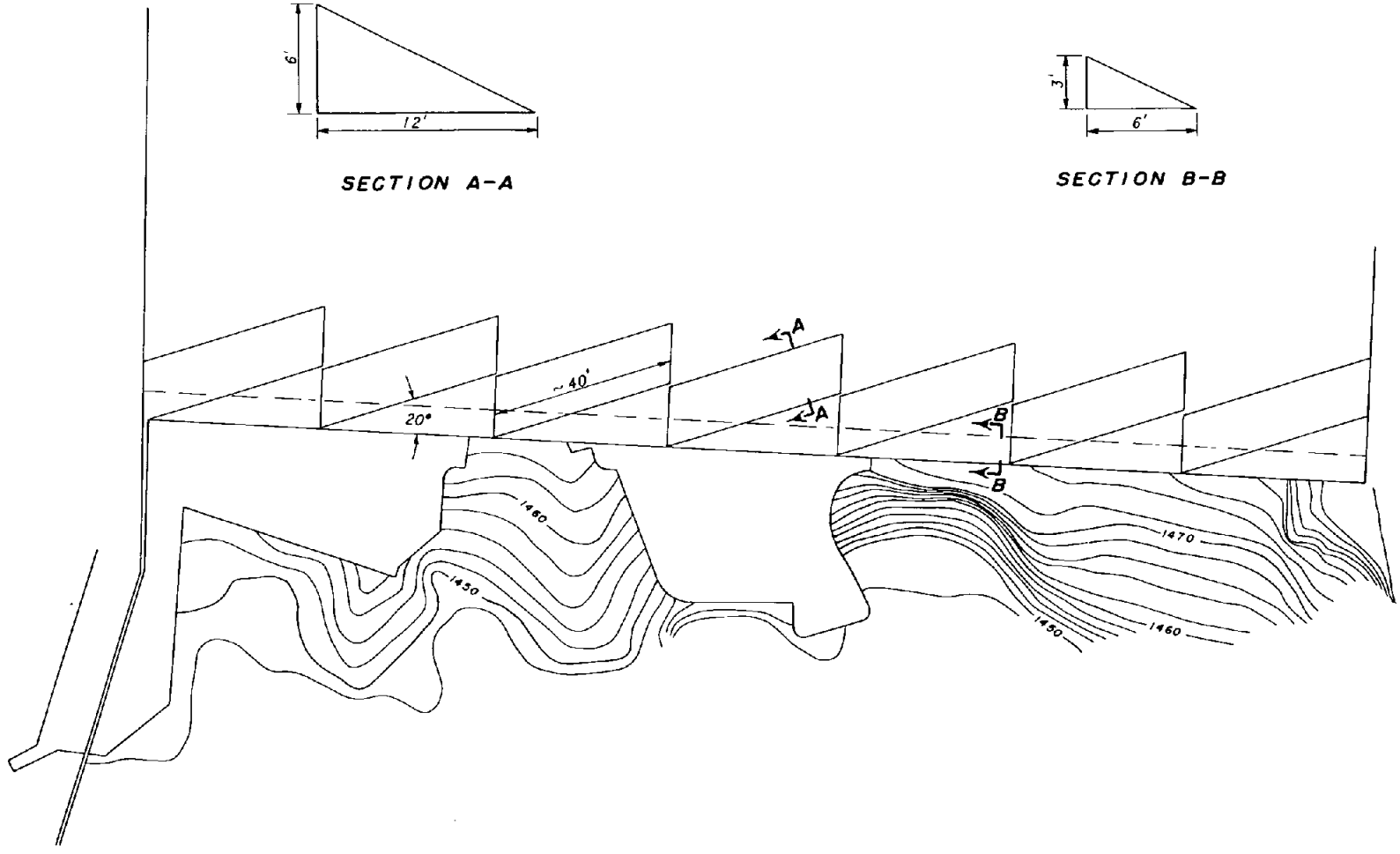

Figure 9. Drawing of flip structures.

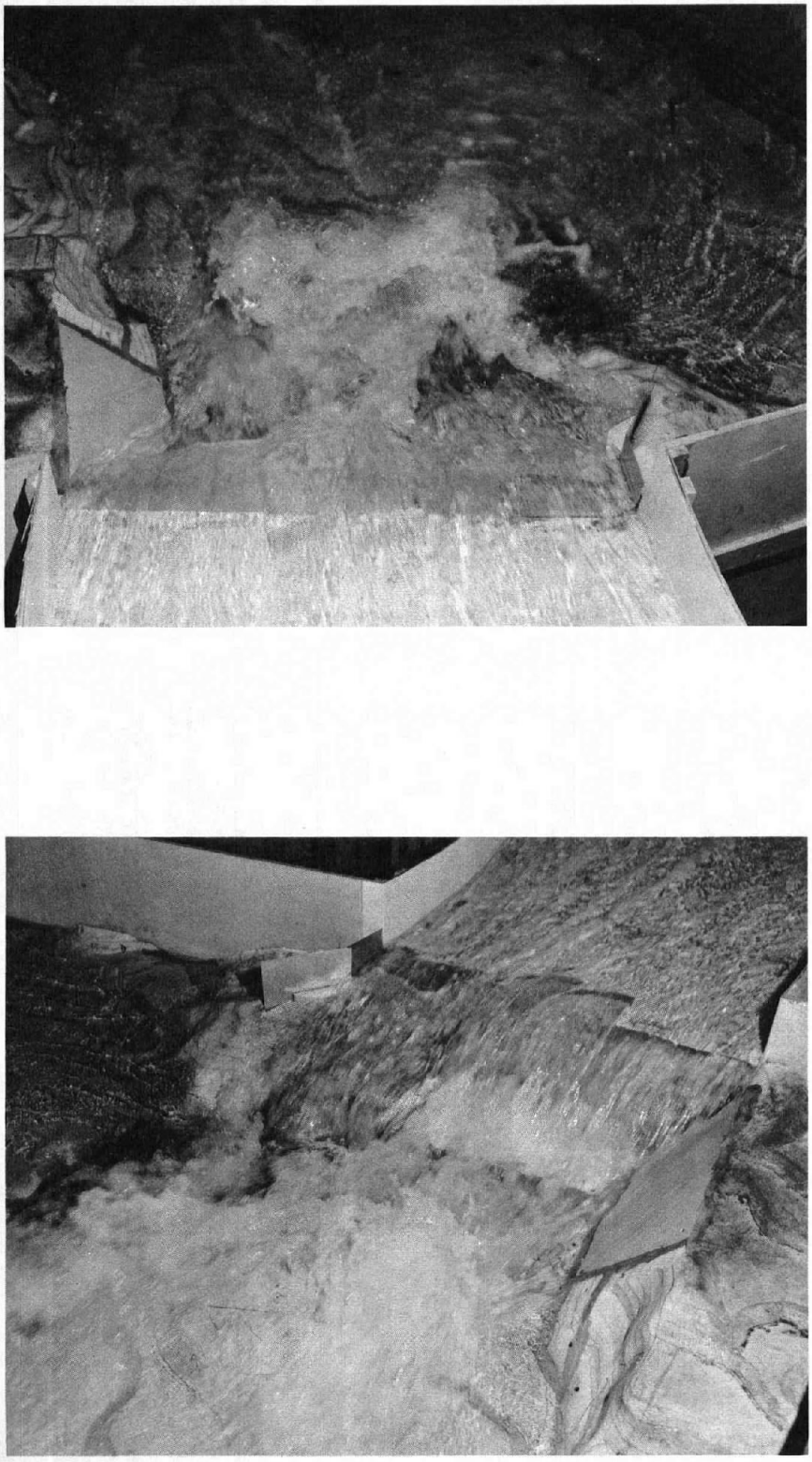

Figure 10. Operating toothed flip. Photos P25-D-75891 and P25-D-75892.

chute lip (fig. 9). This configuration did not deflect the flow to the right (fig. 11), but both the toothed and solid flip structures do throw the flow farther downstream. This resulted in the impact zones being moved father away from the chute structure for any given discharge. Shifts in the location of the impact zone generally ranged between 10 and 20 feet (3.0 and 6.1 m) and did not significantly improve the flow conditions. Because an entire range of discharges was considered in the model test, the flow still impacted over the same surfaces. It should also be noted that because the elevation drop from the chute lip to the rock is basically fixed, the vertical component of the velocity that results from the drop is also relatively constant. The angle of impingement is, in most cases, somewhat steeper but not greatly changed by the flip structure. The result with either flip configuration is flow patterns that are similar to patterns observed without the flip structures. The impact and flow velocity conditions across the poor quality rock were not significantly improved.

A divider wall along the length of the chute was also tested. The wall, which was nearly 12 feet (3.7 m) high, was parallel to the side walls and isolated operation of the first four gates on the right from the rest of the chute (fig. 12). The wall made it possible to operate the spillway at discharges of up to nearly 60,000 ft^3/s (1,700 c^3/s) and yet have the flow passing over only the right 44 percent of the chute. Flow over the topography was limited to the

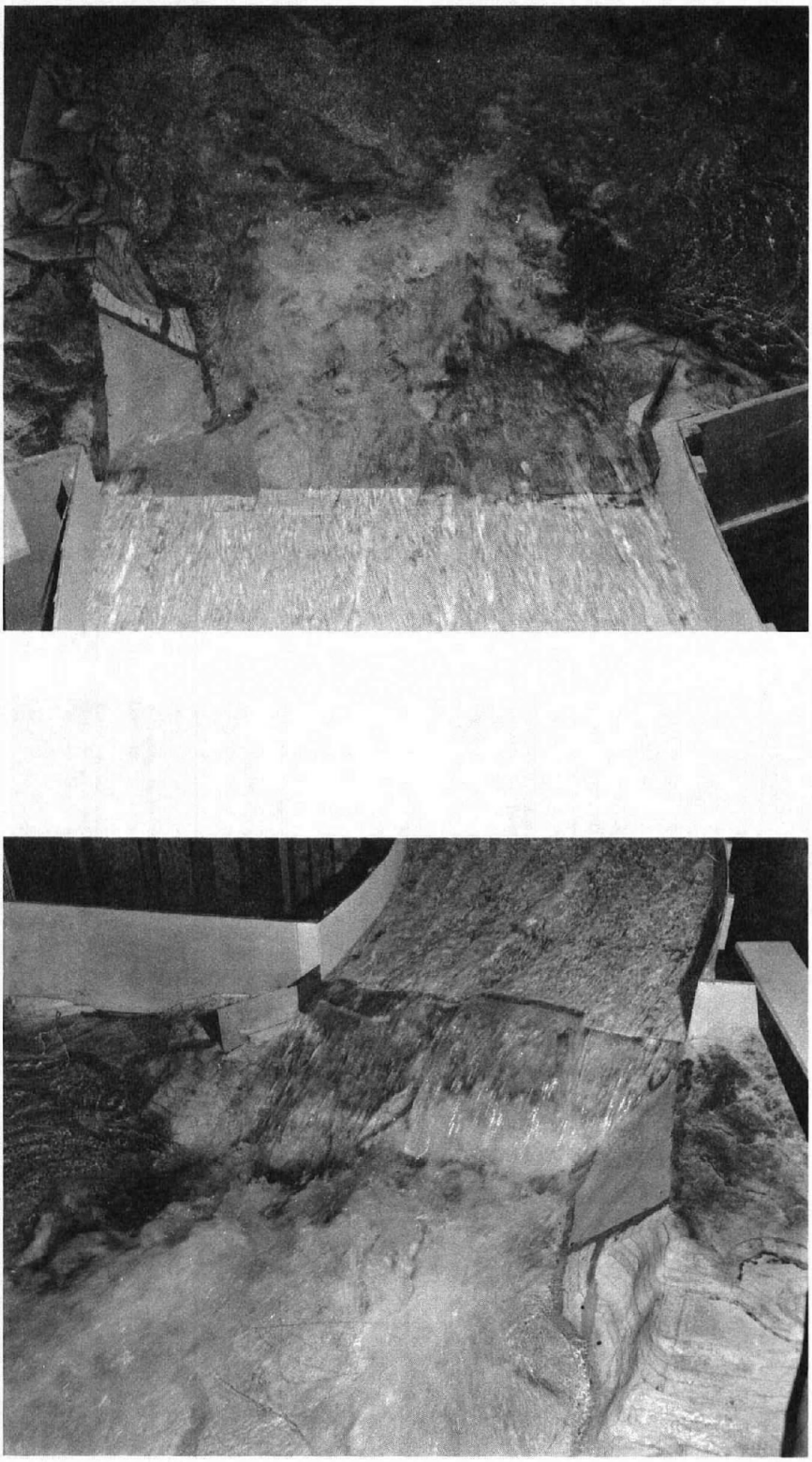

Figure 11. Operating solid flip. Photos P25-D-75893 and P25-D-75894.

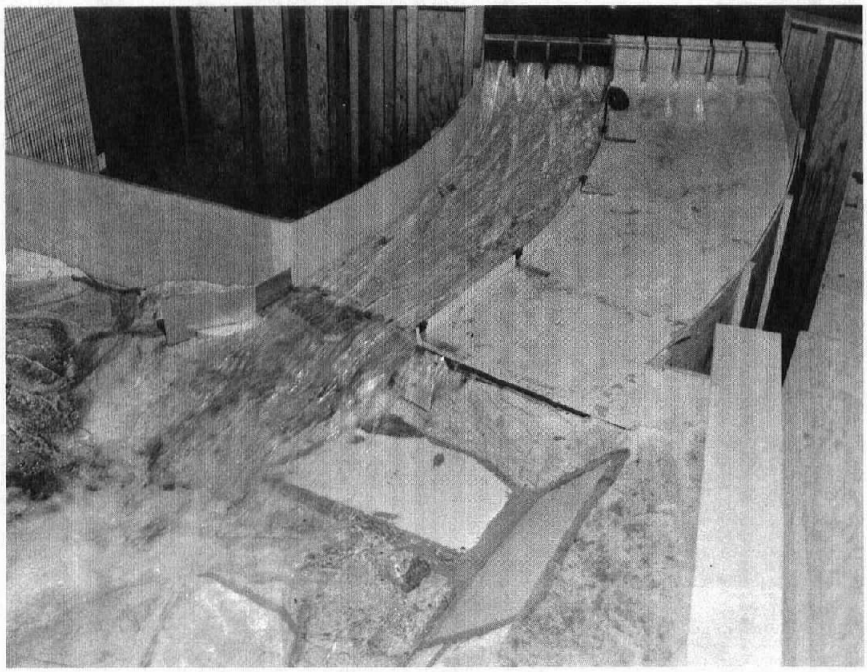

Figure 12. Divider wall. Photo P25-D-75895.

stable rock surfaces on the right side. Thus, there was no flow in the trough, no back eddy, and no flow over the fault. Attempts were made to shorten the wall by terminating it somewhat upstream of the chute lip. Minor reductions in the wall length (30 or 40 feet (9 to 12 m)) significantly reduced the wall's effectiveness. Where the wall ended, the flow would start to spread across the chute. The model study indicates that a wall extending the entire length of the chute is most effective and offers a potential solution to the erosion problem.

Attention was next shifted to possible excavation of the topography below the chute as a means of improving the flow conditions. The first modification considered is shown in figure 13. This arrangement was selected because by opening up the left side of the topography (removing the ridge), the flow would be allowed to move freely away from the chute structure. Thus, the flow would not be deflected back toward the chute structure and the back eddy would be eliminated. The particular shape of the cut was selected to conform with existing slopes in the topography to minimize excavation. Note that the location of the fault, through the cut zone (fig. 13), is only an estimate. The location was determined by using the existing surface contact line for the fault and the geologist's evaluation of the fault plane dip.

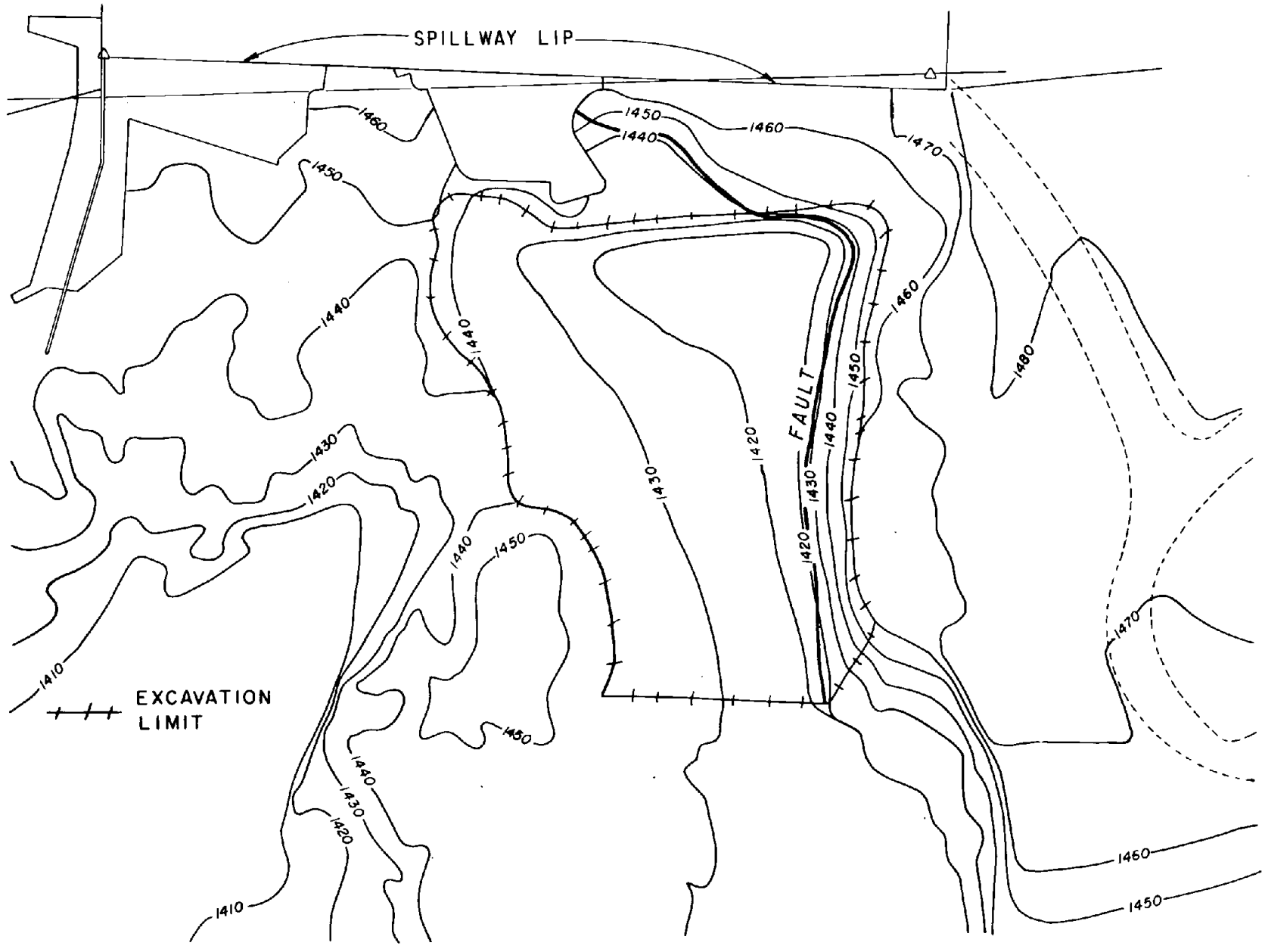

Figure 13. First topographic model modification.

The resulting flow conditions observed are shown in figures A-10 through A-18. Major flow conditions were:

1. The intensity of the back eddy was significantly reduced by the modification. At a discharge of 10,000 ft^3/s (283 m^3/s), no back eddy was observed. At 60,000 ft^3/s (1,700 m^3/s), the maximum velocity in the back eddy had been reduced from 26 to 15 ft/s (8.0 to 4.6 m/s).

2. In the excavated region, the fault contact line lies on a steep surface. Thus, water falling from the chute impinges on the fault with a shallow angle of attack. Assuming a smooth surface along the fault, the impact pressures that develop would be relatively small.

3. For discharges up to 40,000 ft^3/s (1,130 m^3/s), the V-shaped valley near the downstream end of the cut is a control point that forces formation of a hydraulic jump in the upper reaches of the excavated zone. For discharges greater than 40,000 ft^3/s (1,130 m^3/s), the flow swept out of the excavated zone. This indicates that for the discharges below 40,000 ft^3/s (1,130 m^3/s), there is potential for erosion and ball-mill type action in the upper reaches of the excavated zone. On the other hand, significant energy dissipation in the hydraulic jump resulted in reduced flow velocities and reduced erosion potential downstream.

A second topographic modification studied is shown in figure 14. The main objective of this modification was the same as for the previous one; that is, to open up the downstream topography so that the flow could move freely away from the chute. The left flow boundary was moved farther to the left to reduce the control by the downstream portion of the cut. The upstream or nose portion of the center rock mass was streamlined to reduce its resistance to the flow. In addition, the 4:1 (horizontal to vertical) sloping plane in the upstream portion of the cut was added. The plane acts as a deflection surface that cleanly turns the flow downstream with a minimum of turbulence. Thus, there is less potential for ball-mill type of erosion which may result from the turbulence. The roller behind the impinging flow was also reduced, which reduces the potential for the flow to form a back eddy. The sloping surface also reduces the impingement angle of the flow on the rock, thus, reducing the average magnitude of the impact pressures that occur. It should be added that the length of the slope was selected to satisfactorily intercept the free jet for discharges of up to 140,000 ft^3/s (3,960 m^3/s). The slope of the plane was controlled by the toe elevation of the plane and the desire to keep the sloping plane all in cut. The toe elevation is approximately the elevation of the flood plain. The alternative to keeping the 4:1 plane entirely in cut would be a combination fill-and-cut arrangement. Mass concrete would probably have to be used for the fills, which would be

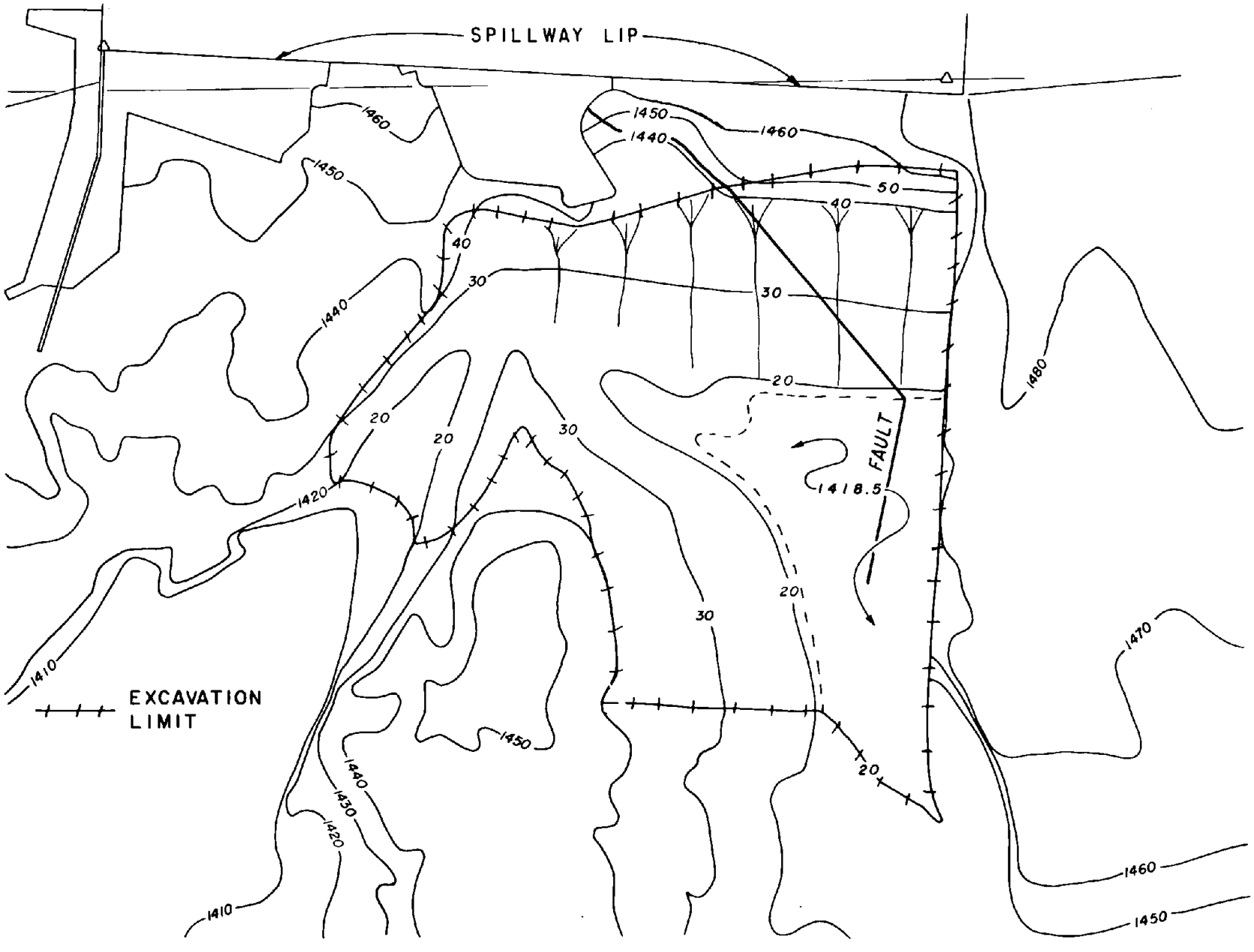

Figure 14. Second topographic model modification.

quite expensive. Although a fill-and-cut arrangement offered a potential solution to the problem, it was considered economically infeasible to pursue in the model study.

The flow conditions observed for the modification shown in figure 14 are shown in figures A-19 to A-27. Major points are:

1. No back eddies were observed over the fault zone near the chute structure for any discharge.

2. The estimated location of the fault zone crosses the 4:1 sloping impact plane, resulting in nearly direct impact on the fault. This impact occurs for all but the smallest discharges.

3. Hydraulic jumps still occurred near the toe of the sloping plane for discharges of up to approximately 40,000 ft^3/s (1,130 m^3/s). The hydraulic jumps resulted from both friction losses and from the increased tailwater depth caused by the crossing flow that comes off the nose of the center rock mass. It should be noted that because of the length of the impact slope, the hydraulic jumps are farther from the chute with this modification than they had been with the initial modification.

One of several intermediate modifications that were considered is shown in figure 15. As can be seen, not only has the left rock mass been

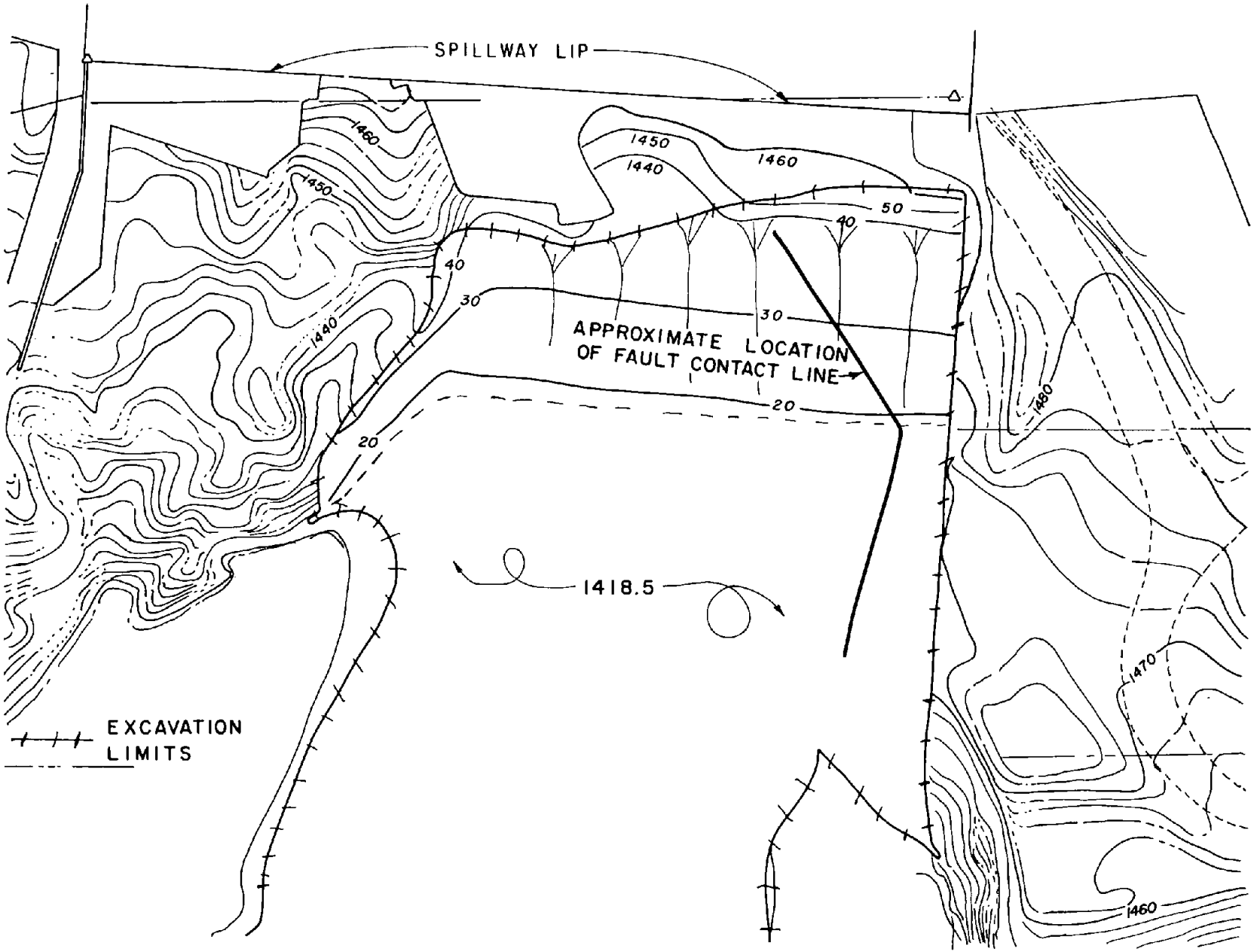

Figure 15. Intermediate topographic model modification.

removed, but also all the center rock mass. The shape and location of the impact slope were determined in a similar manner to the previously discussed modification. As would be expected, the flow at all discharges swept out onto the horizontal plain and then formed a hydraulic jump. The position of the jump depended on the discharge. The larger the discharge, the farther downstream the jump. Again, the estimated fault location crosses the impact slope and, thus, direct flow impact occurred on the fault. No back eddies were observed near the chute structure.

The final modification considered, shown in figure 16, is similar to the previous modification (fig. 15) except for two changes. First, a portion of the center rock mass has been left in place. Observations indicate that this rock mass has very little effect on the flow conditions near the toe of the impact slope. There is violent hydraulic action around this rock mass at high discharges, which probably will erode the rock mass with time. However, such erosion probably will not progress upstream and endanger the chute structure. In addition, the left cut slope was changed from a vertical to a 1:1 slope. The main reason for this change was to establish a slope that could feasibly be excavated. The 1:1 slope turned the flows passing over it to the right. Thus, flow concentrations were created at the intersection of the 4:1 and 1:1 slopes. Also, at higher discharges, flow passed from the 1:1 slope to the horizontal surface with a significant component of velocity to the right. This resulted in a diagonal

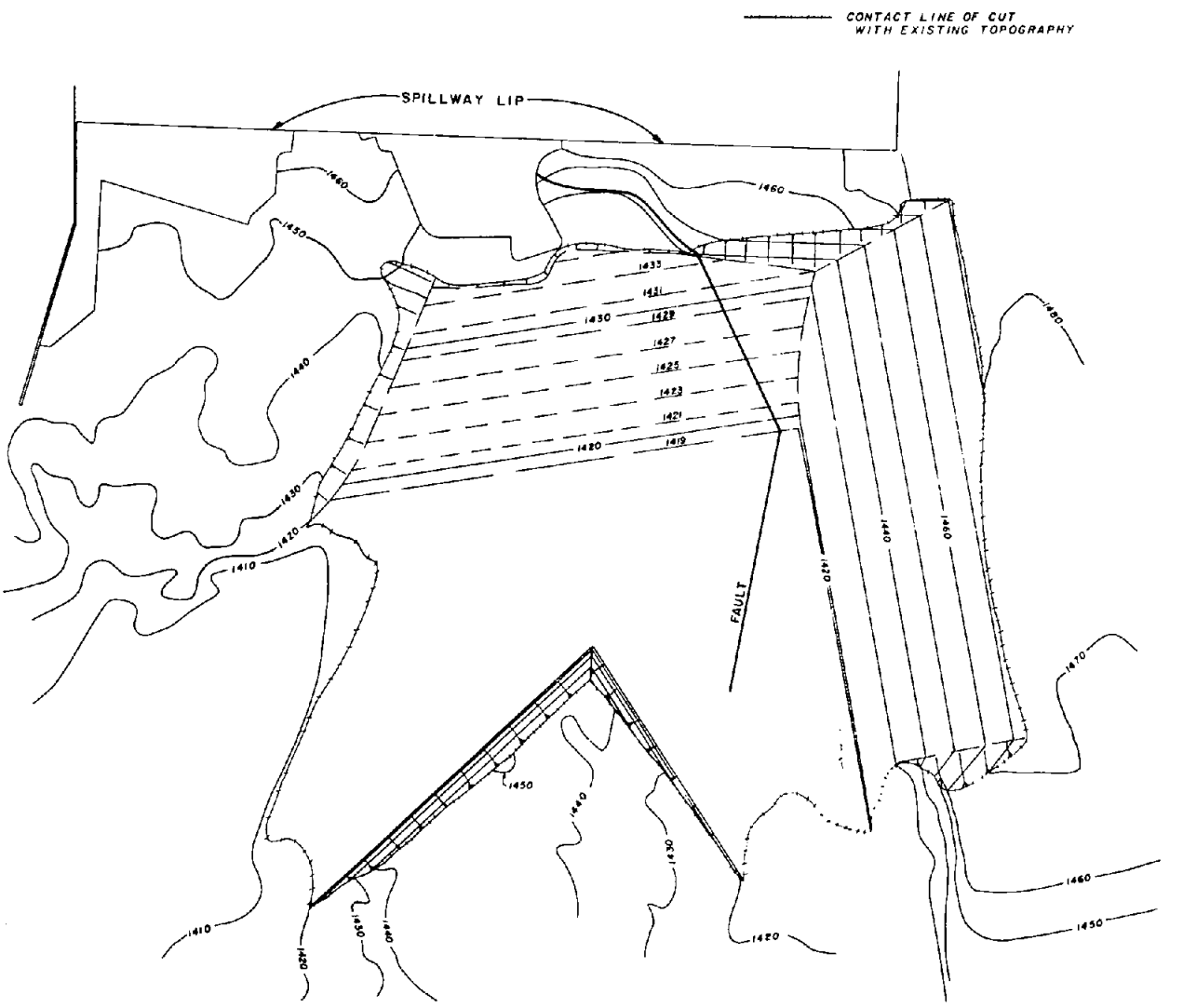

Figure 16. Final topographic configuration with protective surfacing.

crossflow that interacted with the main flow on the horizontal plane and created additional flow concentrations and established a small additional velocity component to the right in this localized section of the horizontal flow.

Figures A-28 to A-36 show the flow conditions that were observed for this final modification. Again, data were taken at discharges of 13,000, 30,000, 60,000, and 140,000 ft^3/s (368, 850, 1,700, and 3,960 m^3/s). As stated earlier, most of the impact pressures shown were computed from measured flow velocities and angles of deflection. These computed pressures (in feet of water) are shown as circled numbers (figs. A-30, A-32, A-34, and A-36). In addition, pressures were also measured, where possible, with piezometers placed in the topography. These measured pressures (in feet of water) are shown inside squares (figs. A-30, A-32, A-34, and A-36).

For the final modification with a discharge of 13,000 ft^3/s (368 m^3/s), there was very little flow on the left 1:1 cut surface. The flow from the chute impinged either on the existing ground surface on the right or on the upper portion of the 4:1 impact plane. At this discharge, the spillway superelevation significantly affects the flow concentrations on the chute. The flow on the right was significantly heavier than the flow on the left. The position of the hydraulic jump as shown (fig. A-29) was quite unstable, and variations in flow surface

roughness could cause significant shifts. It should be noted that the jump was relatively small and that the farthest it could ever locate upstream would be at the toe of the 4:1 slope. Even though there is very little flow over the 1:1 slope, the flow on the 4:1 slope is directed somewhat to the right. The redirection resulted generally from the orientation of the 4:1 impact plane with respect to the chute. A tendency toward the redirection exists at all discharges. At the higher discharges, the flow from 1:1 slope intensifies the redirection and causes flows to impinge a bit more directly on the left side of the center rock mass, developing somewhat higher impact pressures. The flow separation along the left boundary is also a result of the redirection. The maximum velocity observed in the back eddy in this separation zone was 4 ft/s (1.2 m/s), (fig. A-29).

Observed and computed impact pressures for the 13,000 ft^3/s (368 m^3/s) discharge are shown in figure A-30. As can be seen, there are four major zones where impact pressures were noted. One is the impact line along which the flow falling from the chute impinges. The greatest impact pressures observed were along this line. The small impact pressures on both ends of this zone resulted from the somewhat shallow angles of impingement that occur in these areas and from the relatively small vertical drop that the flow passes through to these impact areas. Throughout the middle of this impact zone, rather steep angles of impact occur. This is especially true in the region just to the right

of the center concrete mass. In this region the flow strikes the upstream slope of the ridge at a very steep angle and, consequently, a very large portion of the total velocity head is converted to impact pressure. Across the 4:1 impact slope, moderately steep impingement angles (45° to 50°) were noted, but the flow has dropped 40 feet (12.2 m) from the chute lip and the total velocity head of the flow is quite high, resulting in the high impact pressures noted. In addition, impact pressures were observed at the upstream end of the 1:1 slope where the flow off the steeper slopes is deflected, at the toe of the 4:1 slope where the flow is turned to the horizontal, and on the nose of the center rock mass. Some low average impact pressures were observed at the toe of the 4:1 slope, even though the velocity of the flow was quite high because of the flat angle through which the flow was deflected.

At 30,000 ft^3/s (850 m^3/s), the flow conditions shown in figures A-31 and A-32 were observed. Generally, the pattern is similar to that observed at 13,000 ft^3/s (368 m^3/s). A larger flow across the 1:1 slope, in turn causes a larger flow concentration at and downstream from the intersection of the 4:1 and 1:1 slopes. This flow concentration results in the higher velocity region shown. In addition, the higher velocities and the heavier flow moved the hydraulic jump farther downstream. On the left, the jump moved to a position downstream from the center rock mass except for the small region at

the nose of the separation zone. As can be seen in figure A-31, all velocities have increased considerably from those at 13,000 ft^3/s (368 m^3/s). Likewise, as shown on figure A-32, the impact pressures have also increased. The impact pressure distributions have a similar pattern to those observed at 13,000 ft^3/s (368 m^3/s), except that the initial impact line has shifted downstream. It should be noted that an impact zone is created when the flow turns from the 1:1 slope to the horizontal. Both computed and measured impact pressures are indicated on figure A-32.

At 60,000 ft^3/s (1,700 m^3/s), flow patterns were again similar to the previous discharges. Velocities were somewhat higher, and this, coupled with the heavier flow, resulted in the hydraulic jumps being moved even farther downstream. The maximum velocity in the back eddy of the separation zone on the left was somewhat lower (fig. A-33). The impact pressure zone distribution was similar to those previously observed except that the initial impact zone was shifted farther downstream (fig. A-34). This shifting occurs because the flow leaving the chute has a higher velocity, which causes the free jet to carry farther downstream before it impinges. Observed impact pressures were again higher than for the previous discharges.

At 140,000 ft^3/s (3,960 m^3/s), the flow patterns were again similar to that observed at the lower discharges. The hydraulic jump on the

right (fig. A-35) is confined to the deeper water of the pool. The position and size of the separation zone on the left is approximately the same as for the 60,000 ft^3/s (1,700 m^3/s) discharge. The flow velocities (fig. A-35) and measured impact pressures (fig. A-36) had increased.

Some generalized observations can be made about the flow across the final modification. First, because the estimated location of the fault zone crosses the 4:1 impact plane, there is direct impact on the fault zone over the full range of discharges. The average impact pressures increase with discharge from 9 feet (2.7 m) of water at 13,000 ft^3/s (368 m^3/s) to 35 feet (10.7 m) of water at 140,000 ft^3/s (3,960 m^3/s). These pressures are more than enough to cause hydraulic jacking in jointed rock. Second, the estimated fault contact location is such that high-velocity flows will pass over the fault for most discharges. The velocities increase with discharge from approximately 40 ft/s (12.2 m/s) at 13,000 ft^3/s (368 m^3/s) to 70 ft/s (21.3 m/s) at 140,000 ft^3/s (3,960 m^3/s). Third, a high-velocity region with corresponding higher impact pressures exists from approximately the middle of the 4:1 impact slope, downstream. This higher velocity region was an extension of a flow concentration that tended to occur in the center of the spillway chute. Velocities in this region were about 5 ft/s (1.5 m/s) above the average velocities across the slope. Fourth, the flow separation on the left occurred for all discharges

observed. At discharges above 30,000 ft^3/s (850 m^3/s), the maximum velocity of the back eddy within this separation stabilized at a value between 10 and 13 ft/s (3.0 and 4.0 m/s). The separation was primarily caused by the spillway chute orientation with respect to the 4:1 and 1:1 slopes. To determine the effect of the center rock mass on the separation, the rock mass was removed and the model was operated. The flow separation and back eddy still existed for all discharges; however, the maximum velocity in the back eddy was reduced about one-third by the removal of the rock mass. Fifth, over the entire discharge range, no back eddy was observed in the region near the fault zone immediately downstream from the chute. This is the region where the chute structure is now being threatened. This major objective of the study was considered satisfied by the modification. Sixth, the flow moved directly and smoothly away from the immediate vicinity of the chute structure for all discharges observed.

Concern was expressed about the possible effects of downstream rock or debris deposits on the hydraulic performance in the vicinity of the cut. It was found that a massive blockage of the left channel less than 250 feet (76.2 m) downstream from the end of the cut would cause an increase in the tailwater level on the left side. For higher discharges (above 20,000 ft^3/s), the flow separation zone did not move measurably upstream even though the depth of water was increased. At small discharges, however, the increased tailwater

depth would cause the hydraulic jump to move closer to the toe of the 4:1 slope. Likewise, a massive blockage, to the water surface and 100 feet long normal to the flow, downstream of the pool on the right caused the hydraulic jump on the right to advance upstream. The blockages placed in the model downstream and on both sides were probably more massive than anything that could conceivably occur in the prototype. In addition, the resulting hydraulic actions from the blockages were not considered severely detrimental.

After the final modification was evaluated, two other points of concern were raised. The first was that the intersection of the 4:1 and 1:1 slopes would not be excavated as a sharp corner, but instead would probably be more rounded. The intersection was built with a 20-foot (6.1-m) radius fillet, and the model was tested again. No appreciable differences in the flow conditions were noted.

Once the flow covers the entire chute surface, the region behind the free jet nappe is sealed off from the atmosphere. When such a condition occurs, negative pressures will develop under the jet nappe. The negative pressures occur because air in the sealed-off region is entrained by the water and carried away. Because there are no openings through which the air can be replenished, a partial vacuum develops. Such negative pressures would cause additional uplift loadings on the rock and on any protective surfacing that was placed

on the rock. To relieve this condition, some type of venting was desirable. Splitter piers, or piers that divide the flow and create openings through which aeration can occur, were studied in the model. Because the end of the chute is cantilevered, any pier used would have to be attached approximately 8 feet (2.4 m) upstream from the chute lip. Figure 17 shows some of the pier shapes considered. Initially, shape (a) was tested and performed well for all discharges up to 60,000 ft^3/s (1,700 m^3/s). The pier cleanly and stably separated the flow with a minimum amount of flow disruption. The pier height, 7 feet (2.1 m), was the limiting performance factor at discharge above 60,000 ft^3/s (1,700 m^3/s). At this discharge, the piers were overtopped. Once overtopped, the piers could no longer separate the flow and their effectiveness was lost. To be effective at discharges of 140,000 ft^3/s (3,960 m^3), the required height of the piers would be 15 feet (4.57 m). Attempts were made to find a compact-shaped pier that would be more structurally desirable. Pier (e) seemed to be nearly satisfactory structurally and seemed to function well in that it separated most of the flow cleanly with little disruption. However, a shallow flow would close behind the pier and seal the opening. At lower discharges (below 20,000 ft^3/s or 566 m^3/s), pier (d) functioned in a similar manner to pier (e). The majority of the flow was separated, but a shallow flow closed behind the pier. At higher discharges, pier (d) successfully separated the flow, but also caused severe finning and flow disruption. It seemed conceivable that the major

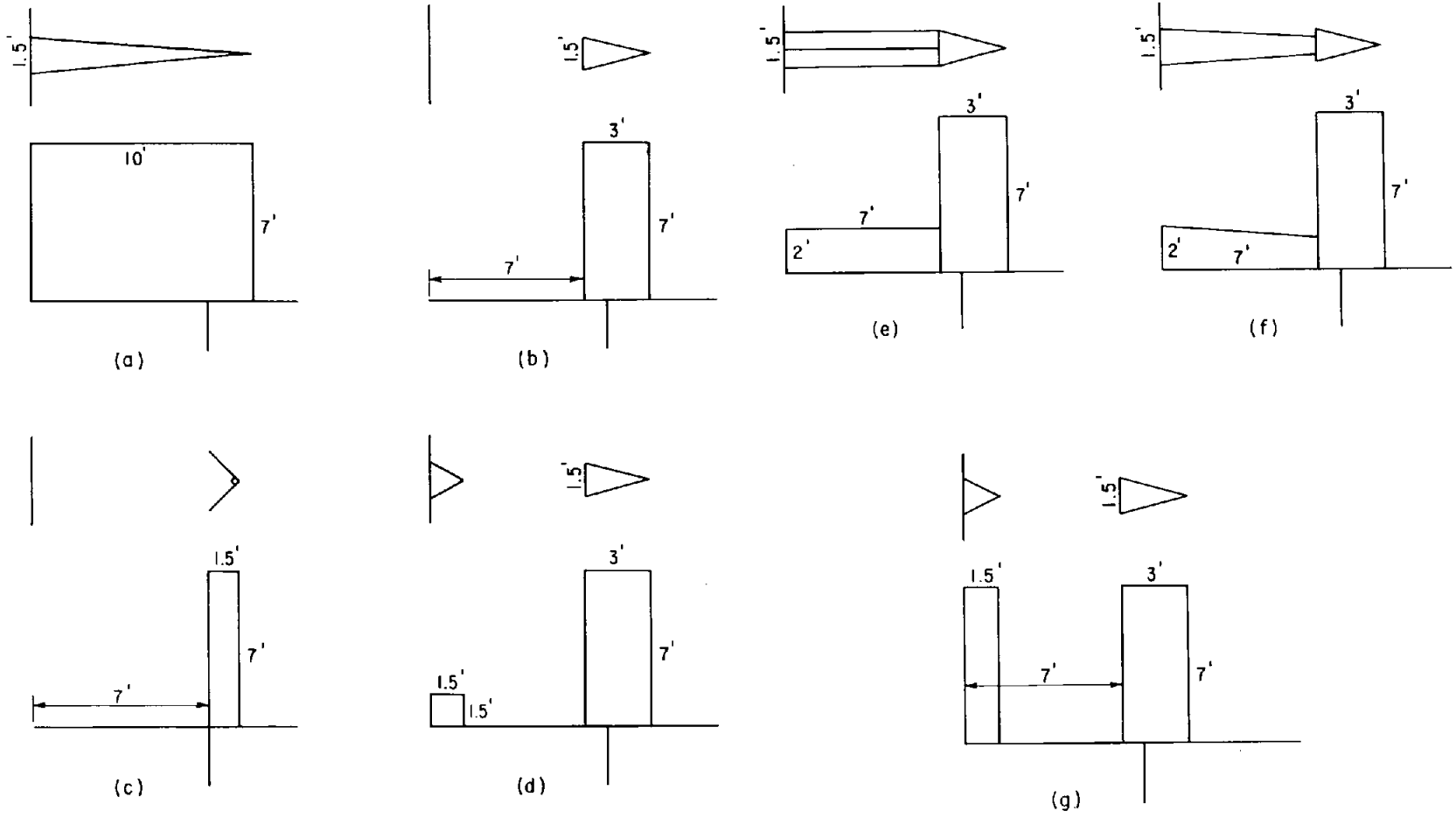

Figure 17. Plan and elevation splitter piers.

flow could be divided by a lead pier (similar to pier (e)) and that a second smaller pier at the chute lip could be used to divide the shallow flows in the wake. The second pier would be subject to much smaller forces than the lead pier. Piers (b), (c), (f), and (g) as well as intermediate-shaped piers between (c) and (g) were based on this concept. All these designs were suitable for discharges between 25,000 and 60,000 ft^3/s (708 and 1,700 m^3/s). At discharges below 25,000 ft^3/s (708 m^3/s), the superelevation of the chute caused the flow to approach the piers from the side. This action increased as the discharge decreased for observed flows down to about 8,000 ft^3/s (227 m^3/s). The resulting crossflow and fins resealed the opening for piers (b), (c), and (f). Pier (g), however, was suitable for these conditions as well as at discharges up to 140,000 ft^3/s (3,960 m^3/s) (fig. 18). The maximum velocities past the piers were approximately 60 ft/s (18.3 m/s). Two piers located at the third points across the chute were considered adequate.

CONCLUSIONS

Assuming that the final modification studied (fig. 16) is the one to be installed in the prototype, several alternatives for flow surface protection can be considered. With each alternative, there is an associated risk that erosion will continue and the modification will be rendered ineffective. The region most susceptible to scour is the fault zone or clay seam which would start eroding as soon as small flows came in contact with it. Relatively small and short-duration

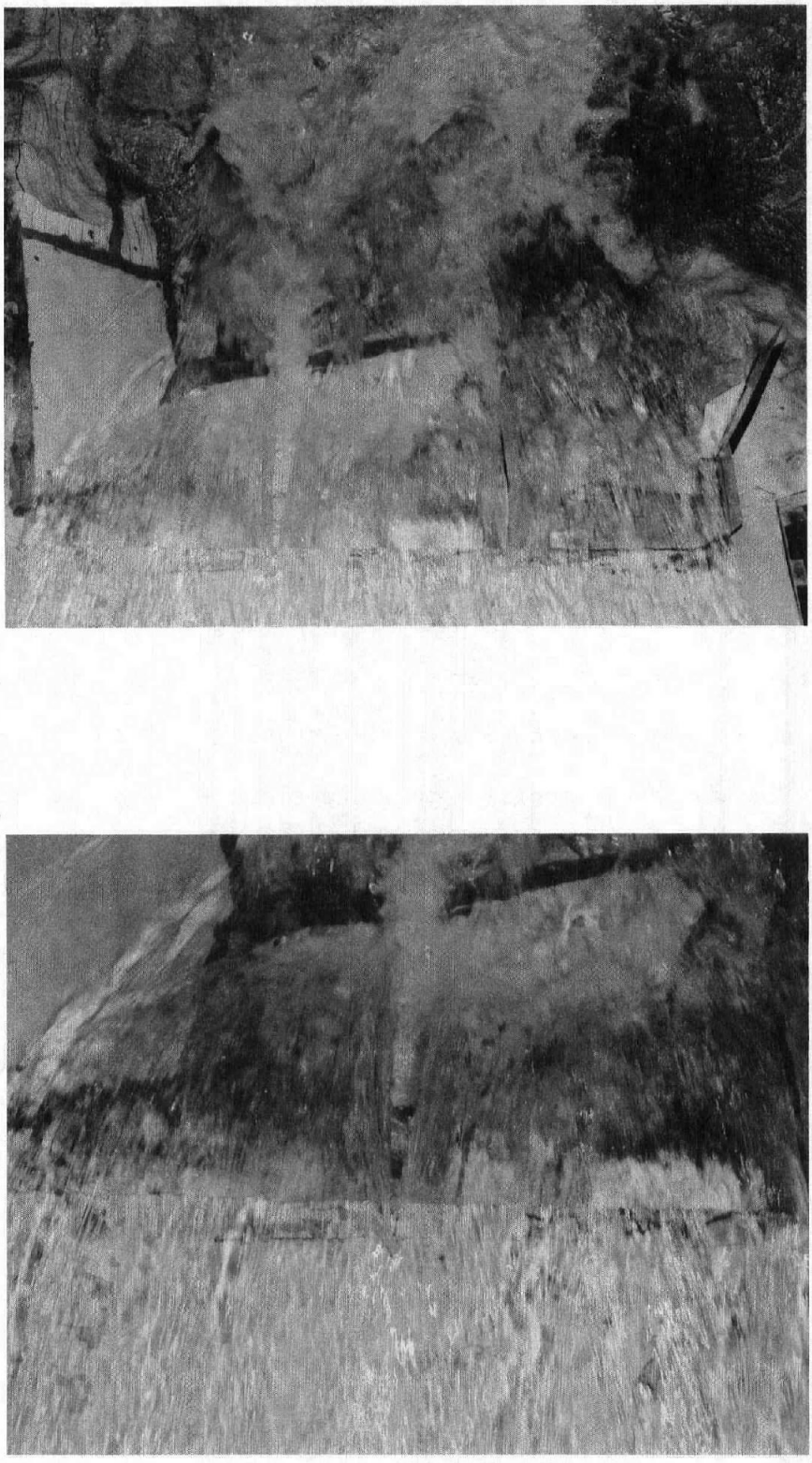

Figure 18. Splitter piers operating. Photos P25-D-75896 and P25-D-75897.

flows could quickly create a trough along the fault zone. The trough would cause back eddies which in turn would cause the erosion to advance upstream and again compromise the structure. A potential region for fault protection, shown in figure 15, contains those zones in which the most severe flow impingement and the highest flow velocities would occur. It is also the region nearest the structure which, if eroded, would result in the most immediate potential damage.

Protective surfacing of general rock zones is also a possibility. As previously explained, jointed rock, even though it may otherwise be sound, is subject to hydraulic jacking when exposed to impact pressures. Jacking could result in undercutting of localized surface protection or in the creation of flow surface irregularities. Irregularities would result in higher impact pressure development and in back eddy action, both of which could cause additional erosion. Such action can be prevented by surfacing the rock so that impact pressure will develop in the joints. Shotcrete surfacing would probably be adequate and concrete surfacing would be more than adequate. A region that offers the potential for surfacing is shown in figure 15. This region contains all the major impact zones that are near the chute structure as well as the zones where the highest flow velocities occur. Surfacing would also isolate the rock from the high-velocity flows. Reduced surfacing or no surfacing at all are possible alternatives, at the risk of resulting damage. Probably the most critical

zones to be lined are those just downstream from the structure (upper portions of the 4:1 slope and between the 4:1 slope and chute). Although these zones are not exposed to extreme impact pressures, their proximity to the structure makes them critical. The zones on which the flow falling from the chute will impinge (the remainder of the 4:1 slope and other such impact zones) will be exposed to the highest impact pressures and, therefore, are most likely to suffer hydraulic jacking. Thus, surfacing of these initial impact zones should, also be seriously considered. Finally, the zones on the horizontal surface at the toes of the 4:1 and 1:1 slopes may also be exposed to some high impact pressures. Even though these toe regions are relatively far away from the chute structure, it may be desirable to protect them from the potential erosion. Possible limits for flow surface protection are shown in figure 19.

Venting of the region behind the free jet falling from the chute lip should also be carefully considered. Without splitter piers or some other venting structure, negative pressures will develop in the region between the free jet and the spillway structure. This negative pressure would result in uplift forces on both the natural rock and any protective surfacing present in the region. Such forces would be of special concern in this region because of the region's close proximity to the structure. Complete venting of the region

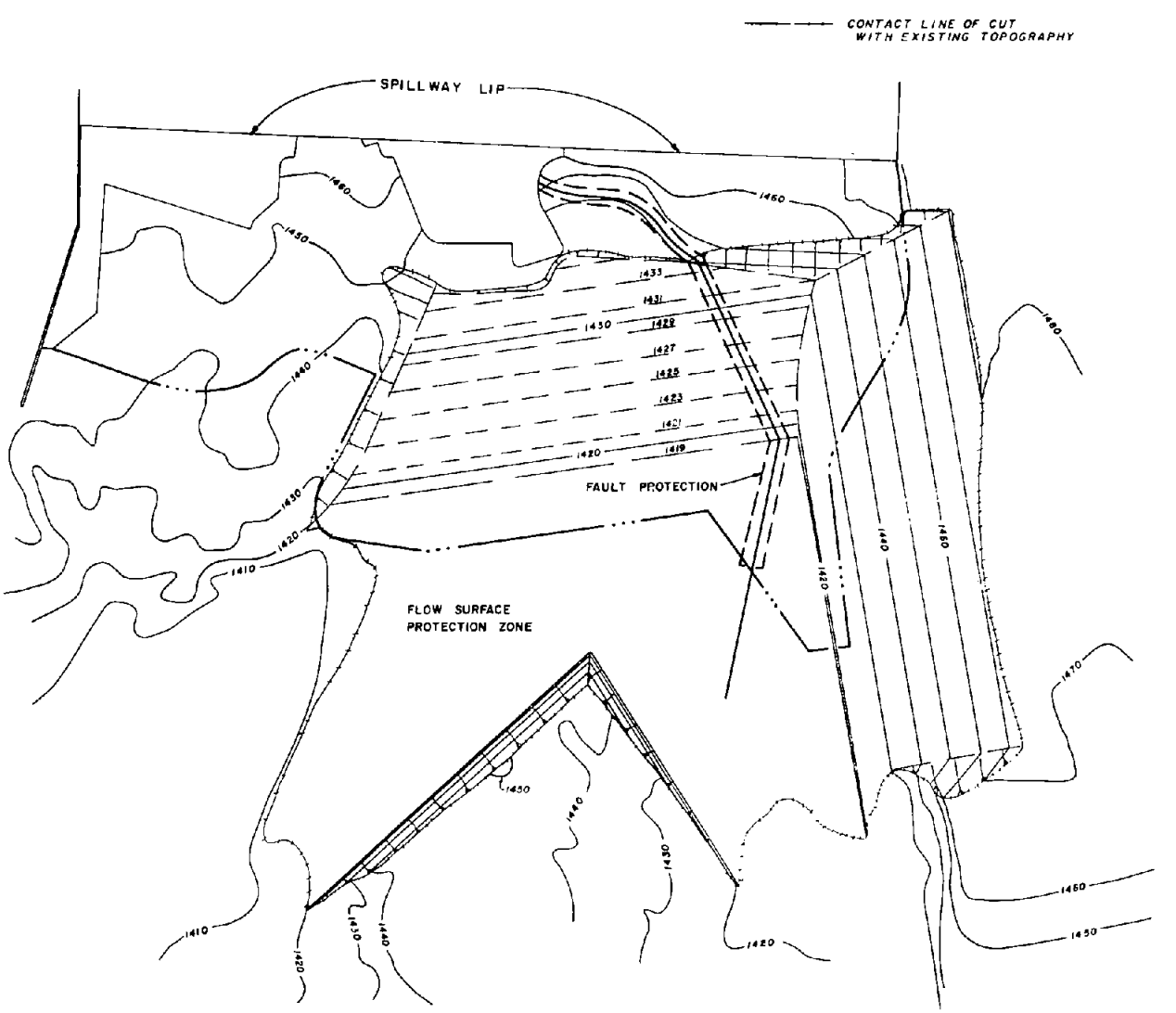

Figure 19. Possible flow surface protection.

would establish atmospheric pressures and, therefore, eliminate the uplift forces and possible vibration caused by unstable flow.

One proposal is to install a venting structure, protect the fault zone, monitor erosion after spills, and take corrective actions as needed. If the rock in the impact and high-velocity zones proves to be nearly joint-free, the potential for hydraulic jacking would be minimized and the proposal would appear feasible. The more jointed the rock, the more likely that hydraulic jacking will occur and, therefore, unprotected flow surfaces would become less acceptable. There is always the possibility that a major spill would occur which could cause erosion even with good rock. It should also be recognized that if damages needed repairing the repair would probably require massive concrete fill, which would be quite expensive.

APPENDIX A

In the following figures all flow velocities are shown in feet per second.

All impact pressures are given in feet of water. Where measured impact pressures are given, the observed values are enclosed in a square. Computed pressures are either enclosed by a circle or are freestanding in the indicated impact regions. Major impact regions are shown by the following symbol:

In some cases, the regions where minor impacts may occur are indicated by the following symbol:

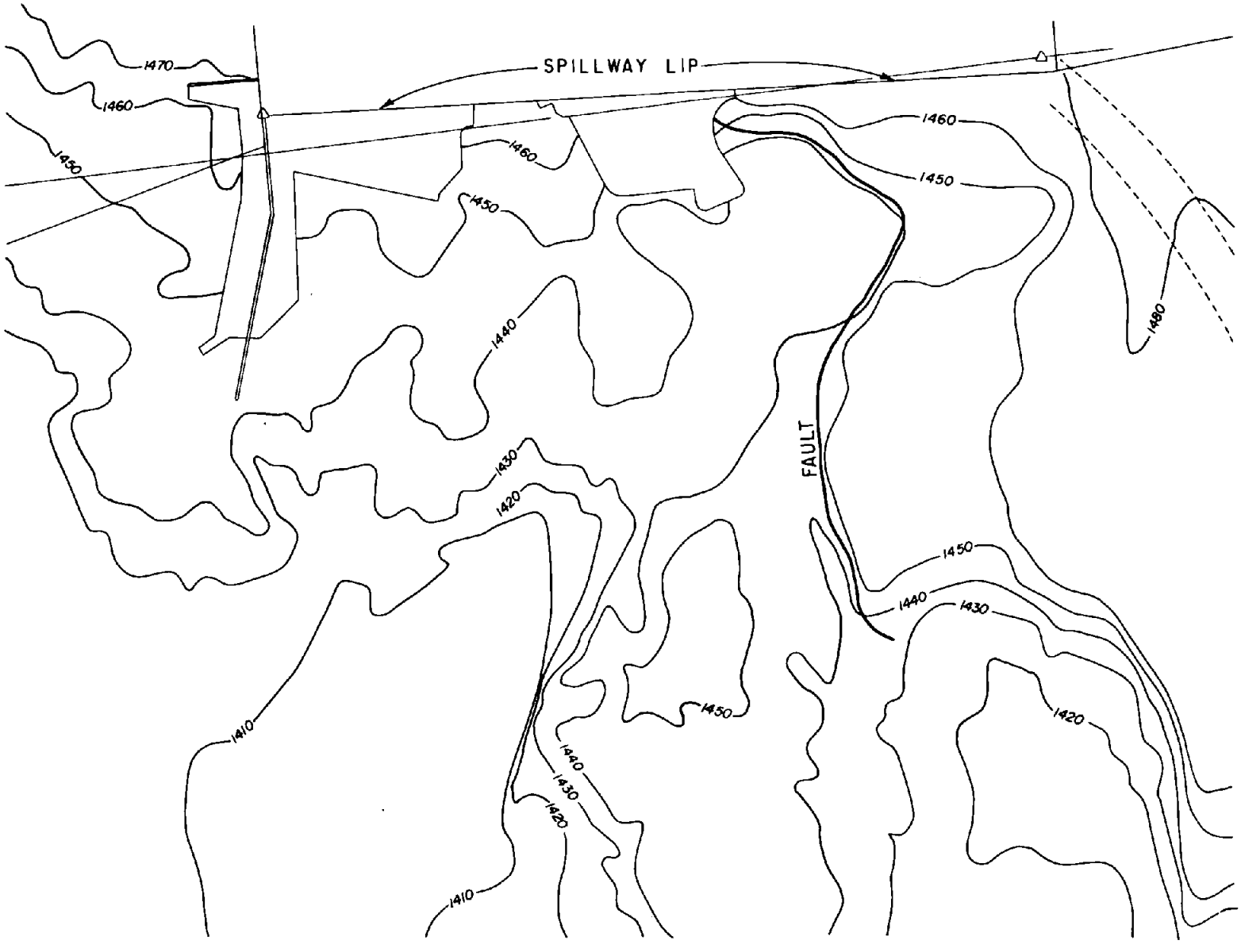

Figure A-1. Initial model topography.

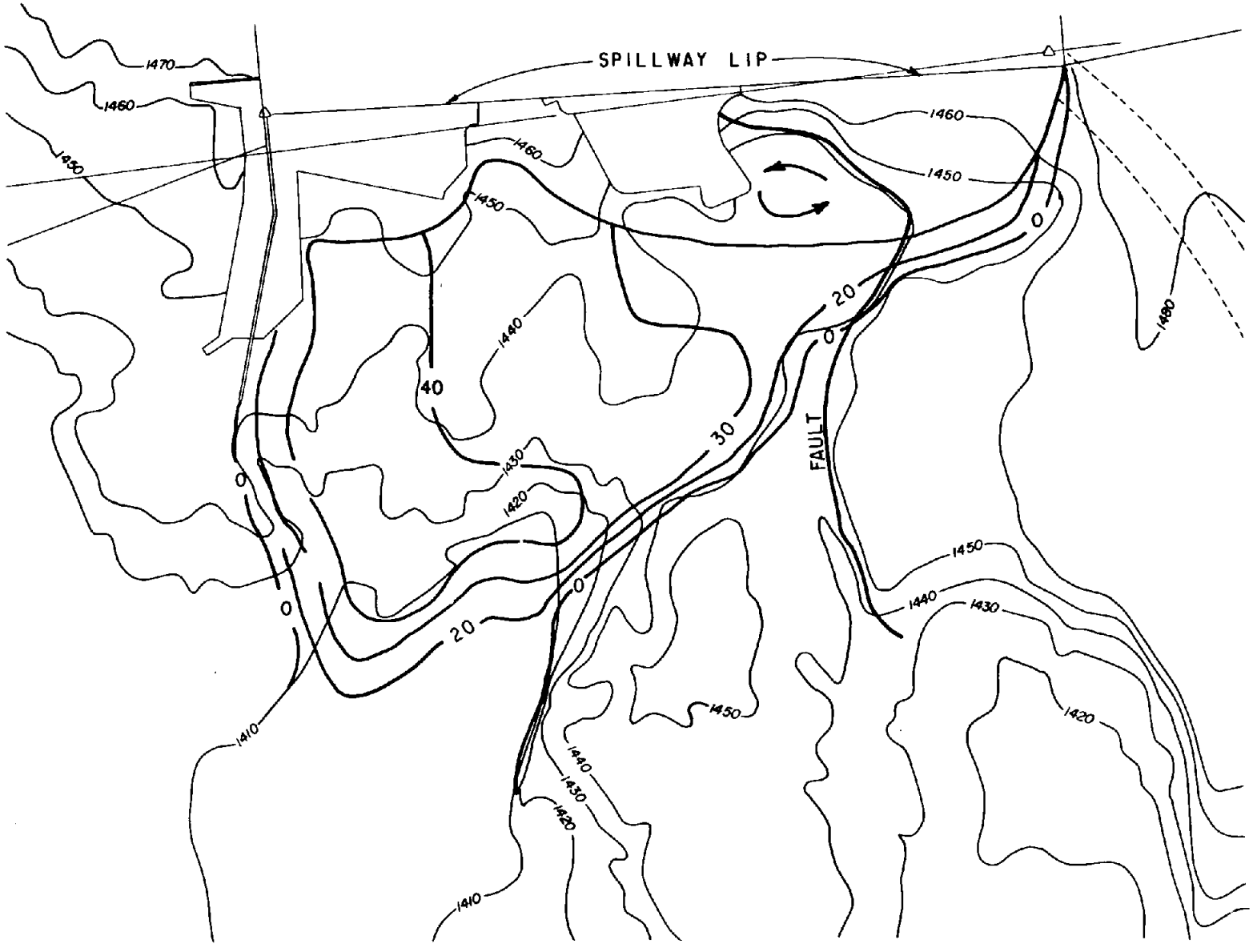

Figure A-2. Velocity contours for a discharge of 13,000 ft^3/s (initial model topography).

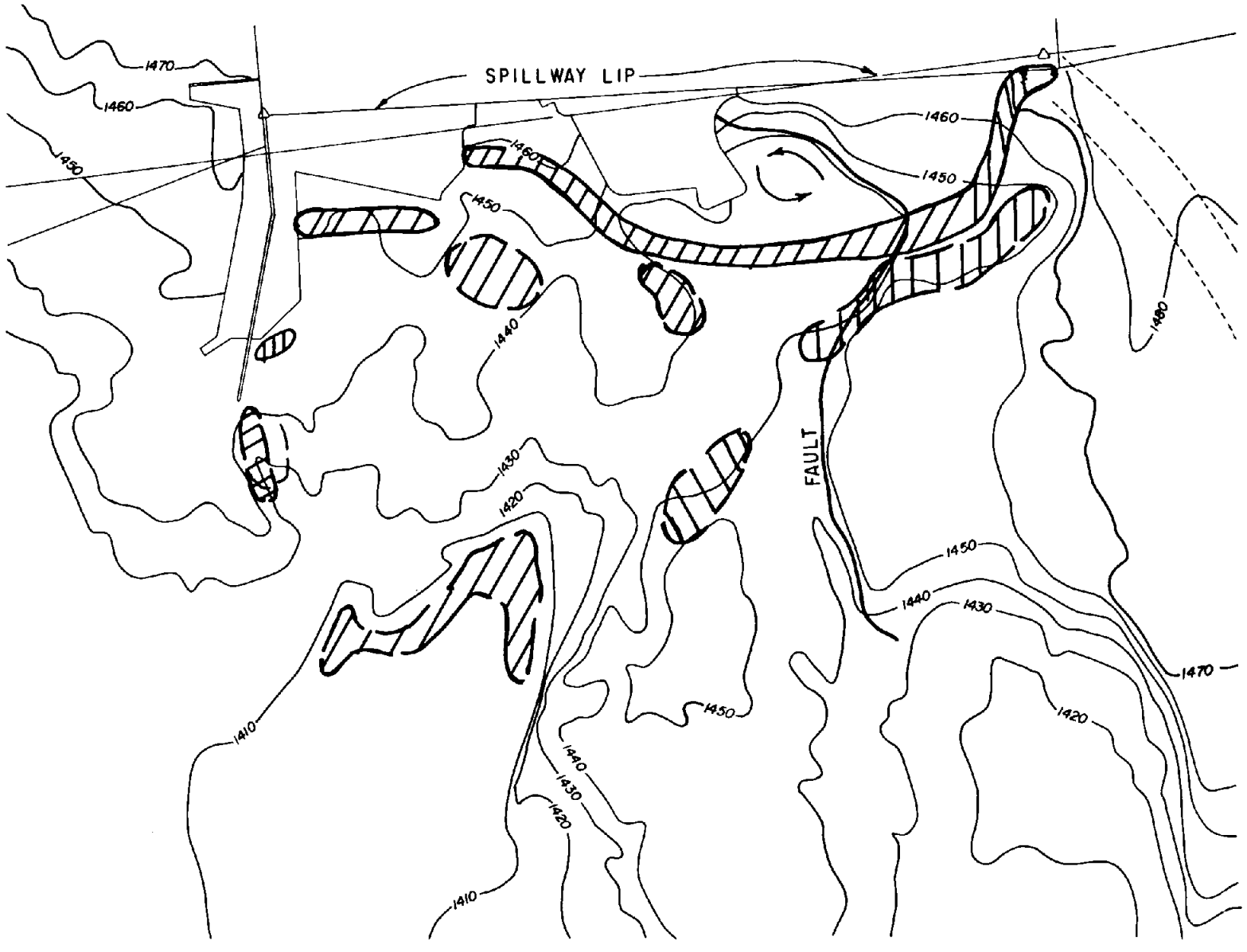

Figure A-3. Impact pressures for a discharge of 13,000 ft^3/s (initial model topography).

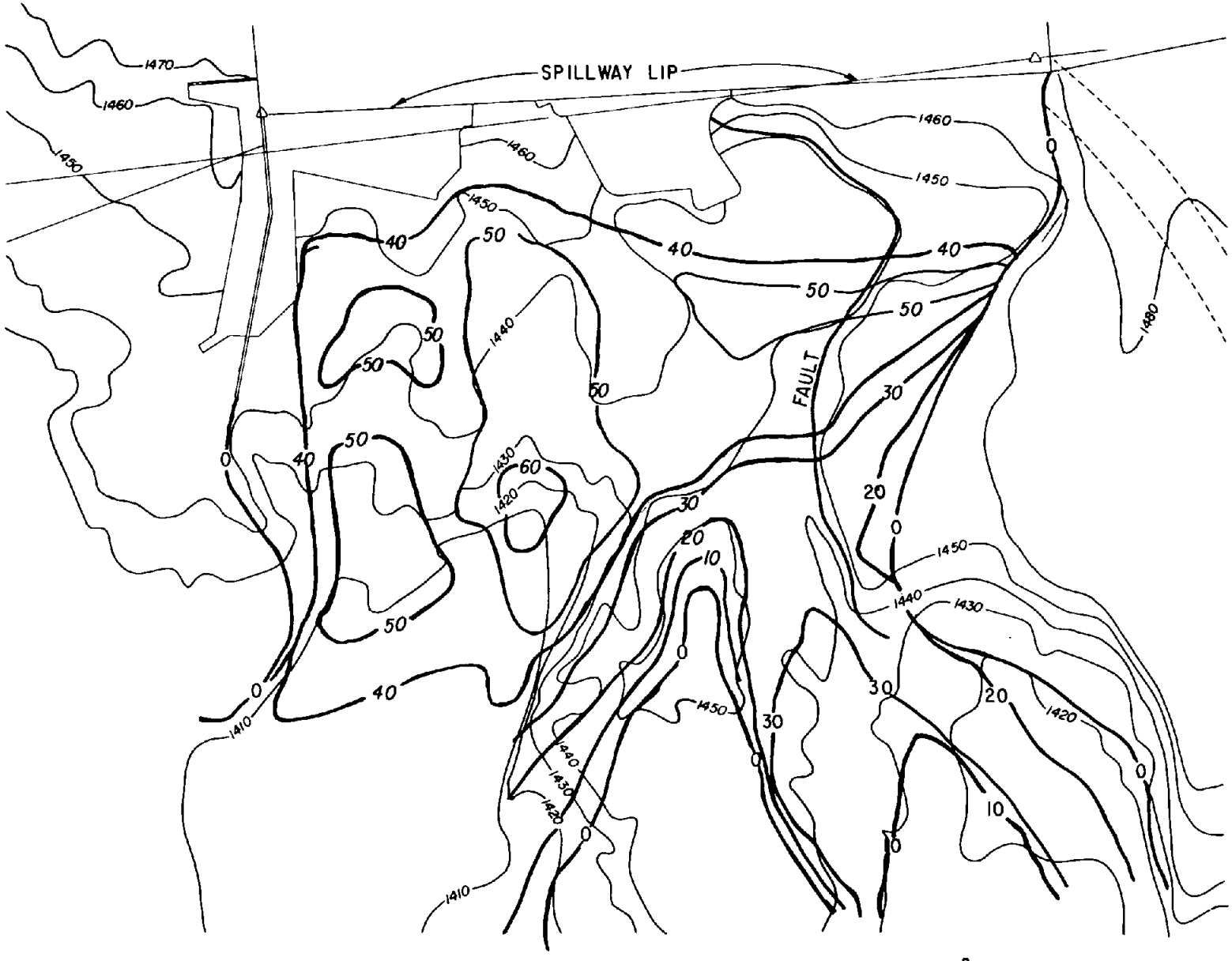

Figure A-4. Velocity contours for a discharge of 30,000 ft^3/s (initial model topography).

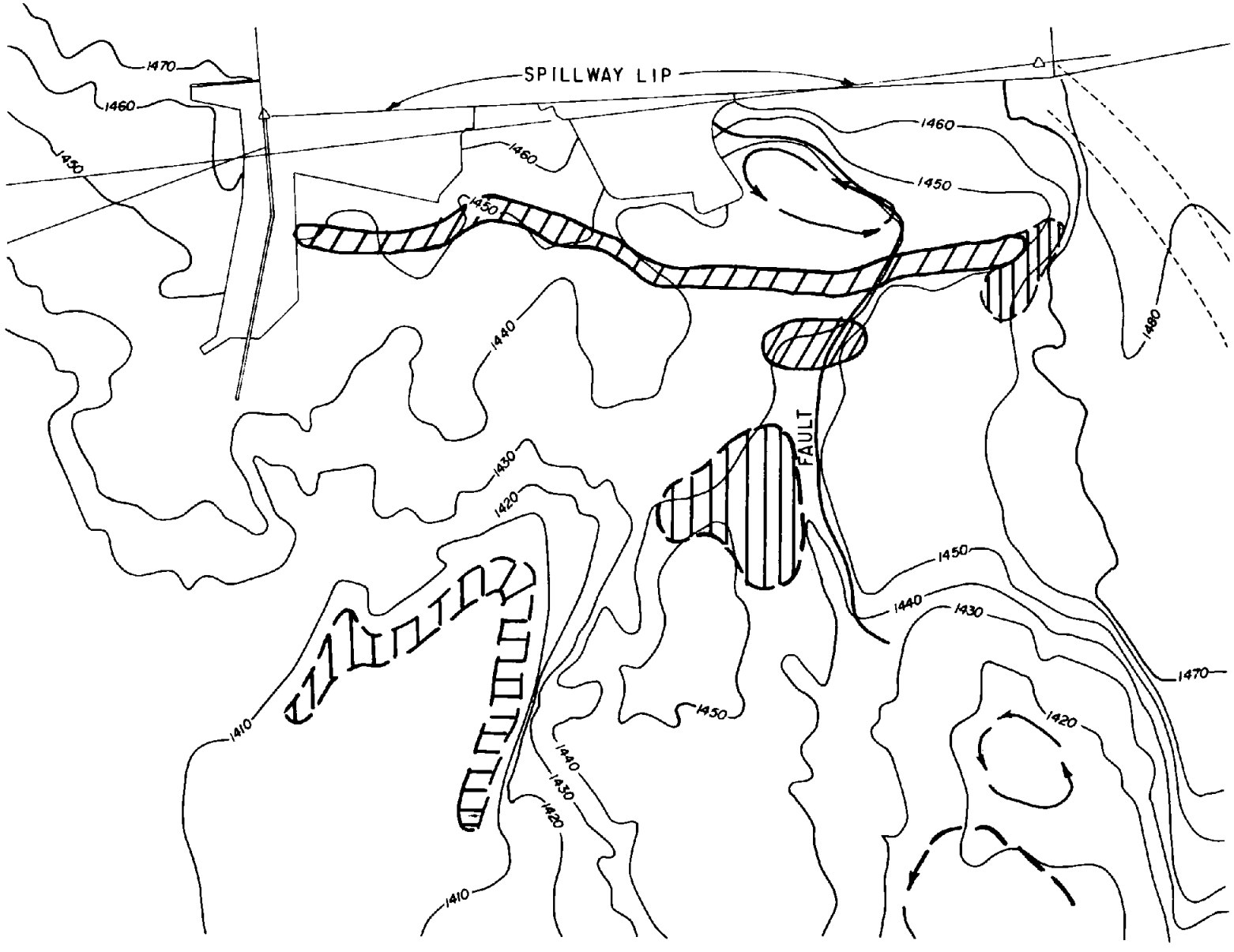

Figure A-5. Impact pressures for a discharge of 30,000 ft^3/s (initial model topography).

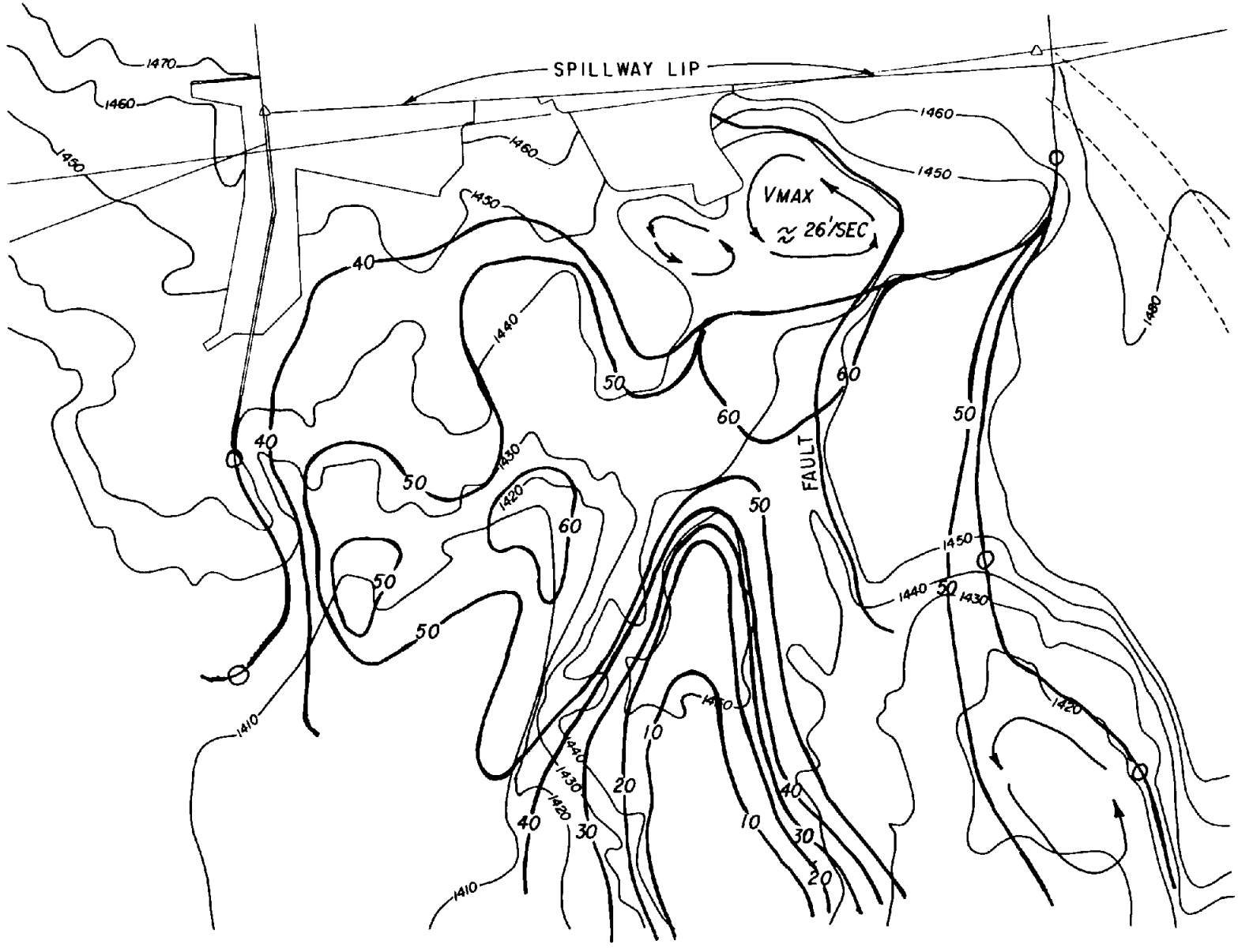

Figure A-6. Velocity contours for a discharge of 60,000 ft^3/s (initial model topography).

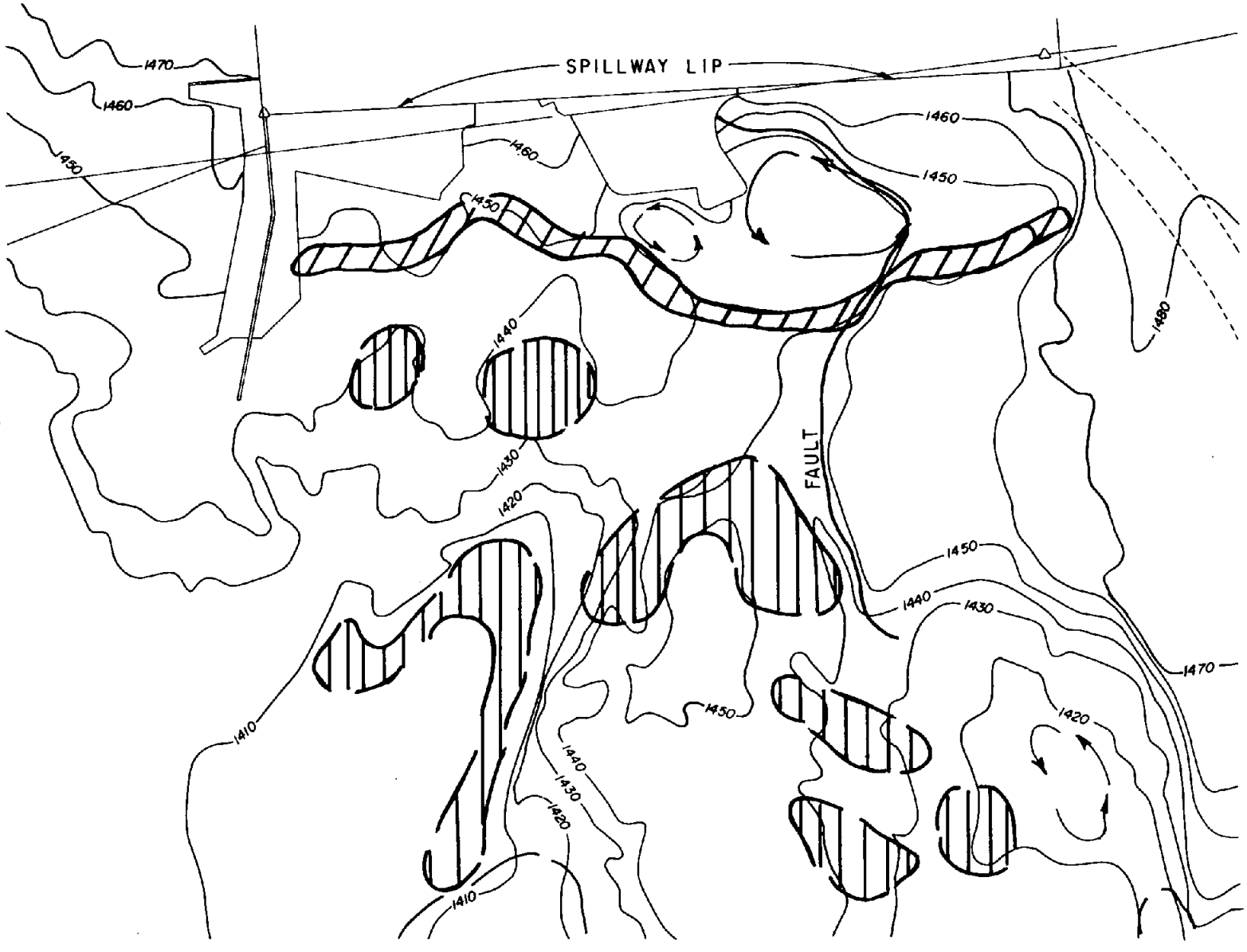

Figure A-7. Impact pressures for a discharge of 60,000 ft^3/s (initial model topography).

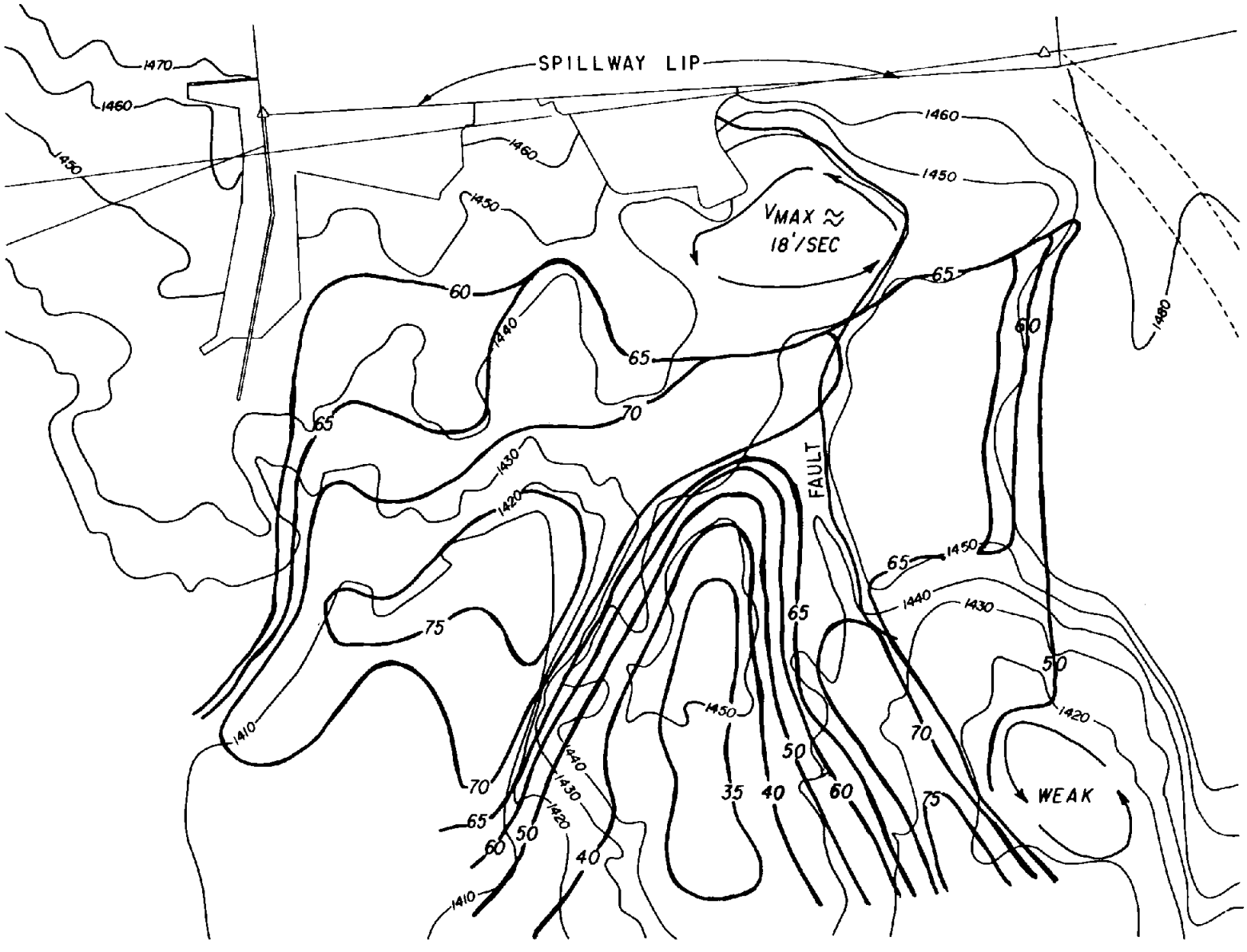

Figure A-8. Velocity contours for a discharge of 140,000 ft^3/s (initial model topography).

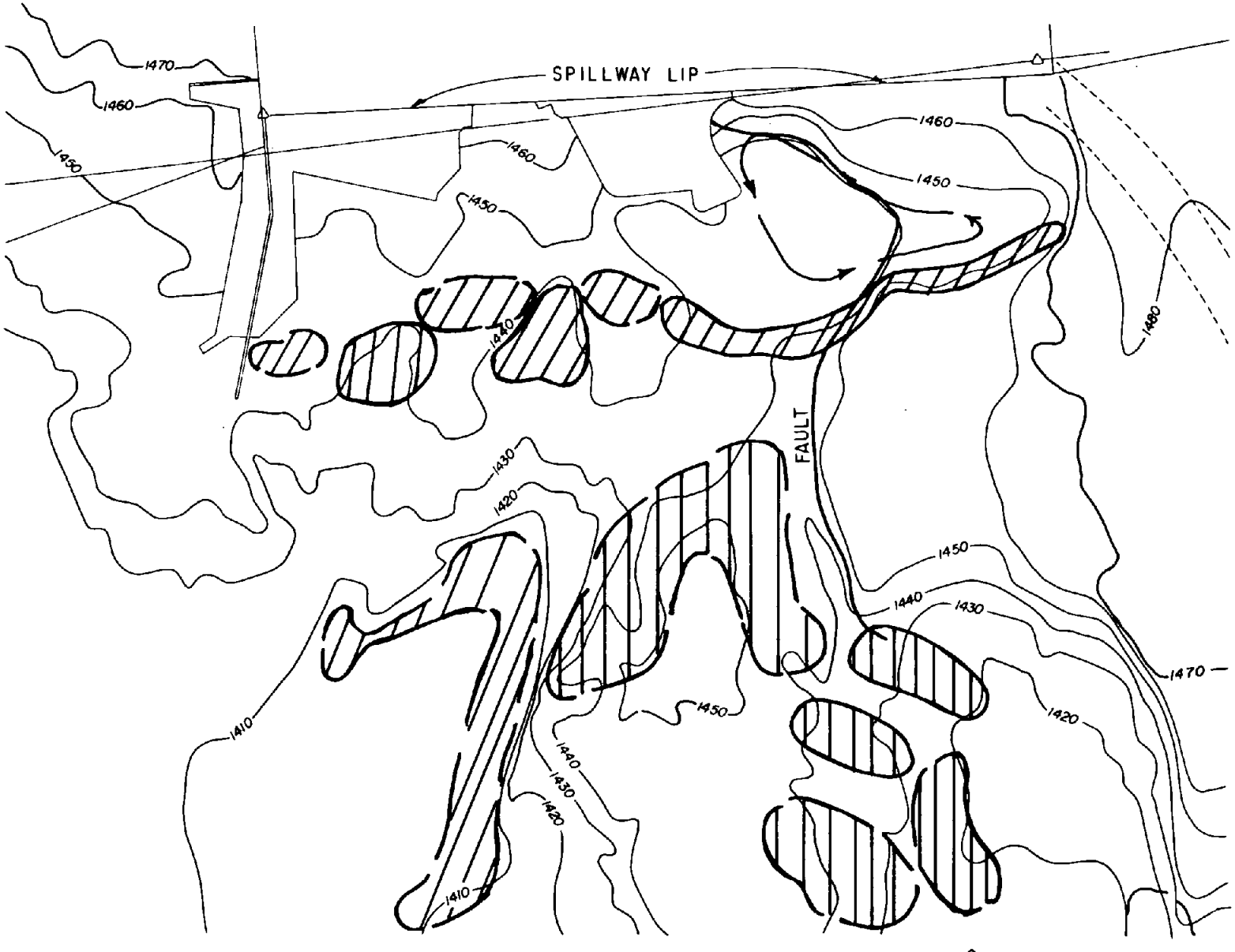

Figure A-9. Impact pressures for a discharge of 140,000 ft^3/s (initial model topography).

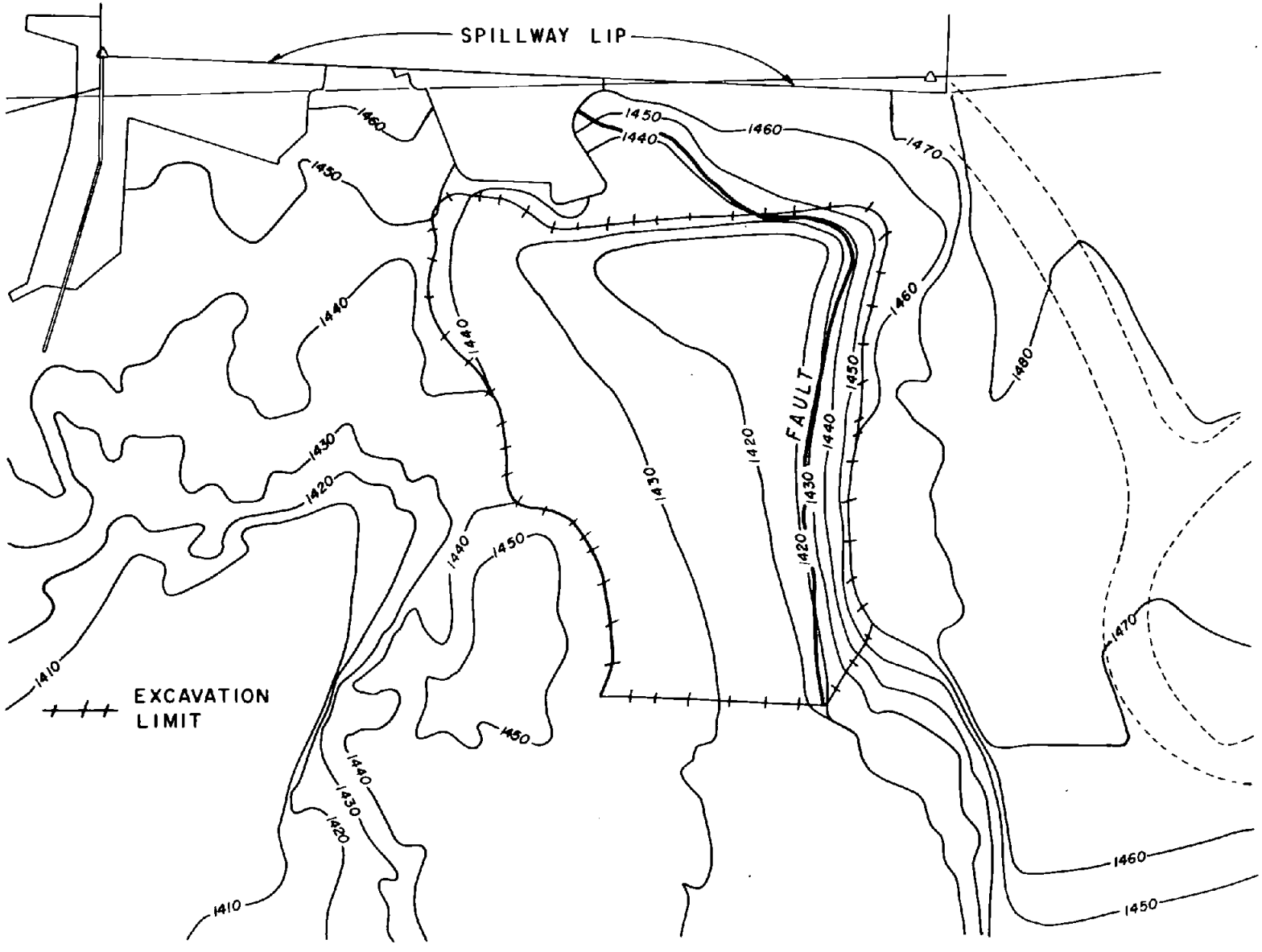

Figure A-10. First topographic model modification.

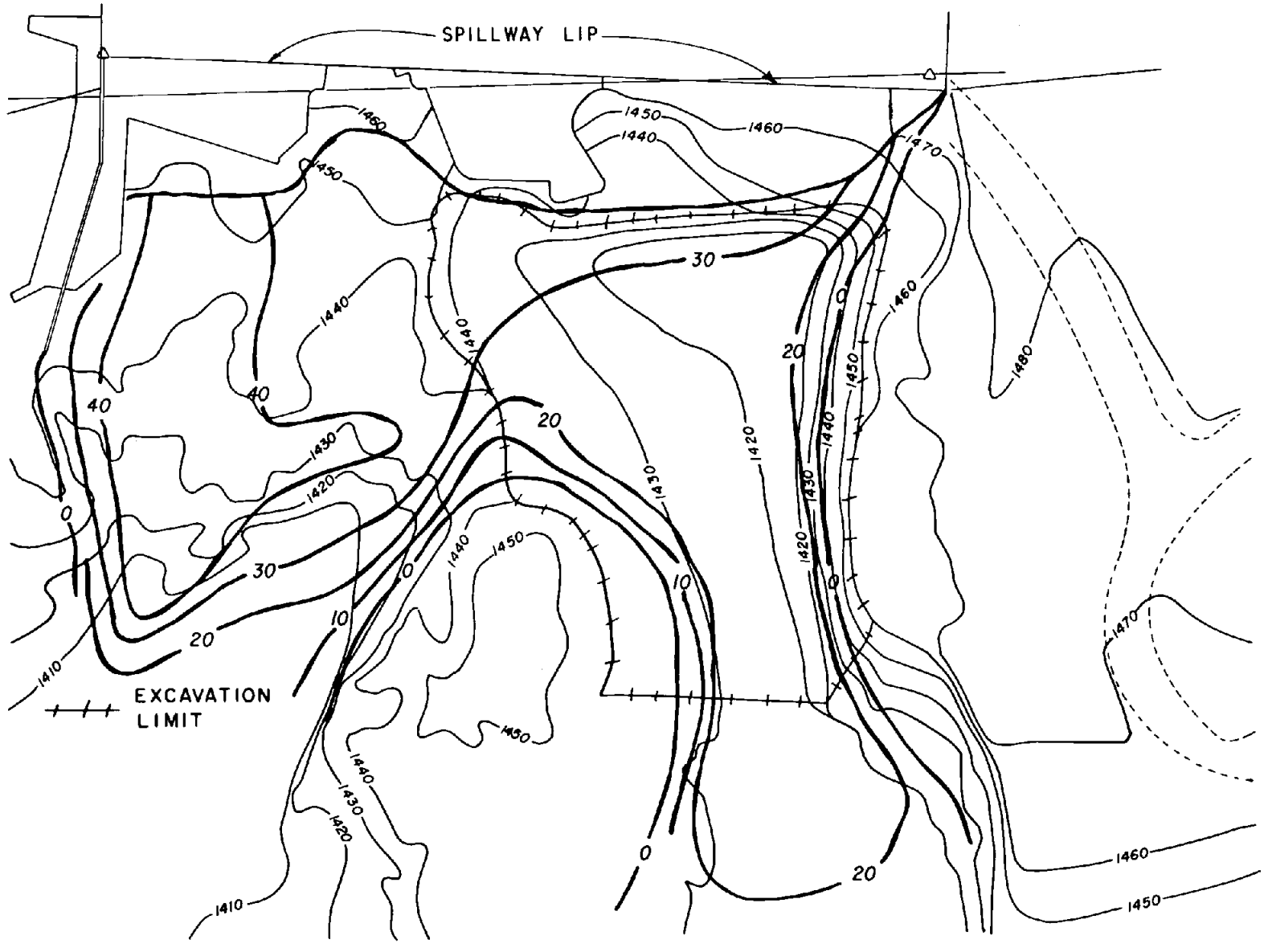

Figure A-11. Velocity contours for a discharge of 13,000 ft^3/s (first topographic model modification).

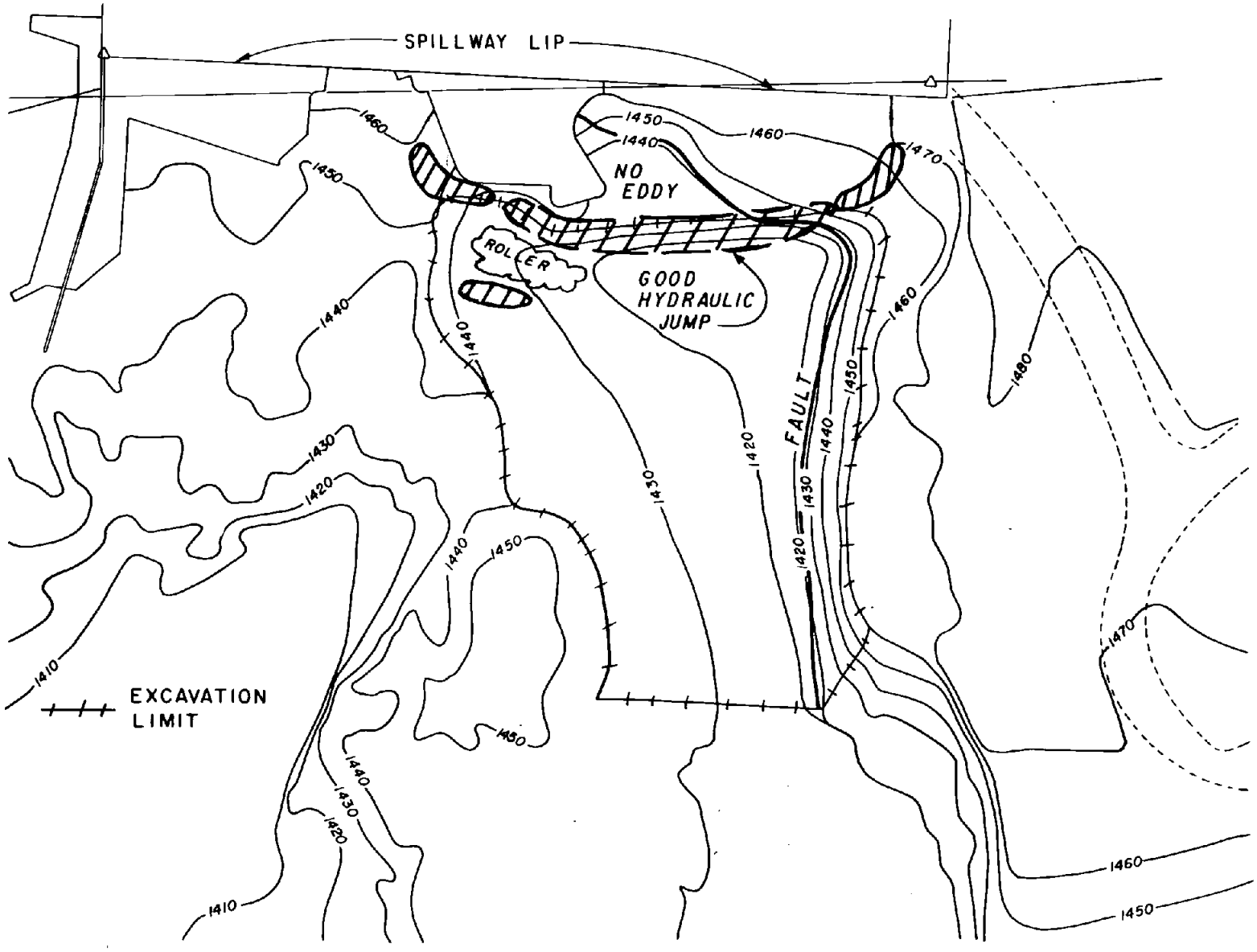

Figure A-12. Impact pressures for a discharge of 13,000 ft^3/s (first topographic model modification).

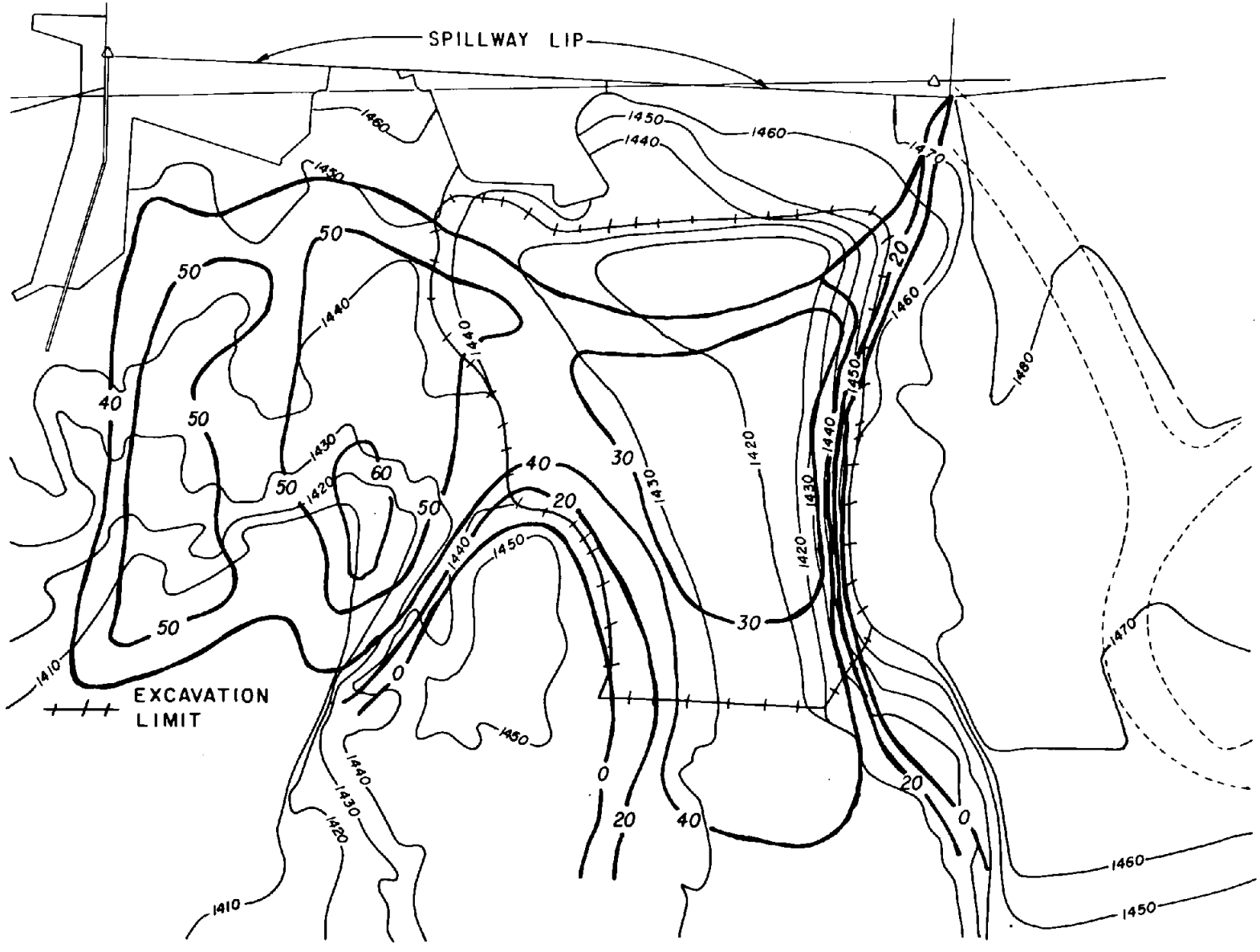

Figure A-13. Velocity contours for a discharge of 30,000 ft^3/s (first topographic model modification).

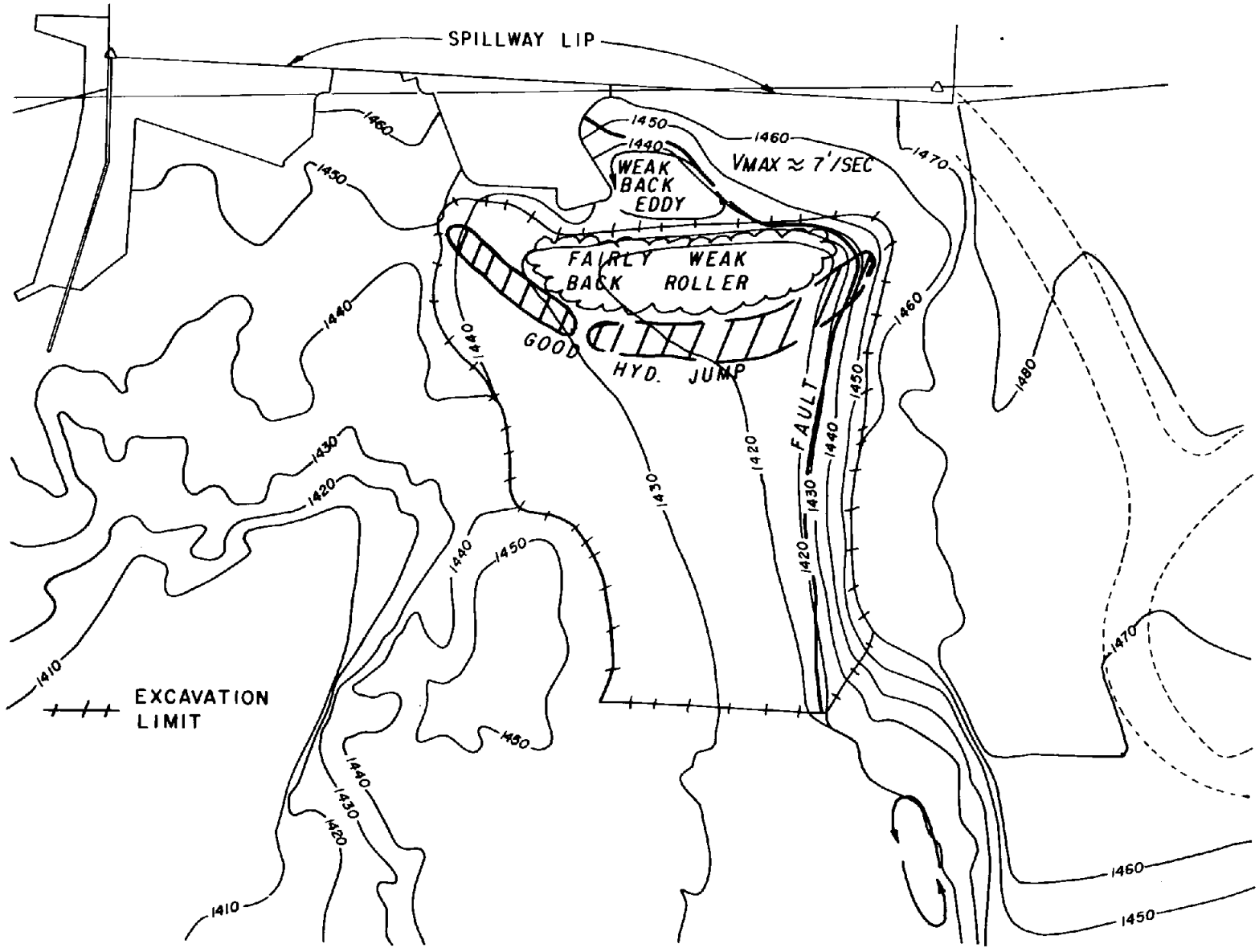

Figure A-14. Impact pressures for a discharge of 30,000 ft^3/s (first topographic model modification).

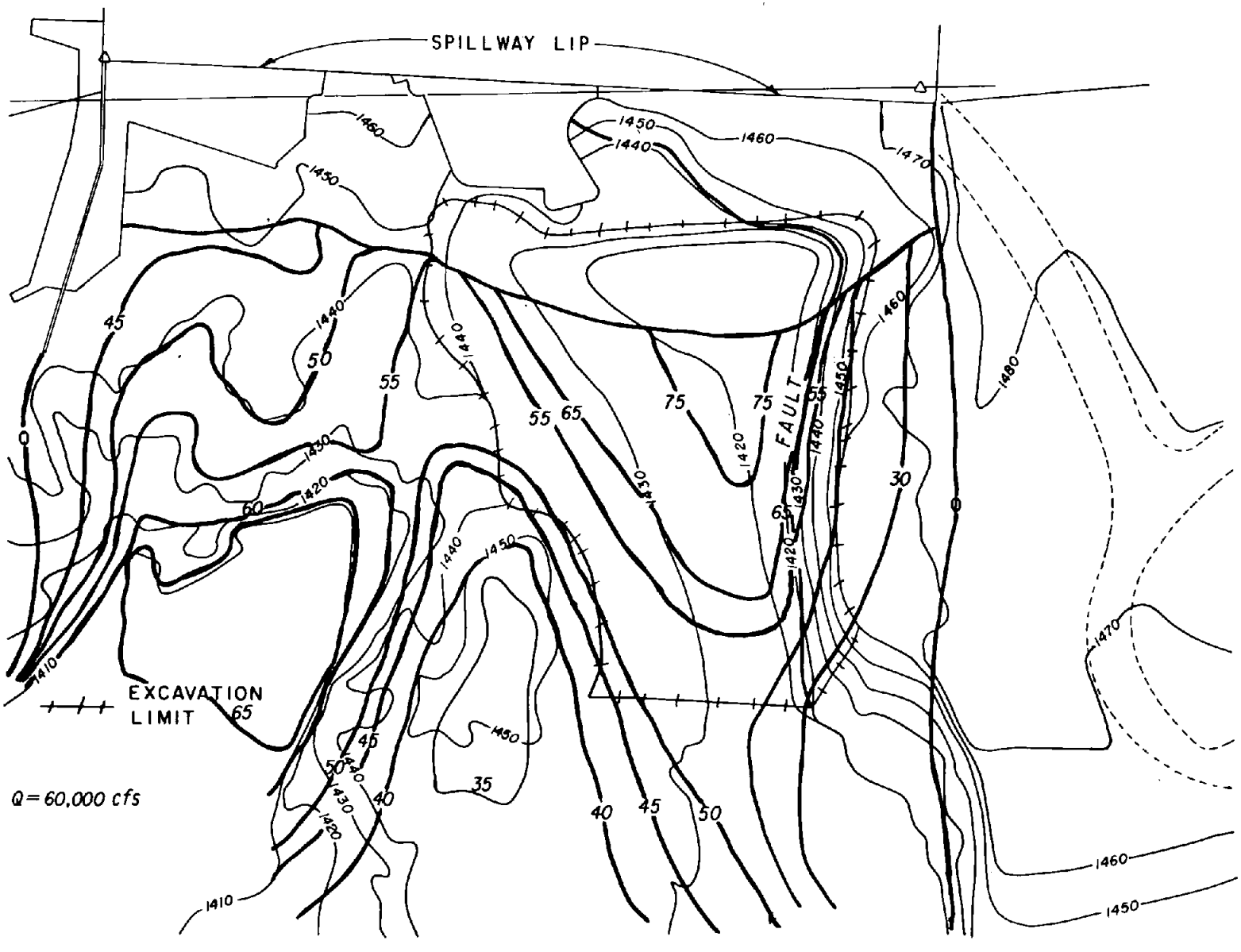

Figure A-15. Velocity contours for a discharge of 60,000 ft^3/s (first topographic model modification).

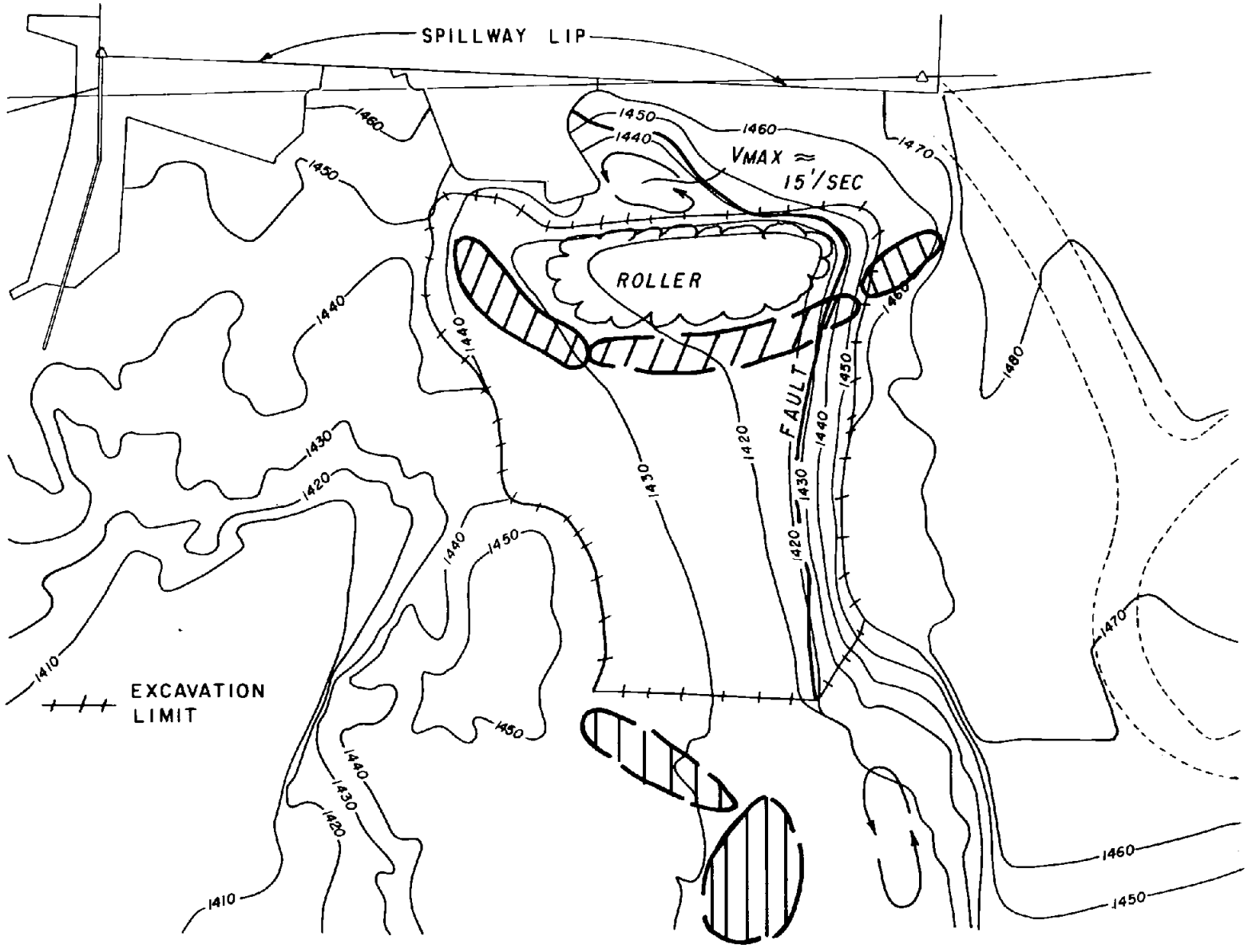

Figure A-16. Impact pressures for a discharge of 60,000 ft^3/s (first topographic model modification).

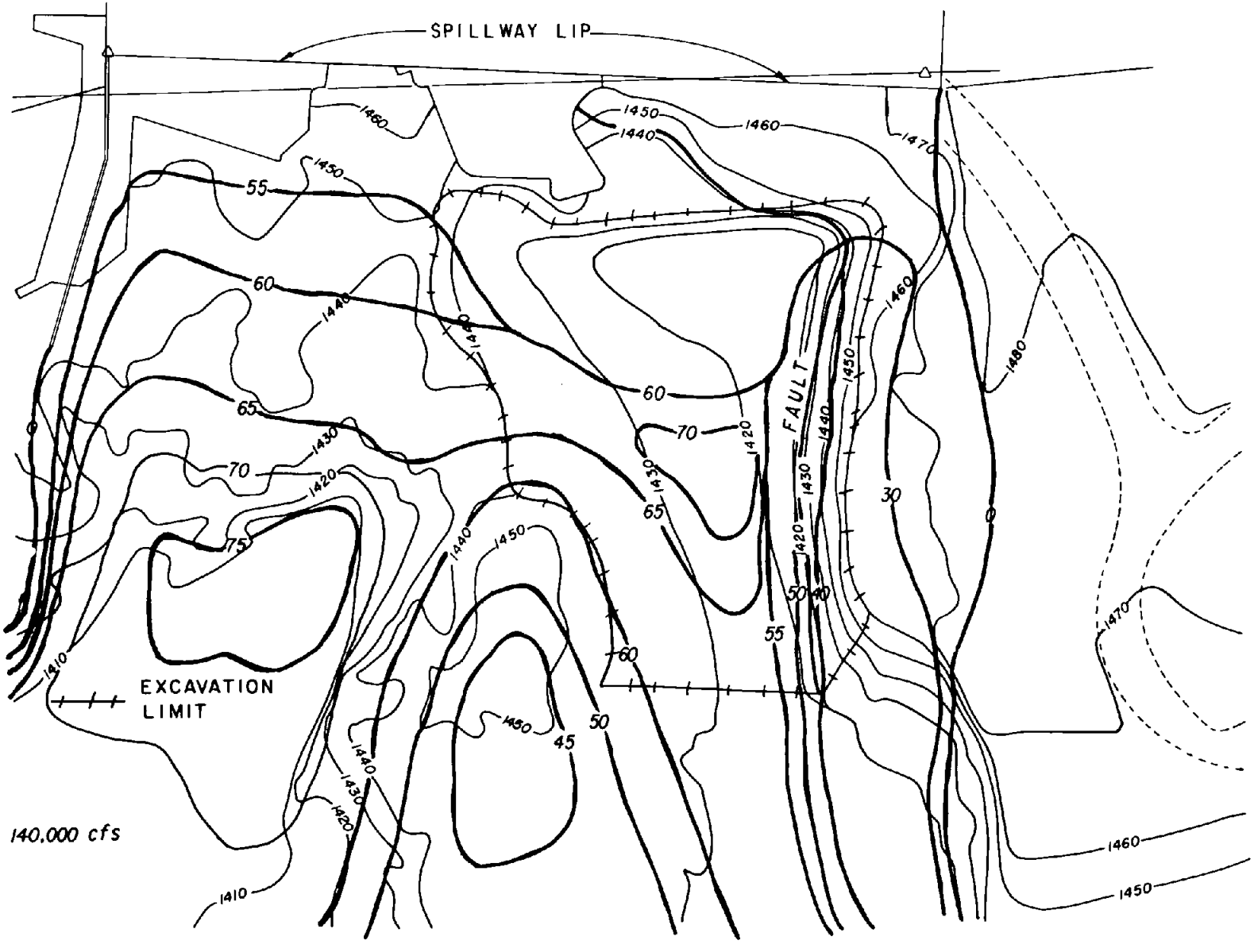

Figure A-17. Velocity contours for a discharge of 140,000 ft^3/s (first topographic model modification).

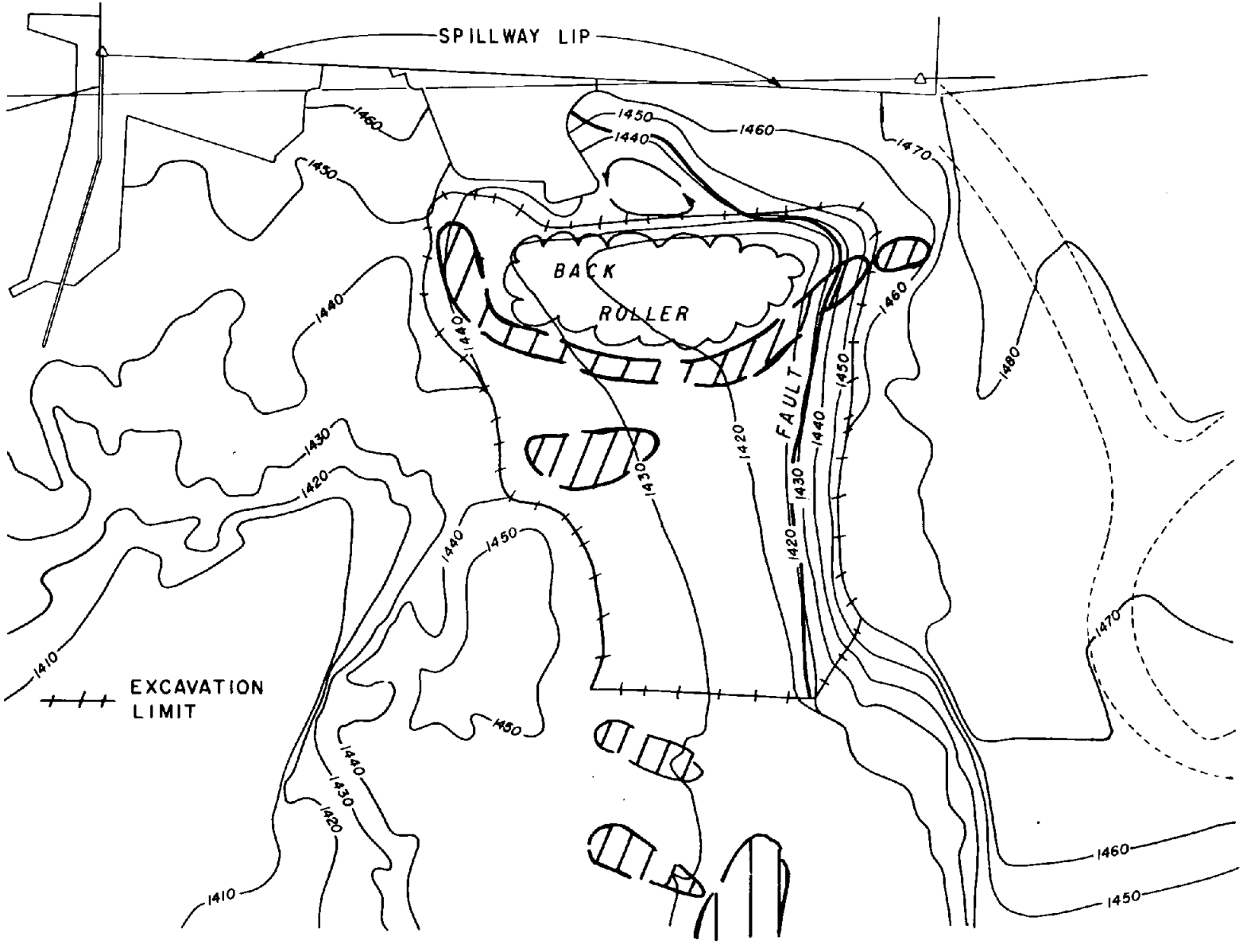

Figure A-18. Impact pressures for a discharge of 140,000 ft^3/s (first topographic model modification).

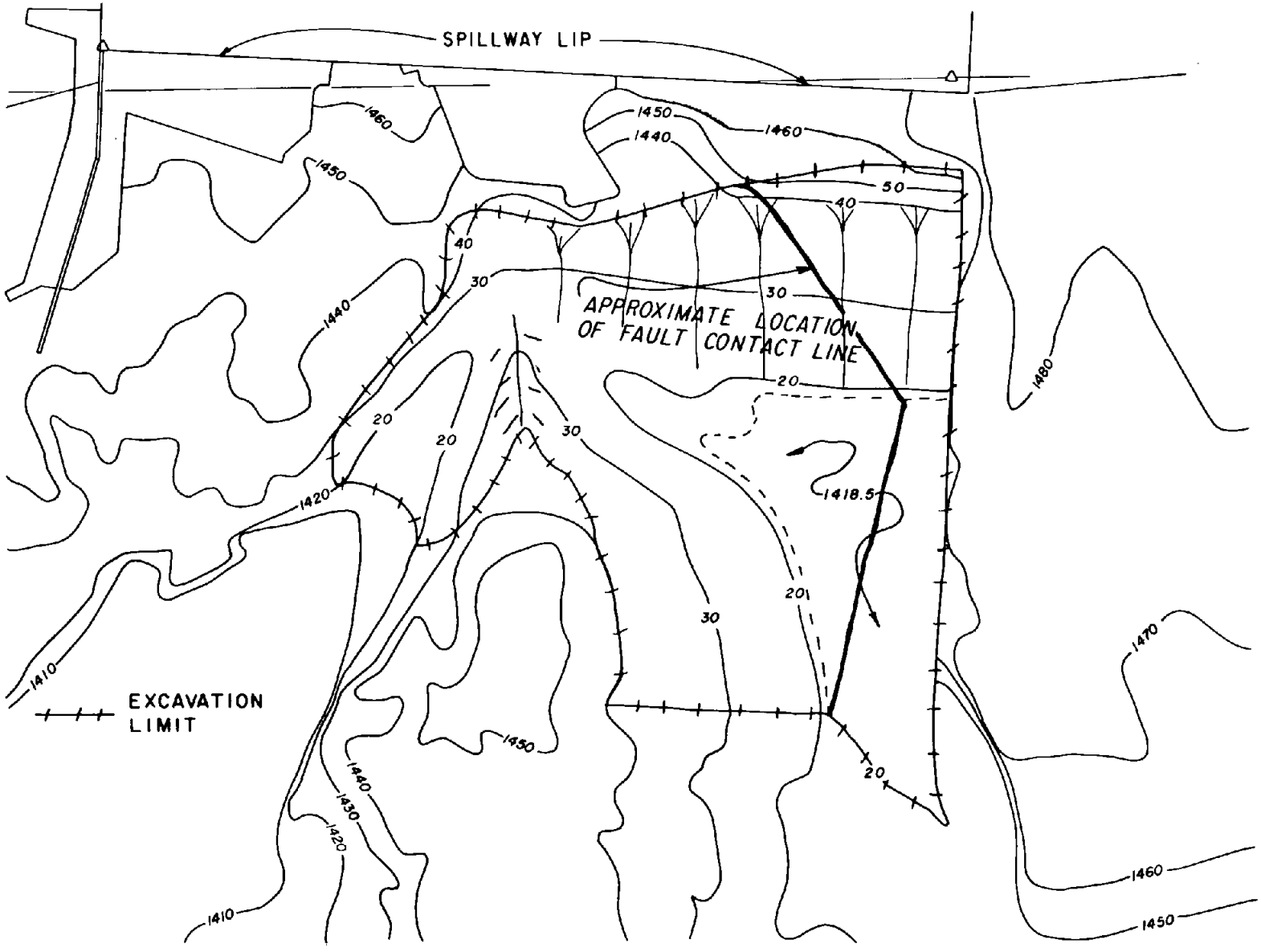

Figure A-19. Second topographic model modification.

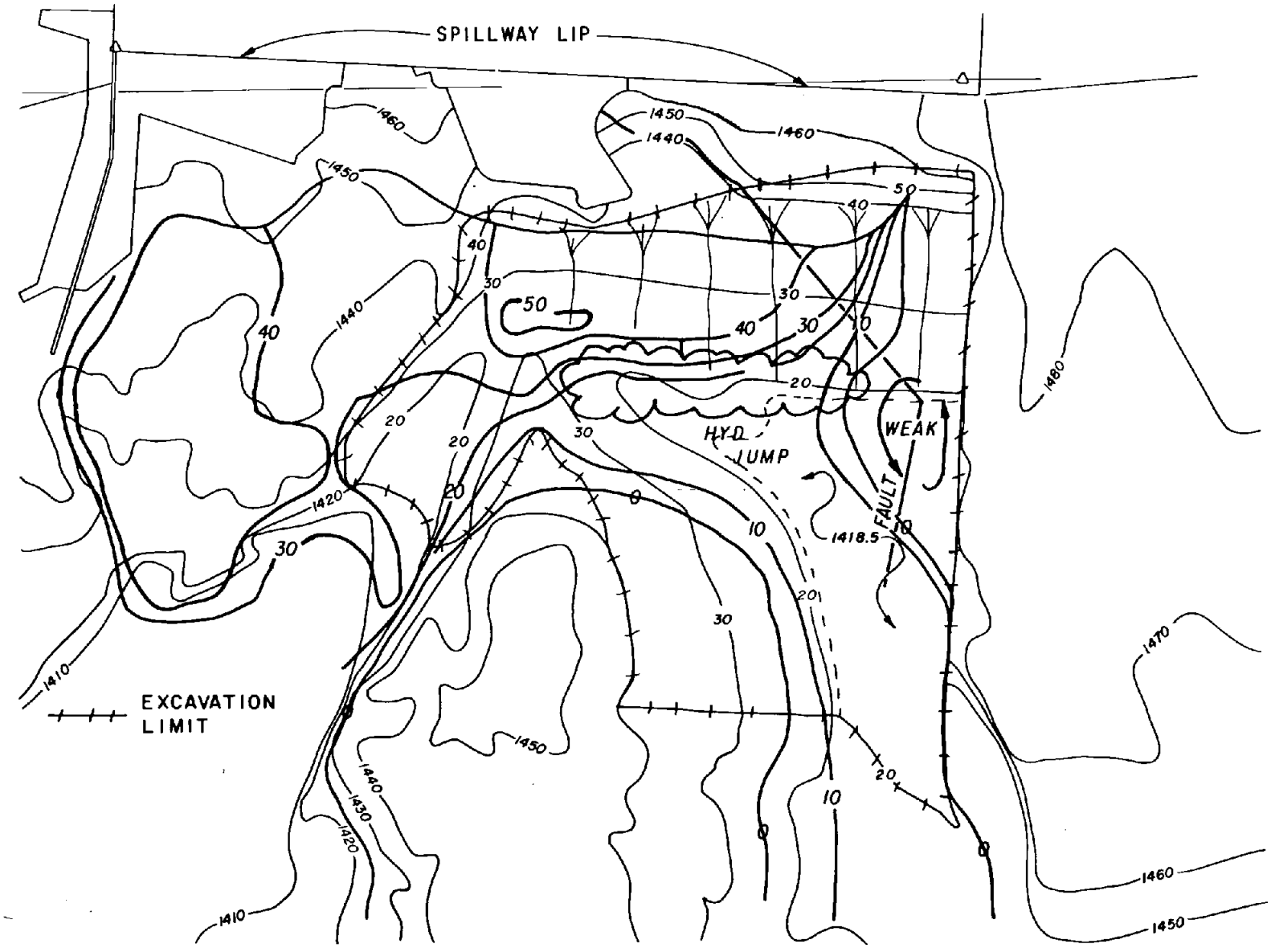

Figure A-20. Velocity contours for a discharge of 13,000 ft^3/s (second topographic model modification).

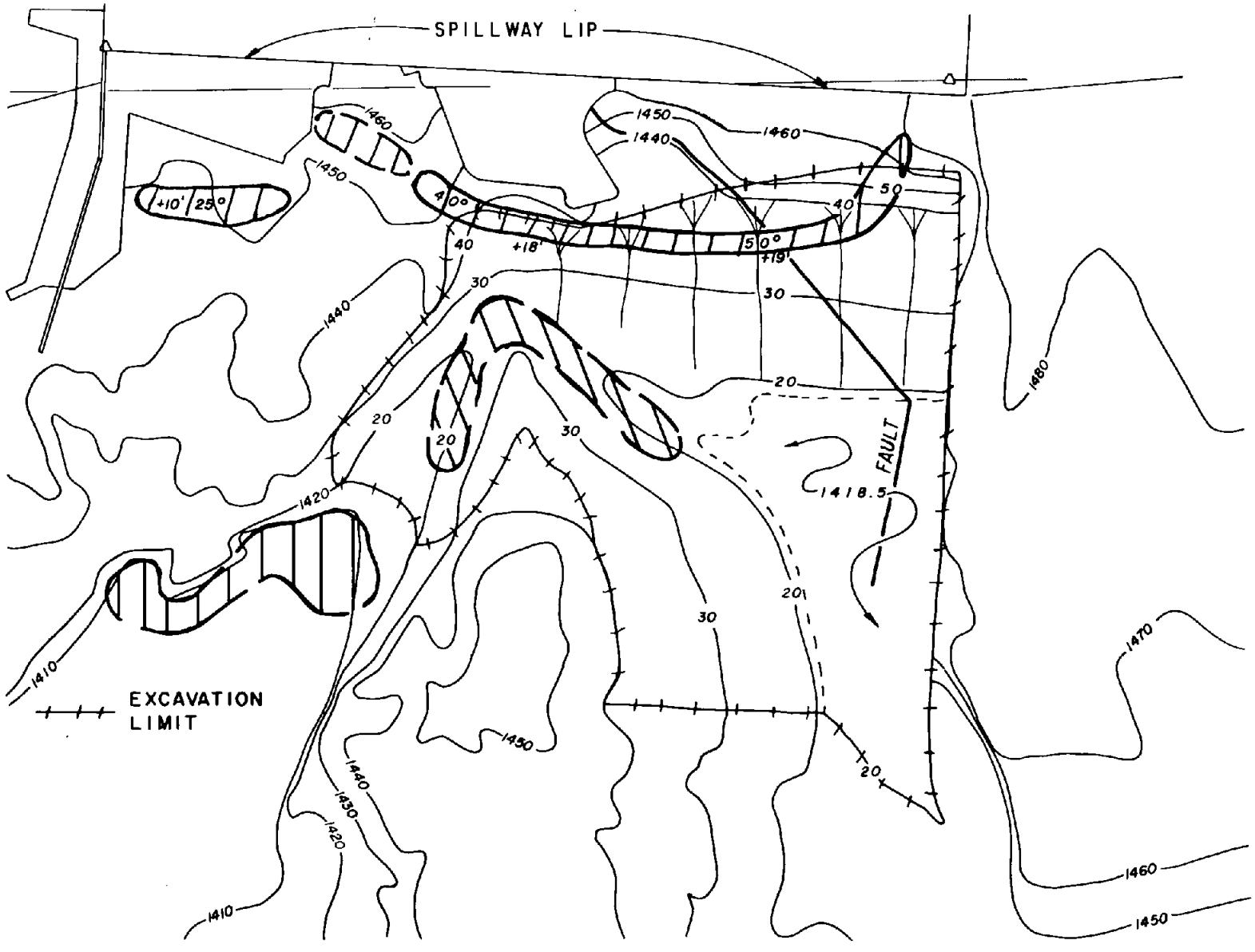

Figure A-21. Impact pressures for a discharge of 13,000 ft^3/s (second topographic model modification).

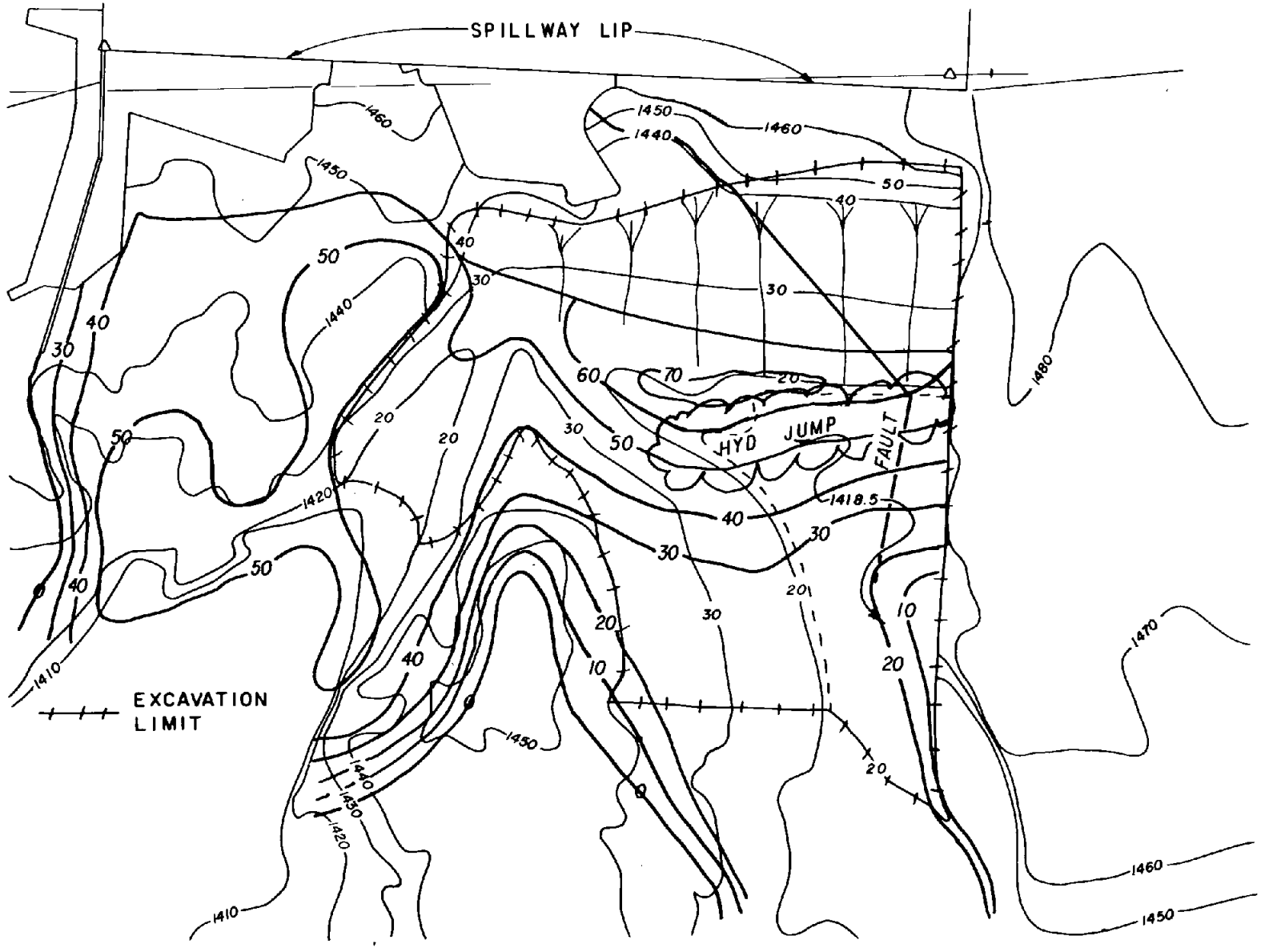

Figure A-22. Velocity contours for a discharge of 30,000 ft^3/s (second topographic model modification).

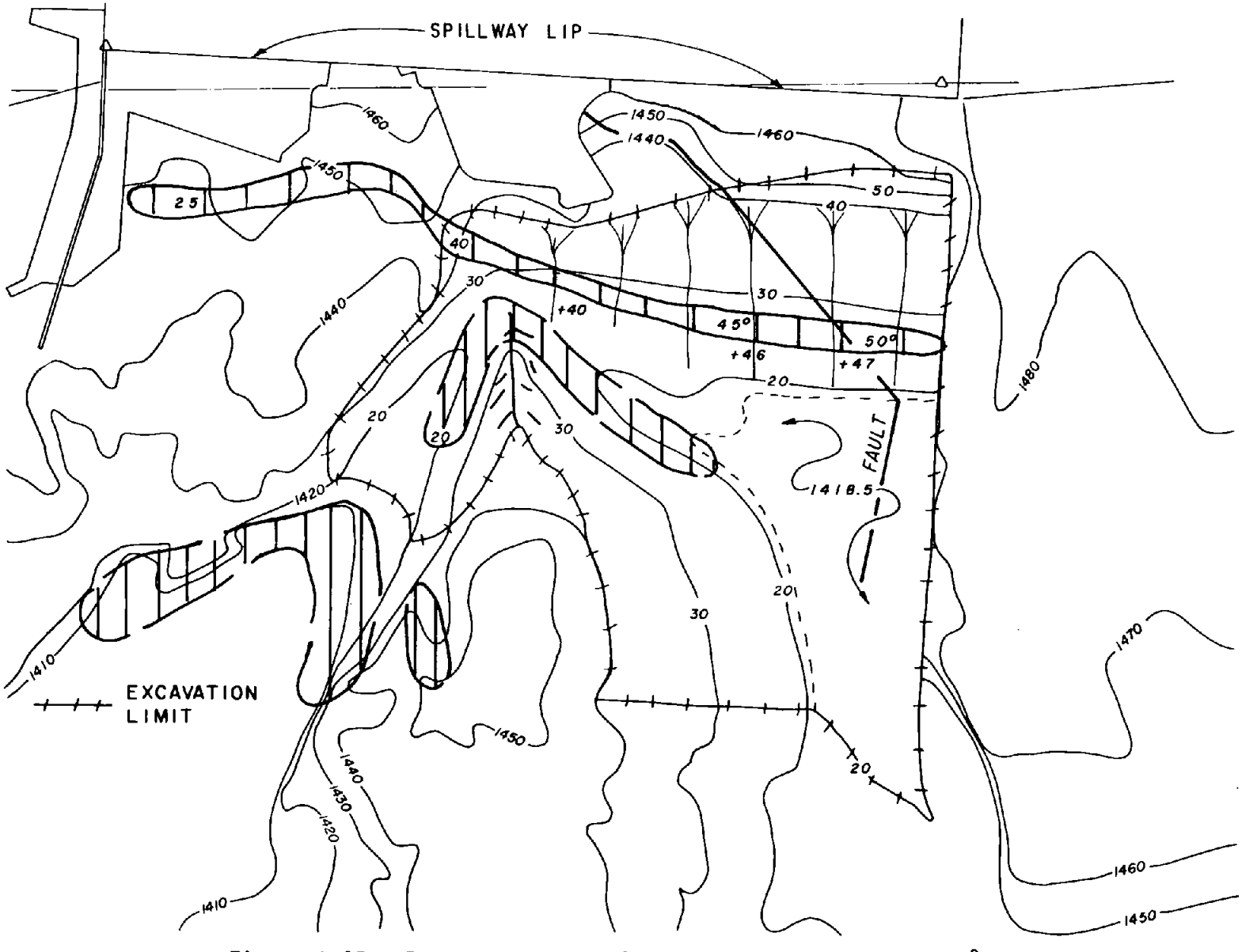

Figure A-23. Impact pressures for a discharge of 30,000 ft^3/s (second topographic model modification).

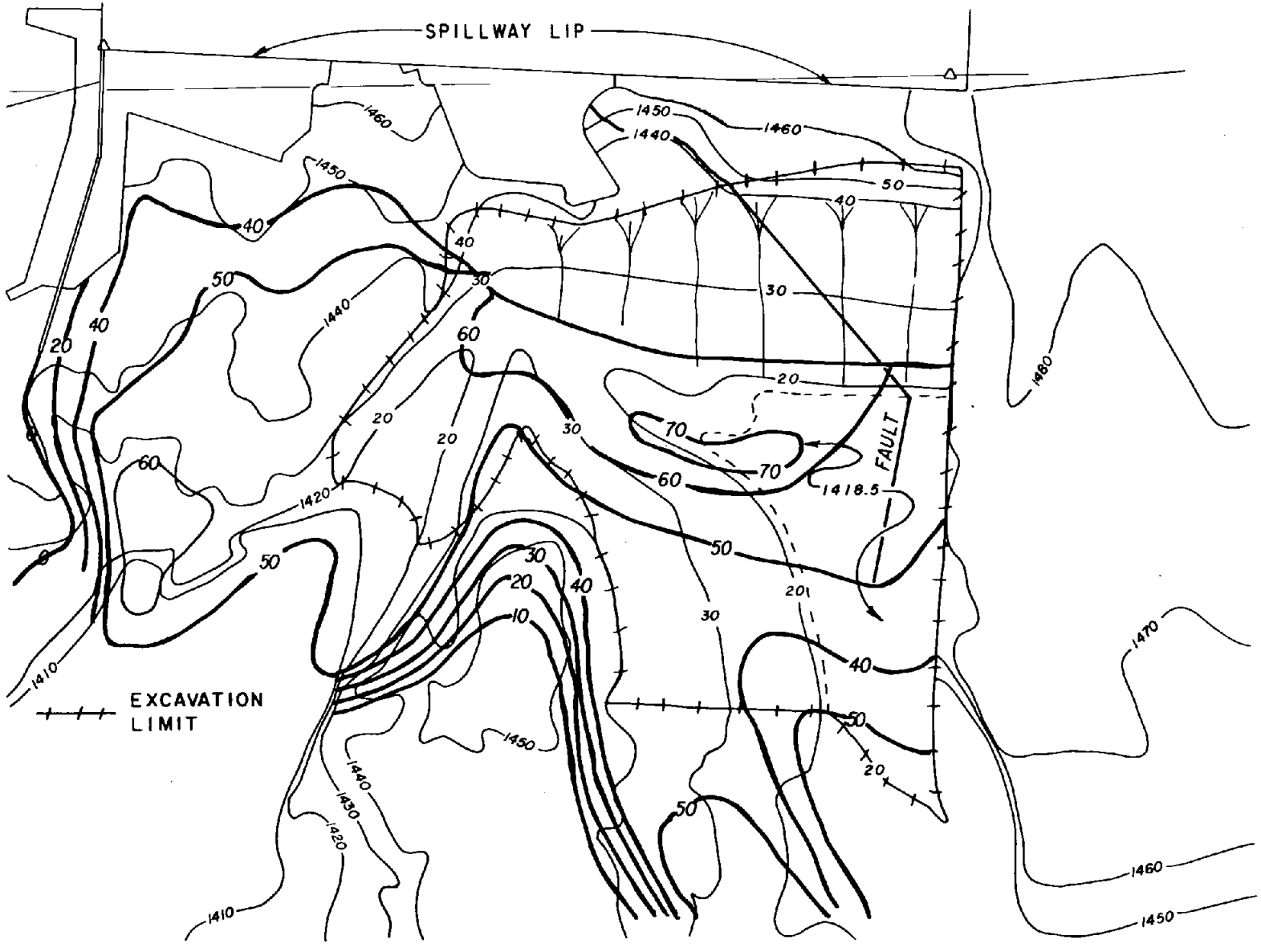

Figure A-24. Velocity contours for a discharge of 60,000 ft^3/s (second topographic model modification).

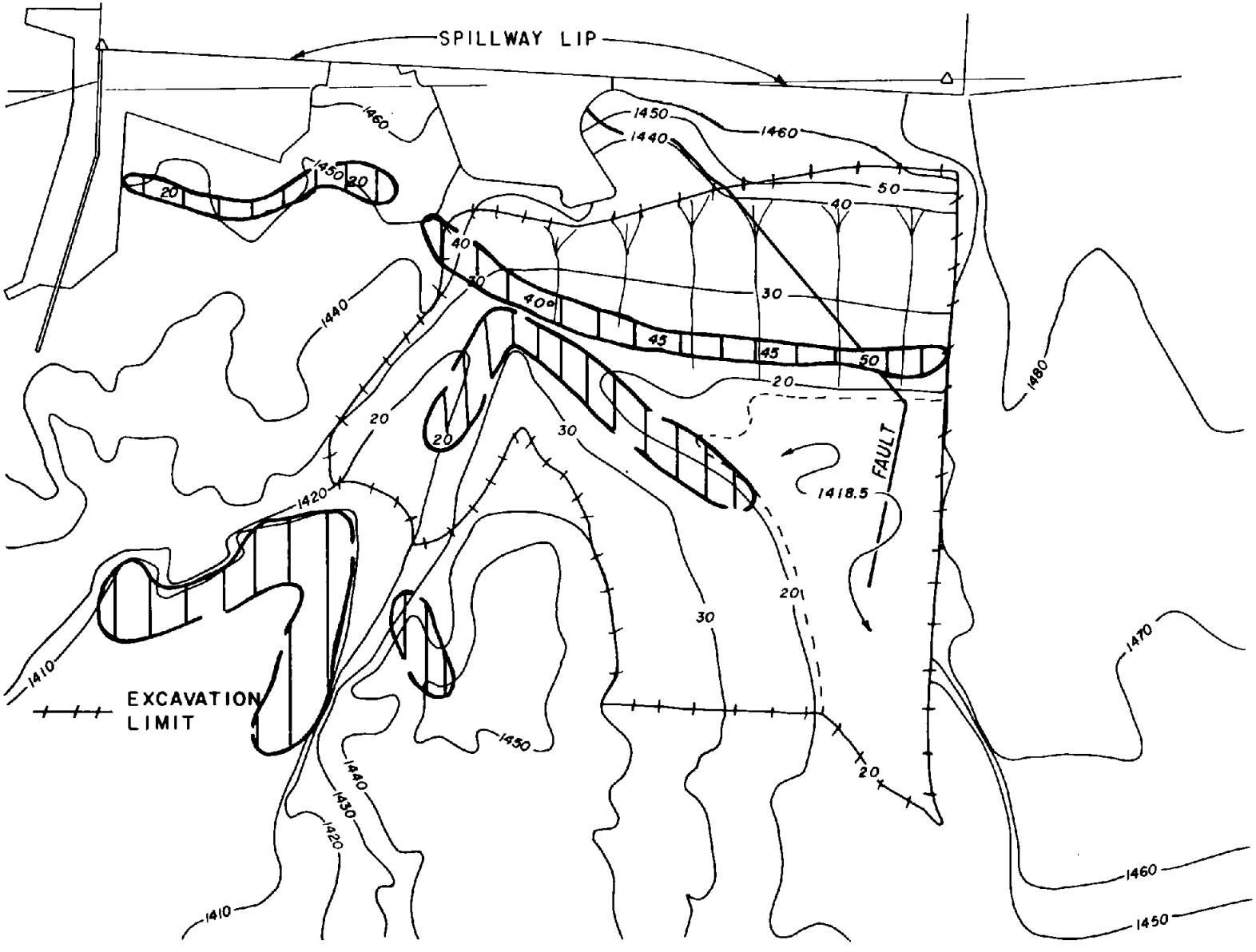

Figure A-25. Impact pressures for a discharge of 60,000 ft^3/s (second topographic model modification).

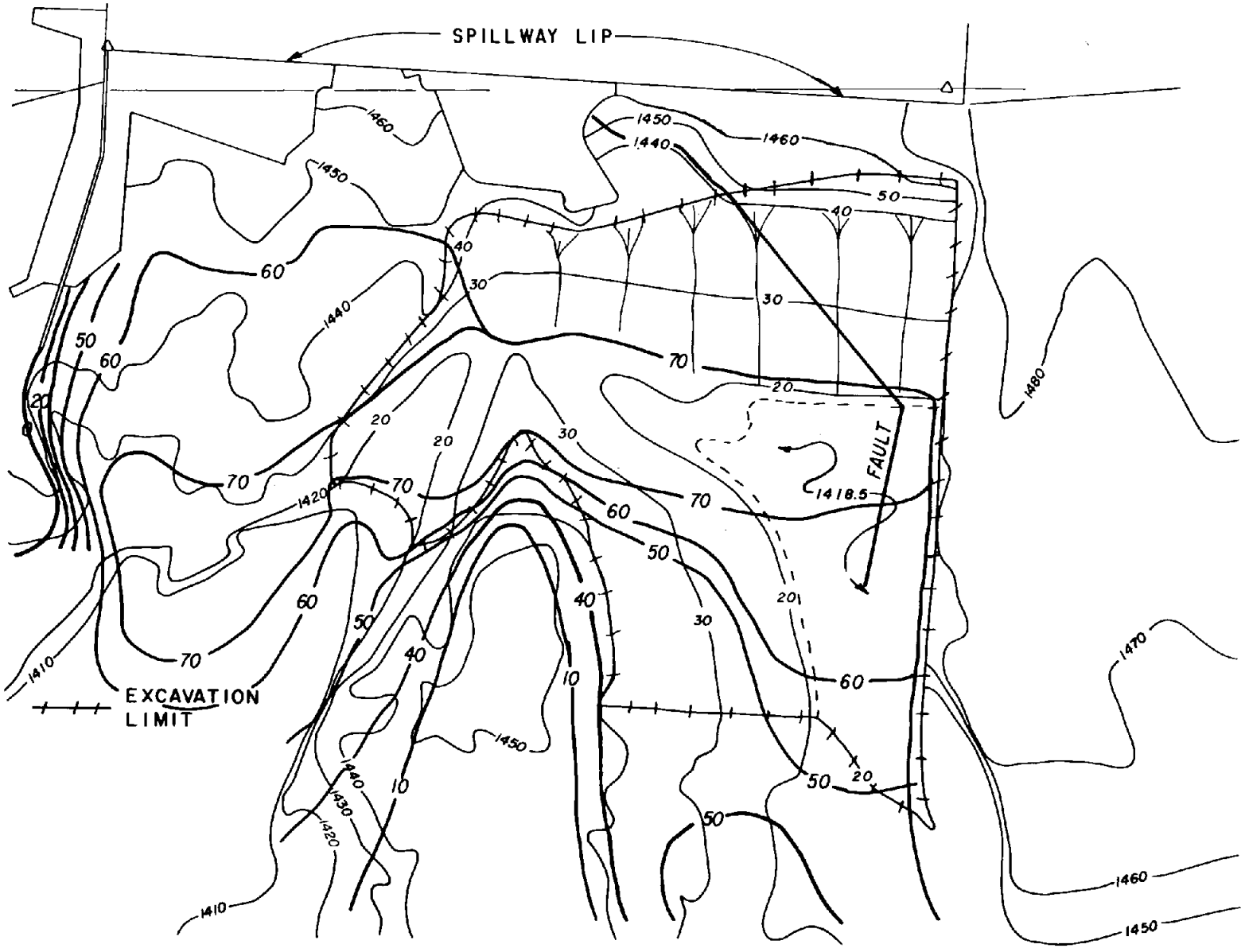

Figure A-26. Velocity contours for a discharge of 140,000 ft^3/s (second topographic model modification).

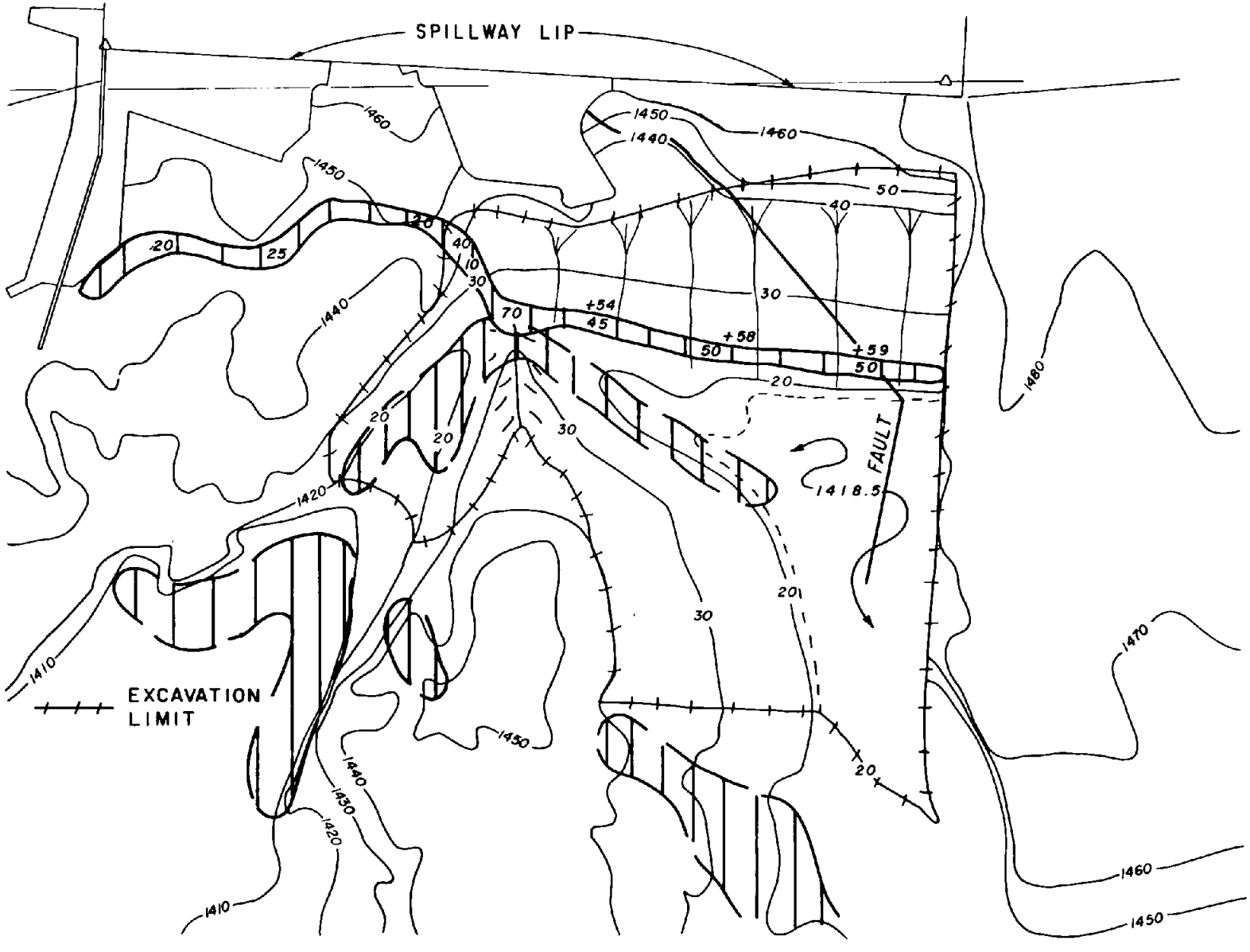

Figure A-27. Impact pressures for a discharge of 140,000 ft^3/s (second topographic model modification).

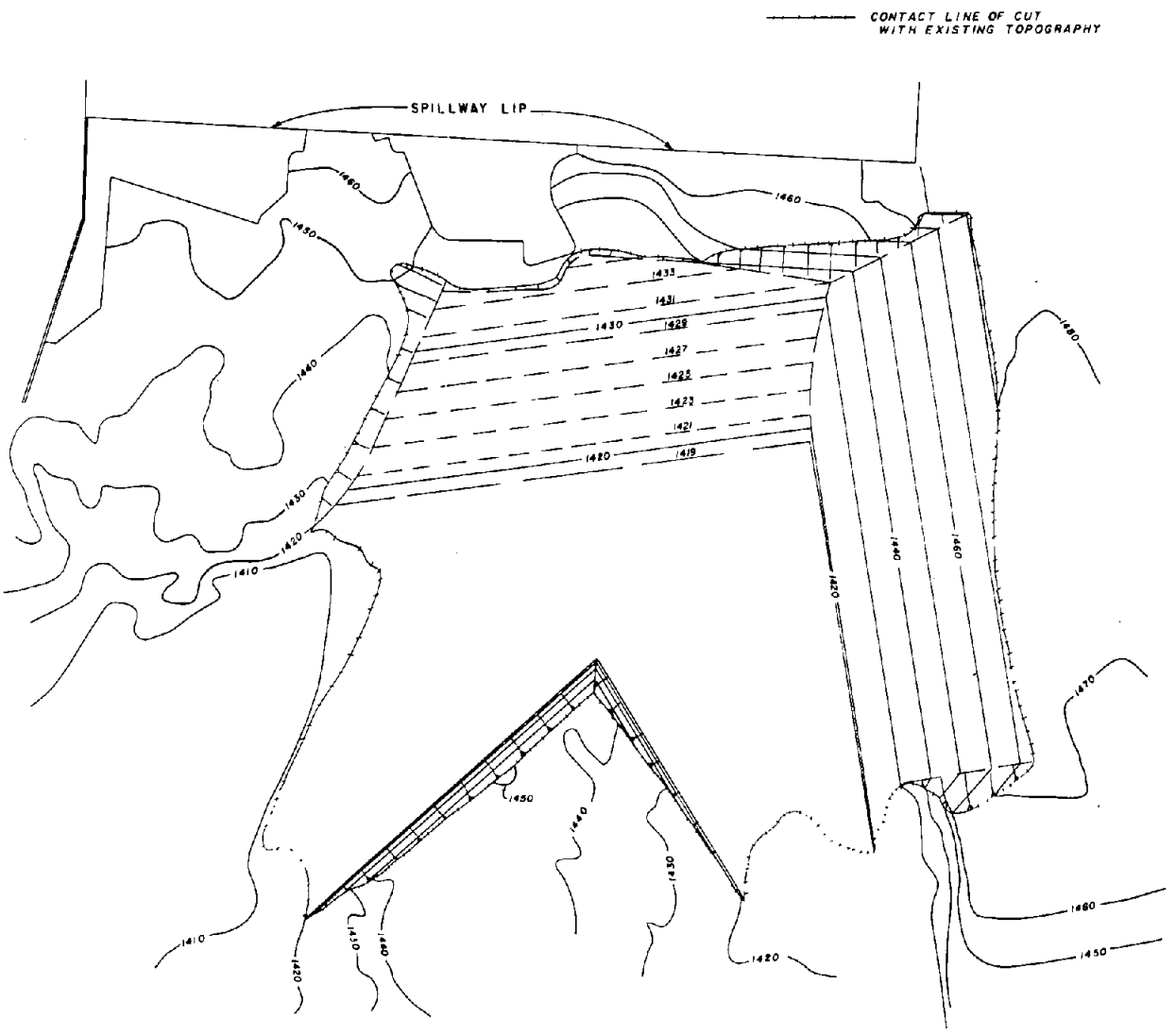

Figure A-28. Final topographic model configuration.

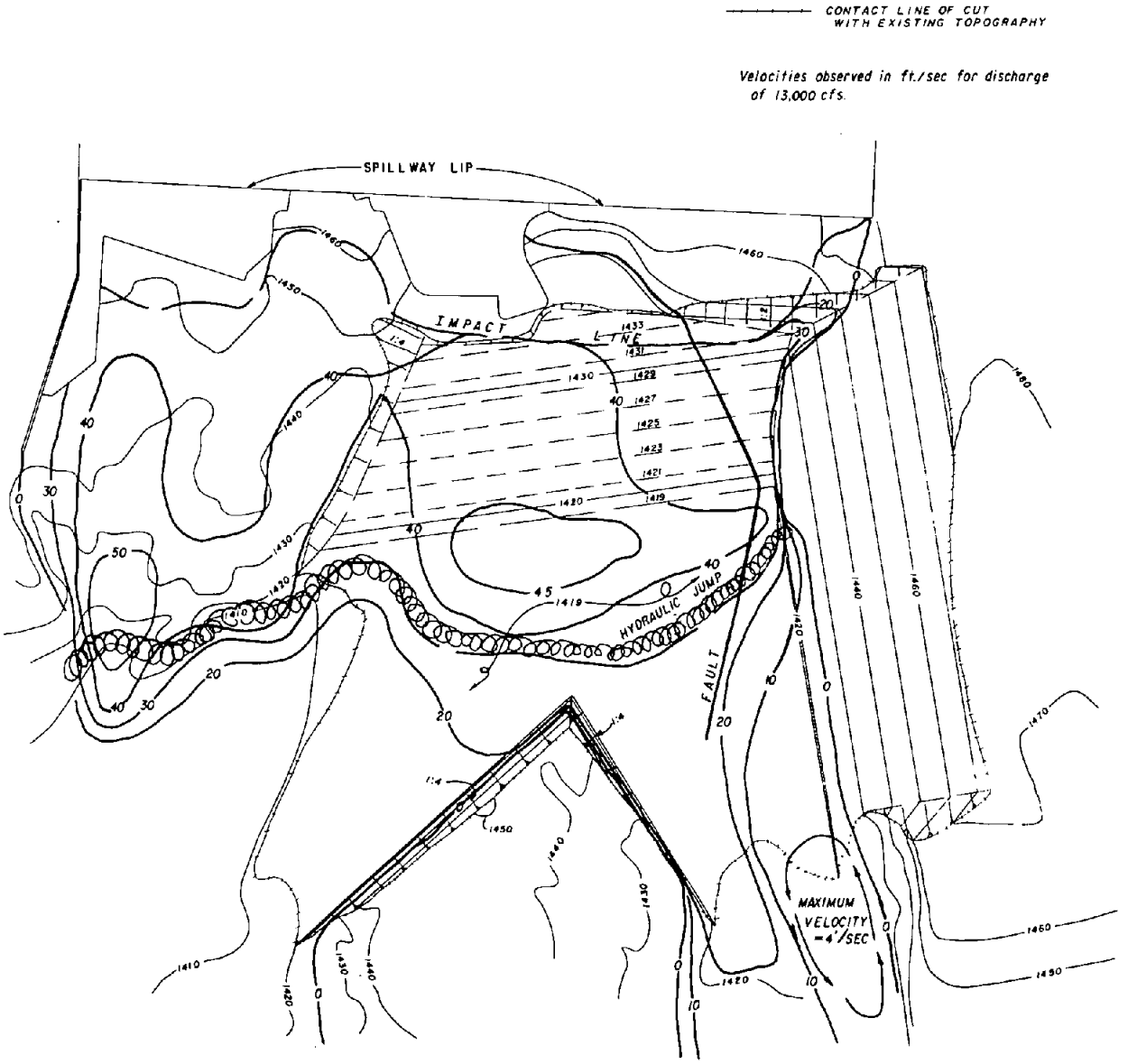

Figure A-29. Velocity contours for a discharge of 13,000 ft^3/s (final topographic model configuration).

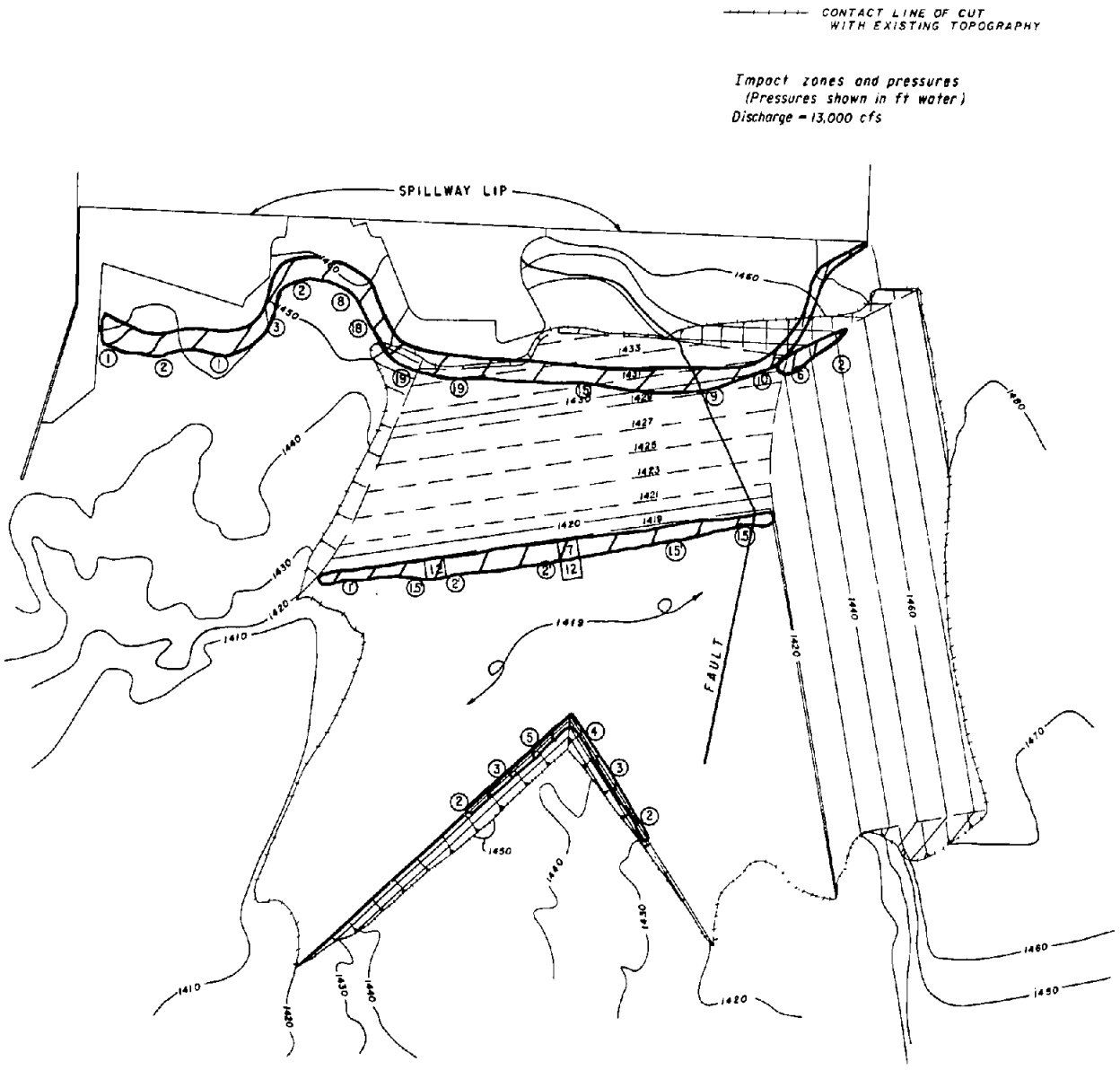

Figure A-30. Impact pressures for a discharge of 13,000 ft^3/s (final topographic model configuration).

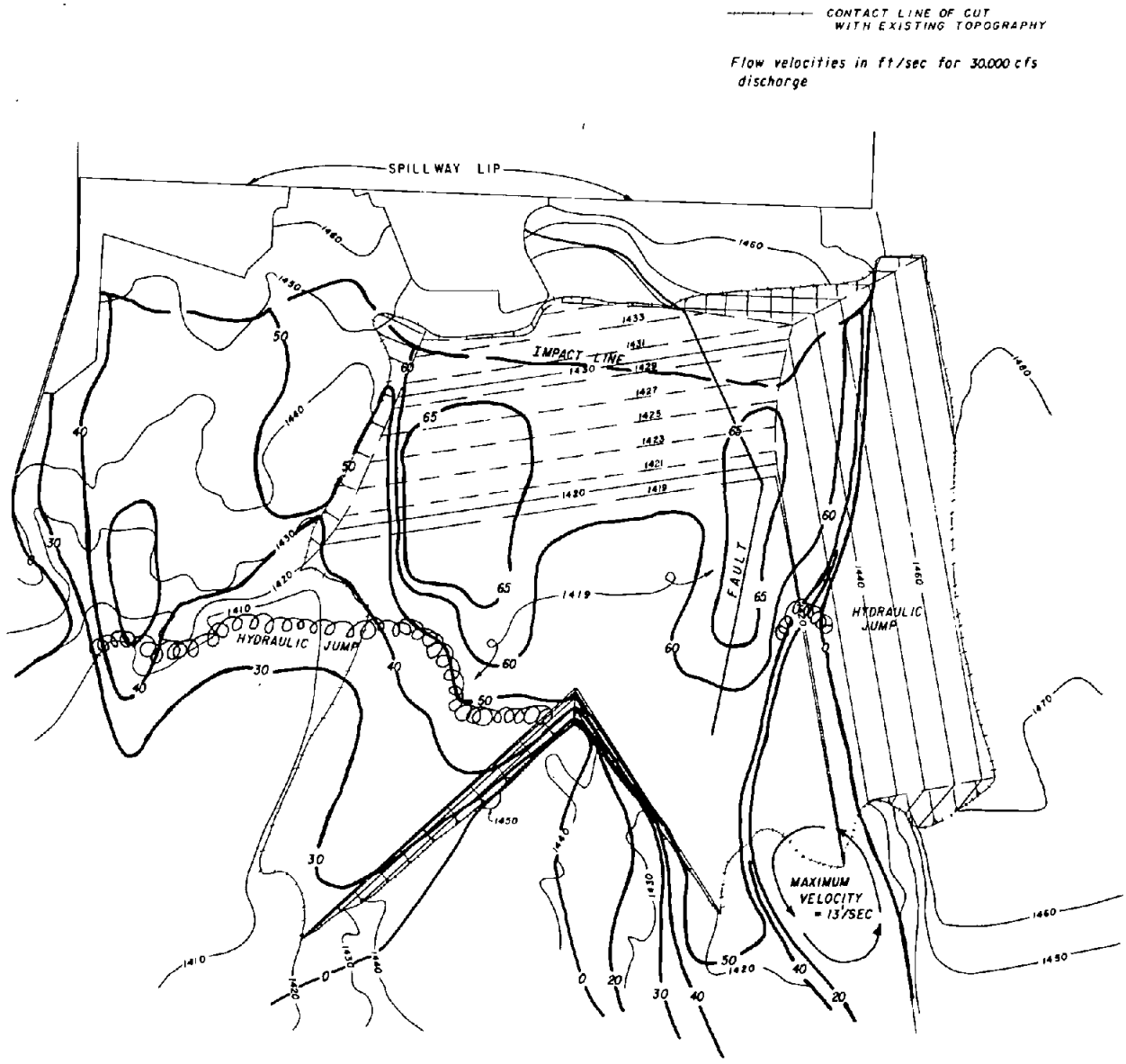

Figure A-31. Velocity contours for a discharge of 30,000 ft^3/s (final topographic model configuration).

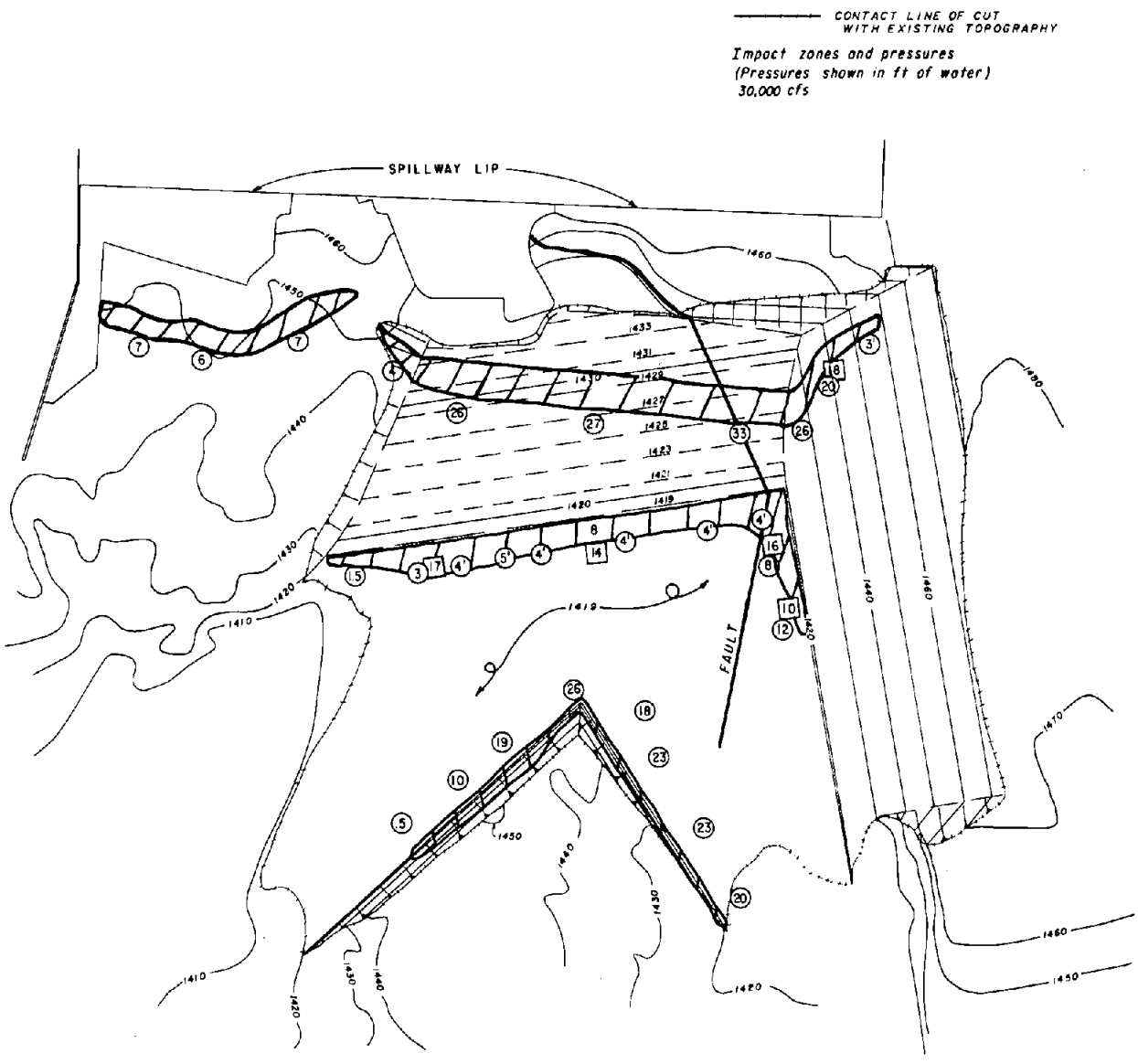

Figure A-32. Impact pressures for a discharge of 30,000 ft^3/s (final topographic model configuration).

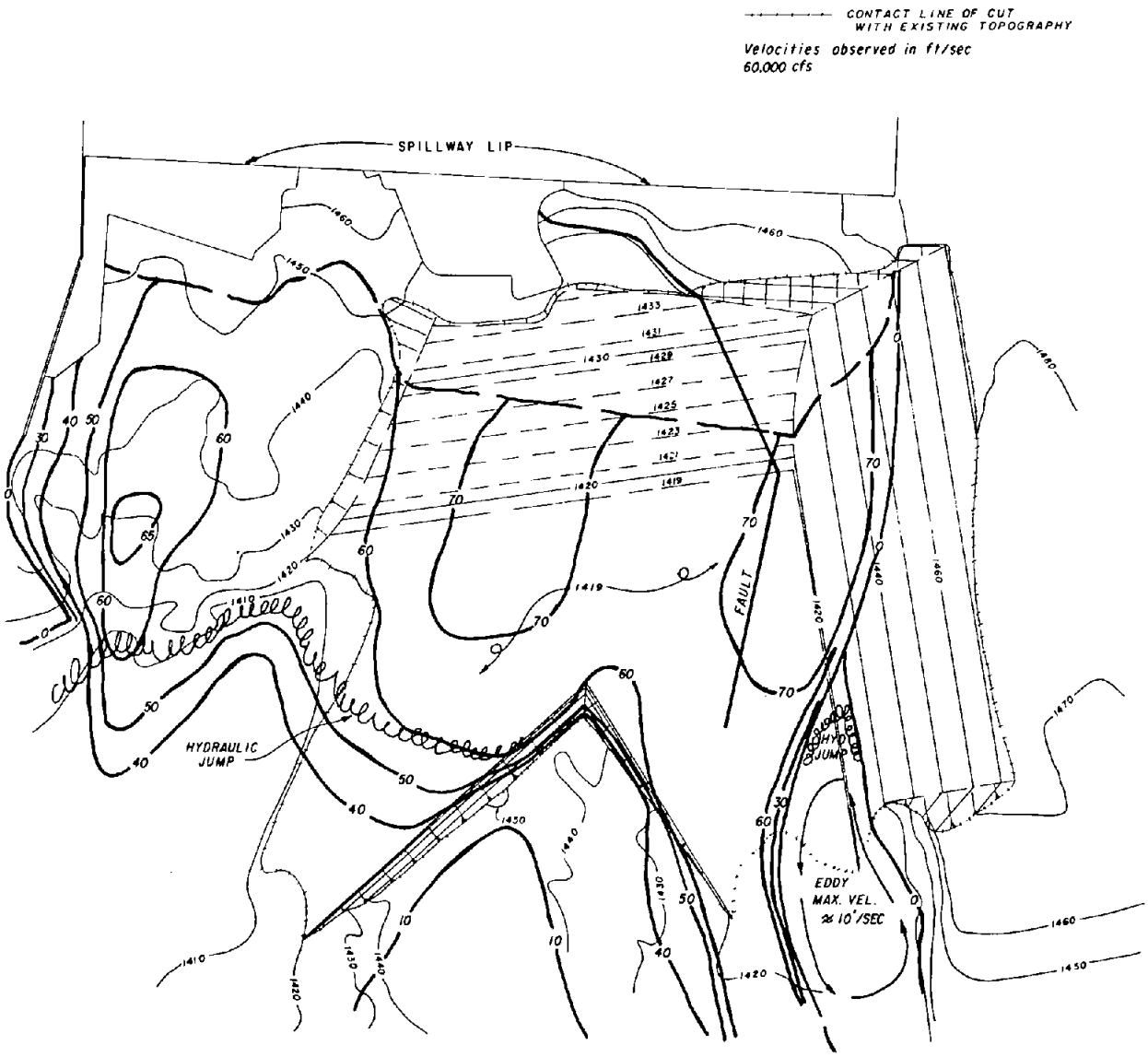

Figure A-33. Velocity contours for a discharge of 60,000 ft^3/s (final topographic model configuration).

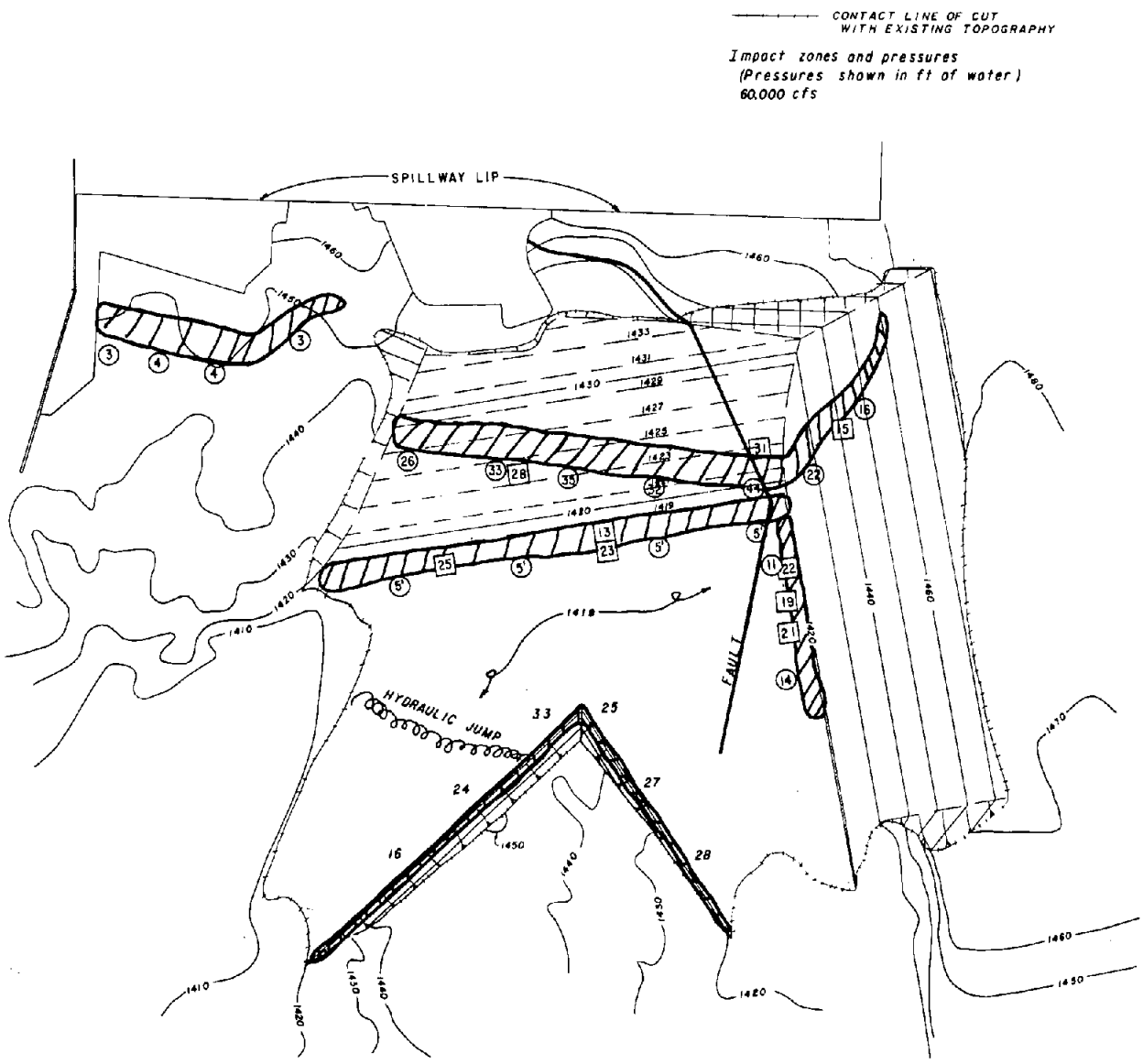

Figure A-34. Impact pressures for a discharge of 60,000 ft^3/s (final topographic model configuration).

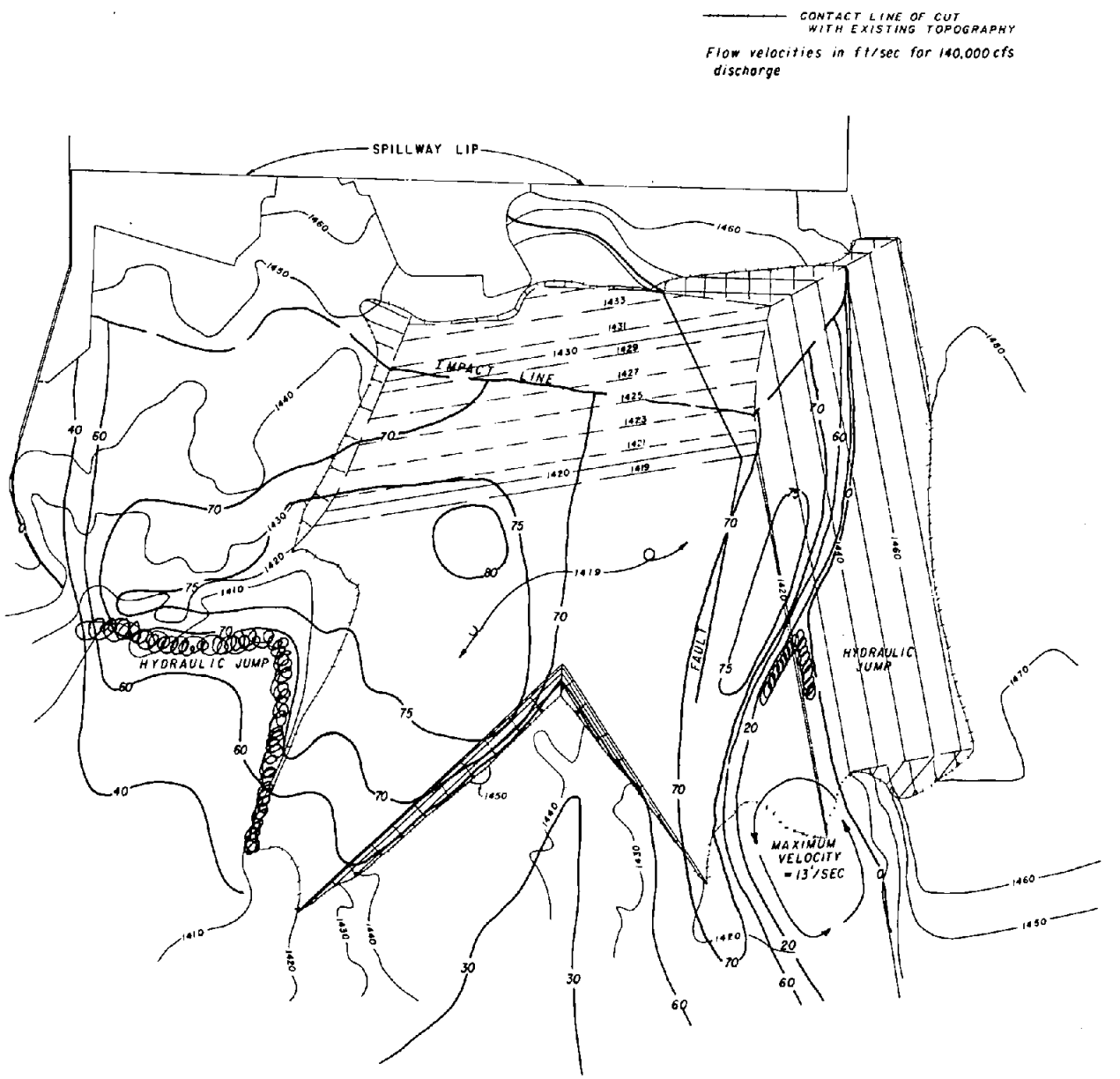

Figure A-35. Velocity contours for a discharge of 140,000 ft^3/s (final topographic model configuration).

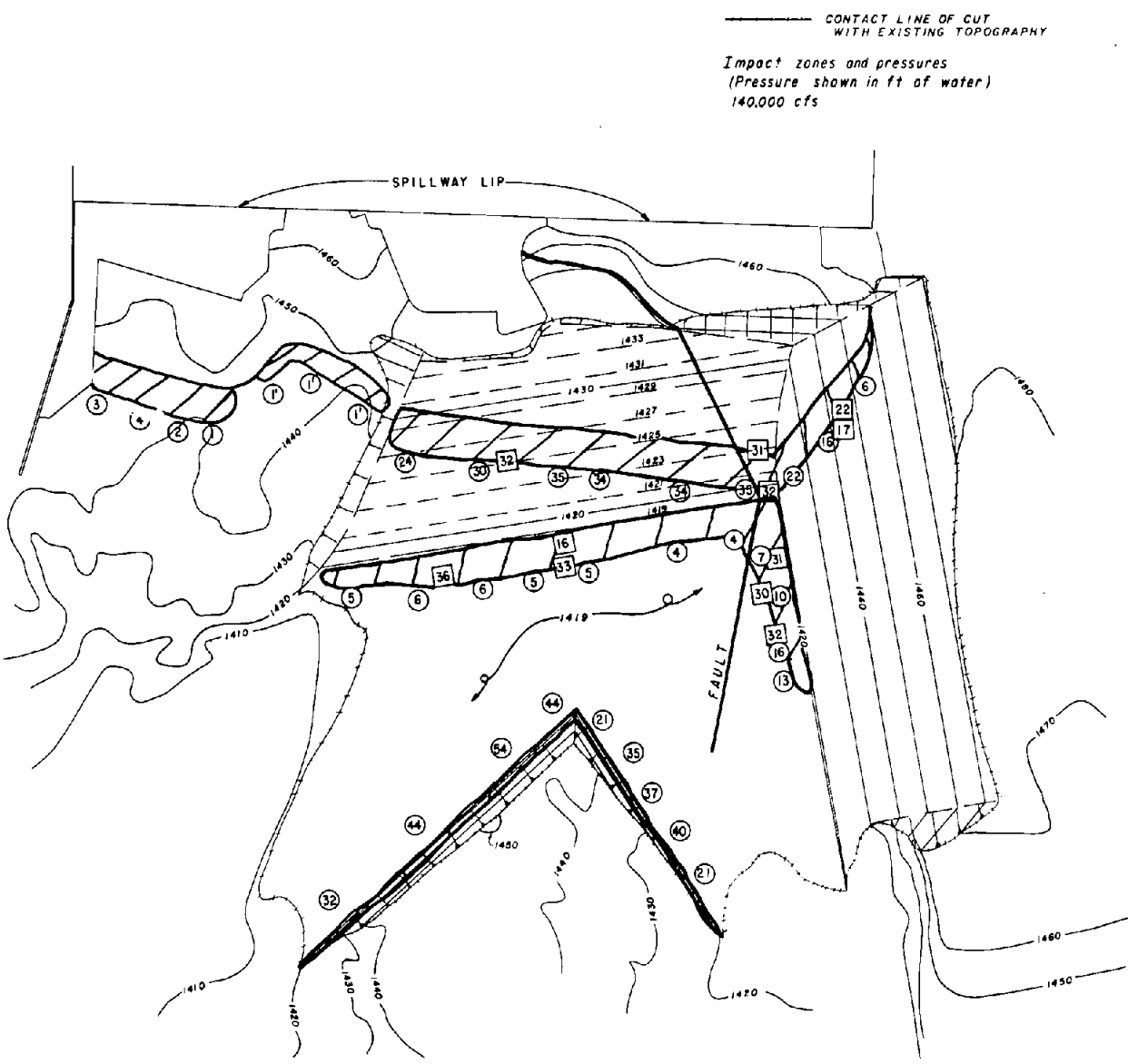

Figure A-36. Impact pressures for a discharge of 140,000 ft^3/s (final topographic model configuration).

GPO 831 - 103

7-1750 (3-71)
Bureau of Reclamation

CONVERSION FACTORS—BRITISH TO METRIC UNITS OF MEASUREMENT

The following conversion factors adopted by the Bureau of Reclamation are those published by the American Society for Testing and Materials (ASTM Metric Practice Guide, E 380-68) except that additional factors (*) commonly used in the Bureau have been added. Further discussion of definitions of quantities and units is given in the ASTM Metric Practice Guide.

The metric units and conversion factors adopted by the ASTM are based on the "International System of Units" (designated SI for Systeme International d'Unites), fixed by the International Committee for Weights and Measures; this system is also known as the Giorgi or MKSA (meter-kilogram (mass)-second-ampere) system. This system has been adopted by the International Organization for Standardization in ISO Recommendation R-31.

The metric technical unit of force is the kilogram-force; this is the force which, when applied to a body having a mass of 1 kg, gives it an acceleration of 9.80665 m/sec/sec, the standard acceleration of free fall toward the earth's center for sea level at 45 deg latitude. The metric unit of force in SI units is the newton (N), which is defined as that force which, when applied to a body having a mass of 1 kg, gives it an acceleration of 1 m/sec/sec. These units must be distinguished from the (inconstant) local weight of a body having a mass of 1 kg, that is, the weight of a body is that force with which a body is attracted to the earth and is equal to the mass of a body multiplied by the acceleration due to gravity. However, because it is general practice to use "pound" rather than the technically correct term "pound-force," the term "kilogram" (or derived mass unit) has been used in this guide instead of "kilogram-force" in expressing the conversion factors for forces. The newton unit of force will find increasing use, and is essential in SI units.

Where approximate or nominal English units are used to express a value or range of values, the converted metric units in parentheses are also approximate or nominal. Where precise English units are used, the converted metric units are expressed as equally significant values.

Table I

QUANTITIES AND UNITS OF SPACE

Multiply	By	To obtain
LENGTH		
Mil	25.4 (exactly)	Micron
Inches	25.4 (exactly)	Millimeters
Inches	2.54 (exactly)*	Centimeters
Feet	30.48 (exactly)	Centimeters
Feet	0.3048 (exactly)*	Meters
Feet	0.0003048 (exactly)*	Kilometers
Yards	0.9144 (exactly)	Meters
Miles (statute)	1,609.344 (exactly)*	Meters
Miles	1.609344 (exactly)	Kilometers
AREA		
Square inches	6.4516 (exactly)	Square centimeters
Square feet	*929.03	Square centimeters
Square feet	0.092903	Square meters
Square yards	0.836127	Square meters
Acres	*0.40469	Hectares
Acres	*4,046.9	Square meters
Acres	*0.0040469	Square kilometers
Square miles	2.58999	Square kilometers
VOLUME		
Cubic inches	16.3871	Cubic centimeters
Cubic feet	0.0283168	Cubic meters
Cubic yards	0.764555	Cubic meters
CAPACITY		
Fluid ounces (U.S.)	29.5737	Cubic centimeters
Fluid ounces (U.S.)	29.5729	Milliliters
Liquid pints (U.S.)	0.473179	Cubic decimeters
Liquid pints (U.S.)	0.473166	Liters
Quarts (U.S.)	*946.358	Cubic centimeters
Quarts (U.S.)	*0.946331	Liters
Gallons (U.S.)	*3,785.43	Cubic centimeters
Gallons (U.S.)	3.78543	Cubic decimeters
Gallons (U.S.)	3.78533	Liters
Gallons (U.S.)	*0.00378543	Cubic meters
Gallons (U.K.)	4.54609	Cubic decimeters
Gallons (U.K.)	4.54596	Liters
Cubic feet	28.3160	Liters
Cubic yards	*764.55	Liters
Acre-feet	*1,233.5	Cubic meters
Acre-feet	*1,233,500	Liters

Table II

QUANTITIES AND UNITS OF MECHANICS

Multiply	By	To obtain
MASS		
Grains (1/7,000 lb)	64.79891 (exactly)	Milligrams
Troy ounces (480 grains)	31.1035	Grams
Ounces (avdp)	28.3495	Grams
Pounds (avdp)	0.45359237 (exactly)	Kilograms
Short tons (2,000 lb)	907.185	Kilograms
Short tons (2,000 lb)	0.907185	Metric tons
Long tons (2,240 lb)	1,016.05	Kilograms
FORCE/AREA		
Pounds per square inch	0.070307	Kilograms per square centimeter
Pounds per square inch	0.689476	Newtons per square centimeter
Pounds per square foot	4.88243	Kilograms per square meter
Pounds per square foot	47.8803	Newtons per square meter
MASS/VOLUME (DENSITY)		
Ounces per cubic inch	1.72999	Grams per cubic centimeter
Pounds per cubic foot	16.0185	Kilograms per cubic meter
Pounds per cubic foot	0.0160185	Grams per cubic centimeter
Tons (long) per cubic yard	1.32894	Grams per cubic centimeter
MASS/CAPACITY		
Ounces per gallon (U.S.)	7.4893	Grams per liter
Ounces per gallon (U.K.)	6.2362	Grams per liter
Pounds per gallon (U.S.)	119.829	Grams per liter
Pounds per gallon (U.K.)	99.779	Grams per liter
BENDING MOMENT OR TORQUE		
Inch-pounds	0.011521	Meter-kilograms
Inch-pounds	1.12985×10^6	Centimeter-dynes
Foot-pounds	0.138255	Meter-kilograms
Foot-pounds	1.35582×10^7	Centimeter-dynes
Foot-pounds per inch	5.4431	Centimeter-kilograms per centimeter
Ounce-inches	72.008	Gram-centimeters
VELOCITY		
Feet per second	30.48 (exactly)	Centimeters per second
Feet per second	0.3048 (exactly)*	Meters per second
Feet per year	$*0.965873 \times 10^{-6}$	Centimeters per second
Miles per hour	1.609344 (exactly)	Kilometers per hour
Miles per hour	0.44704 (exactly)	Meters per second
ACCELERATION*		
Feet per second^2	*0.3048	Meters per second^2
FLOW		
Cubic feet per second (second-feet)	*0.028317	Cubic meters per second
Cubic feet per minute	0.4719	Liters per second
Gallons (U.S.) per minute	0.06309	Liters per second
FORCE*		
Pounds	*0.453592	Kilograms
Pounds	*4.4482	Newtons
Pounds	$*4.4482 \times 10^5$	Dynes

Table II—Continued

Multiply	By	To obtain
WORK AND ENERGY*		
British thermal units (Btu)	*0.252	Kilogram calories
British thermal units (Btu)	1,055.06	Joules
Btu per pound	2.326 (exactly)	Joules per gram
Foot-pounds	*1.35582	Joules
POWER		
Horsepower	745.700	Watts
Btu per hour	0.293071	Watts
Foot-pounds per second	1.35582	Watts
HEAT TRANSFER		
Btu in./hr ft^2 degree F (k, thermal conductivity)	1.442	Milliwatts/cm degree C
Btu in./hr ft^2 degree F (k, thermal conductivity)	0.1240	Kg cal/hr m degree C
Btu ft/hr ft^2 degree F	*1.4880	Kg cal m/hr m^2 degree C
Btu/hr ft^2 degree F (C, thermal conductance)	0.568	Milliwatts/cm^2 degree C
Btu/hr ft^2 degree F (C, thermal conductance)	4.882	Kg cal/hr m^2 degree C
Degree F hr ft^2/Btu (R, thermal resistance)	1.761	Degree C cm^2/milliwatt
Btu/lb degree F (c, heat capacity)	4.1868	J/g degree C
Btu/lb degree F	*1.000	Cal/gram degree C
Ft^2/hr (thermal diffusivity)	0.2581	Cm^2/sec
Ft^2/hr (thermal diffusivity)	*0.09290	M^2/hr
WATER VAPOR TRANSMISSION		
Grains/hr ft^2 (water vapor transmission)	16.7	Grams/24 hr m^2
Perms (permeance)	0.659	Metric perms
Perm-inches (permeability)	1.67	Metric perm-centimeters

Table III

OTHER QUANTITIES AND UNITS

Multiply	By	To obtain
Cubic feet per square foot per day (seepage)	*304.8	Liters per square meter per day
Pound-seconds per square foot (viscosity)	*4.8824	Kilogram second per square meter
Square feet per second (viscosity)	*0.092903	Square meters per second
Fahrenheit degrees (change)*	5/9 exactly	Celsius or Kelvin degrees (change)*
Volts per mil	0.03937	Kilovolts per millimeter
Lumens per square foot (foot-candles)	10.764	Lumens per square meter
Ohm-circular mils per foot	0.001662	Ohm-square millimeters per meter
Millicuries per cubic foot	*35.3147	Millicuries per cubic meter
Milliamps per square foot	*10.7639	Milliamps per square meter
Gallons per square yard	*4.527219	Liters per square meter
Pounds per inch	*0.17858	Kilograms per centimeter

GPO 835 - 188

ABSTRACT

Hydraulic model studies were performed to develop a means to eliminate the possibility of erosion undercutting the spillway chute at Stewart Mountain Dam, Arizona. The chute, which was completed in 1936, was designed so that the water would flow through the chute down a granitic slope to the river. The granite, which was initially thought to be sound, contains a major fault. Erosion along this fault is compromising the chute structure. Operational modifications, the addition of a divider wall or flip structures, and modifications and protections of the granitic surface were considered. Flow velocities across the surface and impact pressures on the rock surface were evaluated. The divider wall as well as several of the topographic modifications, when combined with protective surfacing of various extents of the rock, offered potential solutions.

ABSTRACT

Hydraulic model studies were performed to develop a means to eliminate the possibility of erosion undercutting the spillway chute at Stewart Mountain Dam, Arizona. The chute, which was completed in 1936, was designed so that the water would flow through the chute down a granitic slope to the river. The granite, which was initially thought to be sound, contains a major fault. Erosion along this fault is compromising the chute structure. Operational modifications, the addition of a divider wall or flip structures, and modifications and protections of the granitic surface were considered. Flow velocities across the surface and impact pressures on the rock surface were evaluated. The divider wall as well as several of the topographic modifications, when combined with protective surfacing of various extents of the rock, offered potential solutions.

ABSTRACT

Hydraulic model studies were performed to develop a means to eliminate the possibility of erosion undercutting the spillway chute at Stewart Mountain Dam, Arizona. The chute, which was completed in 1936, was designed so that the water would flow through the chute down a granitic slope to the river. The granite, which was initially thought to be sound, contains a major fault. Erosion along this fault is compromising the chute structure. Operational modifications, the addition of a divider wall or flip structures, and modifications and protections of the granitic surface were considered. Flow velocities across the surface and impact pressures on the rock surface were evaluated. The divider wall as well as several of the topographic modifications, when combined with protective surfacing of various extents of the rock, offered potential solutions.

ABSTRACT

Hydraulic model studies were performed to develop a means to eliminate the possibility of erosion undercutting the spillway chute at Stewart Mountain Dam, Arizona. The chute, which was completed in 1936, was designed so that the water would flow through the chute down a granitic slope to the river. The granite, which was initially thought to be sound, contains a major fault. Erosion along this fault is compromising the chute structure. Operational modifications, the addition of a divider wall or flip structures, and modifications and protections of the granitic surface were considered. Flow velocities across the surface and impact pressures on the rock surface were evaluated. The divider wall as well as several of the topographic modifications, when combined with protective surfacing of various extents of the rock, offered potential solutions.

GR-6-75
Johnson, P. L.
HYDRAULIC MODEL STUDIES OF STEWART MOUNTAIN DAM SPILLWAY
Bur Reclam Rep GR-6-75, Div Gen Res, Jul 1975. Bureau of Reclamation, Denver, 90p, 55 fig, append

DESCRIPTORS--/ hydraulic models/ *chute spillways/ spillway piers/ *model studies/ *model tests/ *rock competency/ impact tests/ slope protection/ erosion control
IDENTIFIERS--/ *Stewart Mountain Dam, AZ
COSATI 13M

GR-6-75
Johnson, P. L.
HYDRAULIC MODEL STUDIES OF STEWART MOUNTAIN DAM SPILLWAY
Bur Reclam Rep GR-6-75, Div Gen Res, Jul 1975. Bureau of Reclamation, Denver, 90p, 55 fig, append

DESCRIPTORS--/ hydraulic models/ *chute spillways/ spillway piers/ *model studies/ *model tests/ *rock competency/ impact tests/ slope protection/ erosion control
IDENTIFIERS--/ *Stewart Mountain Dam, AZ
COSATI 13M

GR-6-75
Johnson, P. L.
HYDRAULIC MODEL STUDIES OF STEWART MOUNTAIN DAM SPILLWAY
Bur Reclam Rep GR-6-75, Div Gen Res, Jul 1975. Bureau of Reclamation, Denver, 90p, 55 fig, append

DESCRIPTORS--/ hydraulic models/ *chute spillways/ spillway piers/ *model studies/ *model tests/ *rock competency/ impact tests/ slope protection/ erosion control
IDENTIFIERS--/ *Stewart Mountain Dam, AZ
COSATI 13M

GR-6-75
Johnson, P. L.
HYDRAULIC MODEL STUDIES OF STEWART MOUNTAIN DAM SPILLWAY
Bur Reclam Rep GR-6-75, Div Gen Res, Jul 1975. Bureau of Reclamation, Denver, 90p, 55 fig, append

DESCRIPTORS--/ hydraulic models/ *chute spillways/ spillway piers/ *model studies/ *model tests/ *rock competency/ impact tests/ slope protection/ erosion control
IDENTIFIERS--/ *Stewart Mountain Dam, AZ
COSATI 13M